NATIONAL AERONAUTICS AND SPACE ADMINISTRATION

Space Programs Summary 37-49, Vol. I

Flight Projects

For the Period November 1 to December 31, 1967

JET PROPULSION LABORATORY
CALIFORNIA INSTITUTE OF TECHNOLOGY
PASADENA, CALIFORNIA

January 31, 1968

NATIONAL AERONAUTICS AND SPACE ADMINISTRATION

Space Programs Summary 37-49, Vol. I

Flight Projects

For the Period November 1 to December 31, 1967

JET PROPULSION LABORATORY
CALIFORNIA INSTITUTE OF TECHNOLOGY
PASADENA, CALIFORNIA

January 31, 1968

SPACE PROGRAMS SUMMARY 37-49, VOL. I

Prepared Under Contract No. NAS 7-100
National Aeronautics & Space Administration

Preface

The Space Programs Summary is a bimonthly publication that presents a review of engineering and scientific work performed, or managed, by the Jet Propulsion Laboratory for the National Aeronautics and Space Administration during a two-month period. Beginning with the 37-47 series, the Space Programs Summary is composed of four volumes:

Vol. I. *Flight Projects* (Unclassified)

Vol. II. *The Deep Space Network* (Unclassified)

Vol. III. *Supporting Research and Advanced Development* (Unclassified)

Vol. IV. *Flight Projects and Supporting Research and Advanced Development* (Confidential)

Approved by:

W. H. Pickering, Director
Jet Propulsion Laboratory

Contents

PLANETARY–INTERPLANETARY PROGRAM

LUNAR PROGRAM

ADVANCED STUDIES

I. *Mariner IV* Project

PLANETARY–INTERPLANETARY PROGRAM

The *Mariner IV* project activities are associated with the continued operation of the *Mariner IV* spacecraft after conclusion of the Mars mission in October 1965. Periodic telecommunications and tracking activities of a largely experimental nature were carried out by the Deep Space Network in the ensuing 17 months; normal operational activities commenced on March 1, 1967. Scientific data were taken, particularly when the geometry of *Mariner IV*, the earth, *Mariner V*, and the sun was of interest; in addition, a number of engineering exercises, tests, and experiments were conducted. These activities were performed in fulfillment of project objectives, to wit: (1) To obtain scientific information on the interplanetary environment in a region of space further from the sun than the orbit of earth during a period of increasing solar activity in 1967, using the *Mariner IV* spacecraft. (2) To obtain additional engineering knowledge about the consequences of extended exposure of spacecraft equipment in the interplanetary space environment and to acquire experience in the operation of a planetary spacecraft after a prolonged lifetime in deep space.

The project is the responsibility of the *Mariner* 1967 project office, which is also responsible for the *Mariner* Venus 67 Project, reported in Section II of this SPS, and the residual activity of the *Mariner* Mars 1964 project, which has consisted of continuing data analysis and the preparation and publication of various final reports.

During the period the *Mariner IV* spacecraft successfully completed three years of operation in solar orbit. Attitude stabilization and maneuver capability ended with the depletion of the cold-gas supply. Gas in one of the two redundant cold-gas-expulsion systems ran out the end of October 1967; the second gas system was exhausted by December 7. The spacecraft is inherently stable in pitch and yaw in sun-acquired attitude; gas exhaustion left it rolling slowly in a counterclockwise direction. Tracking and telemetry acquisition continued intermittently. On December 9, the *Mariner IV* spacecraft entered the cosmic-dust stream associated with the Leonid meteor showers observed on earth each October.

Without active means to maintain pitch and yaw orientation under the disturbances resulting from dust impacts, the spacecraft roll axis began nutating at an increasing angle from the sun line, precluding effective communications. The mission was accordingly terminated officially on December 20. Characteristics of the orbit resulting from the thrust maneuver conducted October 25 have been determined; perihelion was changed from December 25 to December 26, 1967, at a heliocentric radius of 165,615,490 km.

II. *Mariner* Venus 67 Project

PLANETARY–INTERPLANETARY PROGRAM

A. Introduction

The primary objective of the *Mariner* Venus 67 project, authorized in December 1965, was to conduct a flyby mission to Venus in 1967 to obtain scientific information to complement and extend the *Mariner II* results relevant to determining the origin and nature of Venus and its environment. Secondary objectives were to acquire engineering experience in converting and operating a spacecraft designed for flight to Mars into one flown to Venus, and to obtain information on the interplanetary environment during a period of increasing solar activity.

The single flight spacecraft, prepared by converting the *Mariner* Mars 1964 flight spare, was launched June 14, 1967, by an *Atlas/Agena D* launch vehicle, and encountered the planet on October 19, 1967, with a closest approach distance of 2543 m. Launch was conducted from the Air Force Eastern Test Range, at Cape Kennedy, and was supported in addition by elements of the Manned Space Flight Network; space flight operations were supported by the Deep Space Network.

Seven scientific experiments were conducted in the *Mariner* Venus 67 mission; they are listed in Table 1. The S-band occultation and celestial mechanics experiments used tracking and telecommunications elements, but no special flight instruments; the dual-frequency radio experiment required the incorporation of a new instrument into the spacecraft payload. The remaining experiments were essentially as developed for the *Mariner* Mars 1964 mission.

Following the second playback of encounter data from the *Mariner V* tape recorder, calibration operations were conducted for two planetary experiments in November 1967. The spacecraft was rolled while the ultraviolet photometer and dual-frequency radio system (including ground transmitter) were operating. This provided an ultraviolet star chart for comparison with that obtained after the midcourse maneuver in June; the spacecraft celestial longitudes during these two surveys were 180 deg apart. In addition, a free-space antenna pattern was obtained for the dual-frequency receiver antennas.

Table 1. *Mariner* Venus 67 scientific complement

Experiment	Principal investigator
S-band radio occultation	Arvydas J. Kliore, Jet Propulsion Laboratory
Ultraviolet photometer	Charles A. Barth, University of Colorado
Dual-frequency radio propagation	Von R. Eshleman, Stanford University
Helium magnetometer	Edward J. Smith, Jet Propulsion Laboratory
Solar plasma	Herbert S. Bridge, Massachusetts Institute of Technology
Trapped radiation	James A. Van Allen, State University of Iowa
Celestial mechanics	John D. Anderson, Jet Propulsion Laboratory

Table 2. Attitude control OSE

Spacecraft changes	Disposition
Sun sensor cell functions	OSE stimulus controls redesigned
Canopus sensor intensity gate level	OSE stimulus control circuit changed to permit new gate level testing
Primary sun sensor power supply voltage changed	Changed the OSE monitor circuit
Planet sensor added	Stimulus source added
Planet terminator sensor added	Stimulus source added

Table 3. Central computer and sequencer OSE

Spacecraft changes	Disposition
Timing of spacecraft events	OSE automatic test sequence changed to conform to new sequence

Table 4. Power OSE

Spacecraft changes	Disposition
400 Hz single phase supply (4A17) deleted	Deleted OSE monitor circuit for this supply

On November 21, 1967, the *Mariner V* spacecraft was conditioned for a long-term cruise, and the radio frequency signal was switched to the omnidirectional low gain antenna. The RF carrier was detected on December 4, near threshold; it is not expected to be reacquired until September 1968, when, if operating, the spacecraft may participate in operations similar to those conducted with *Mariner IV* in 1967.

B. Guidance and Control

1. Summary of Operational Support Equipment Changes

The *Mariner* Venus 67 Guidance and Control OSE consisted largely of modified *Mariner C* OSE. Three classes of OSE were provided: Laboratory Test Sets, System Test Sets, and Launch Complex Sets. The modifications to this equipment were confined to mandatory changes, including those resulting from flight equipment changes. The redesigned areas are listed in Tables 2–4.

2. Canopus Sensor Stimulus Hood

A new stimulus hood for the Canopus sensor was a major improvement for the *Mariner* Venus 67 attitude control OSE.

The *Mariner C* hood had 15 collimated light sources: a separate source to provide clockwise, counterclockwise, and null errors for each of five different cone angles. These sources were aligned to provide the proper outputs from the Canopus sensor.

During system testing, it was often desired to simulate Canopus acquisition immediately after turning the sensor on. However, there were two problems with this hood that caused delays in the testing until the sources were aligned. First, the warm-up characteristics of the sensor were such that the hood sources were not at the proper angle to provide the proper logic conditions for the simulated acquisition until the sensor had warmed. Second, the calibration resistors for the source intensity were located in both the hood and in the test set. Calibration was accomplished by selecting and matching resistors in the hood and test set, thus complicating the calibration procedure.

The new hood (Fig. 1) has five collimators (one for each cone angle) mounted on a bar which can rotate about the focal point of the Canopus sensor optics. Warm-up drift is no problem, since the bar is rotated by a motor, and the position of the bar provides the error signals for the sensor. The intensity of the sources is controlled by a single circuit in the OSE. This eases the calibration problem, since there are no resistors to select and match.

3. Attitude Control Subsystem Simulator

A second major improvement in the AC OSE was the design and fabrication of an AC flight subsystem simulator (Figs. 2 and 3). The purpose of this portable unit was to provide a means of performing comprehensive

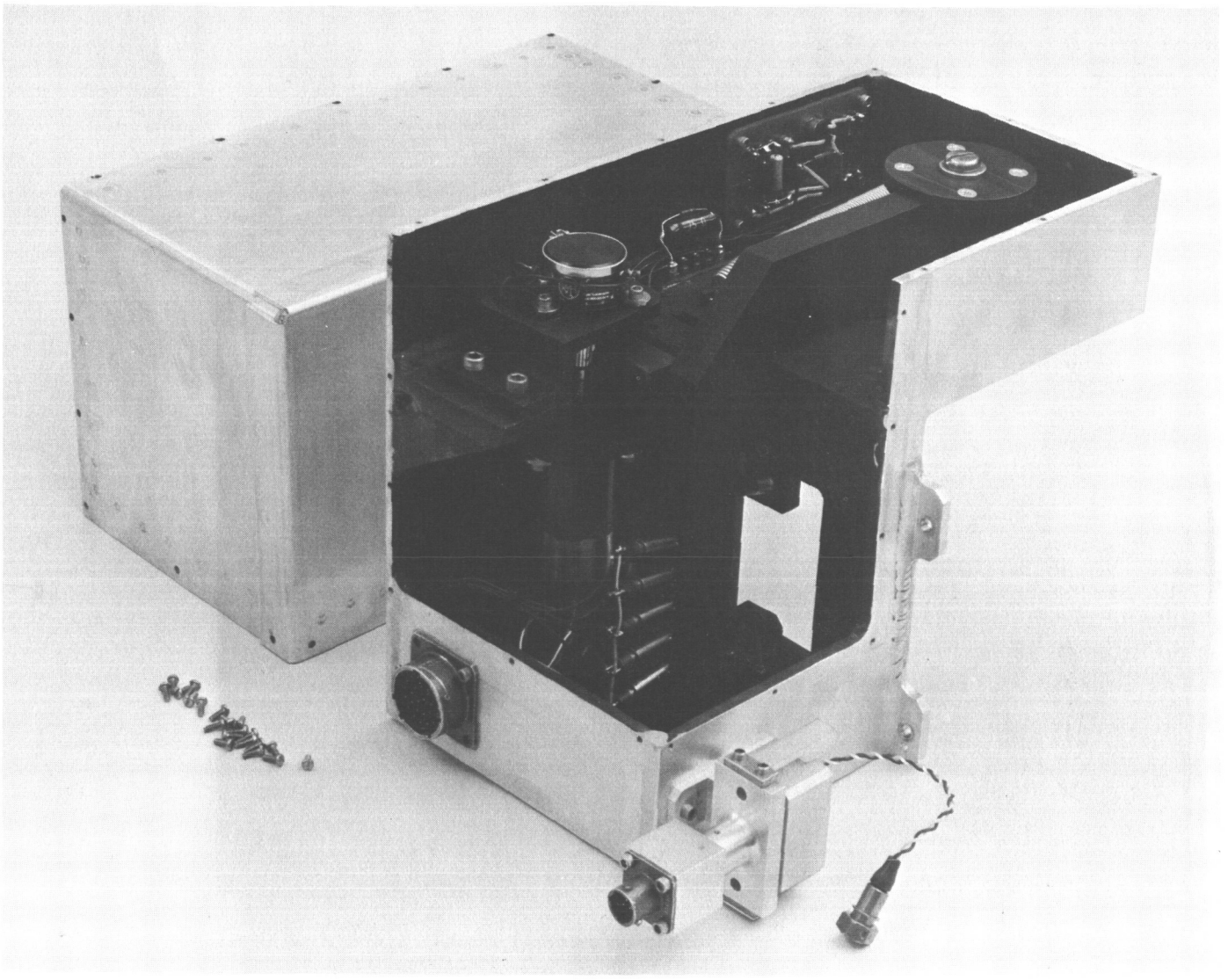

Fig. 1. New Canopus sensor stimulus hood

OSE acceptance testing and troubleshooting without requiring the AC flight hardware. It also permits operator training without accumulating operating time on the flight equipment.

During the *Mariner C* program, there was no simple method of verifying the OSE operation and calibration. The OSE self-test features provide an indication of gross malfunctions and are useful prior to the start of a test. However, calibration and input impedance verification was a time-consuming process and required the use of improvised sources.

Another problem was the training of an operator to use the system test set. The trainee could operate the test set in the laboratory, but it was an open loop process since actuation of a stimulus did not result in a signal to the operator that was indicative of proper spacecraft operation.

The simulator (Fig. 2) was designed to connect to the system test set and to provide the nominal loads and signal sources for the system test set. These loads and sources are normally provided by both the AC flight subsystem and the ancillary OSE.

The ancillary OSE loads and signals are typified by the stimulus lamps for the AC celestial sensors, and by the detectors which indicate proper spacecraft response, such as the jet valve pressure switches. The loads

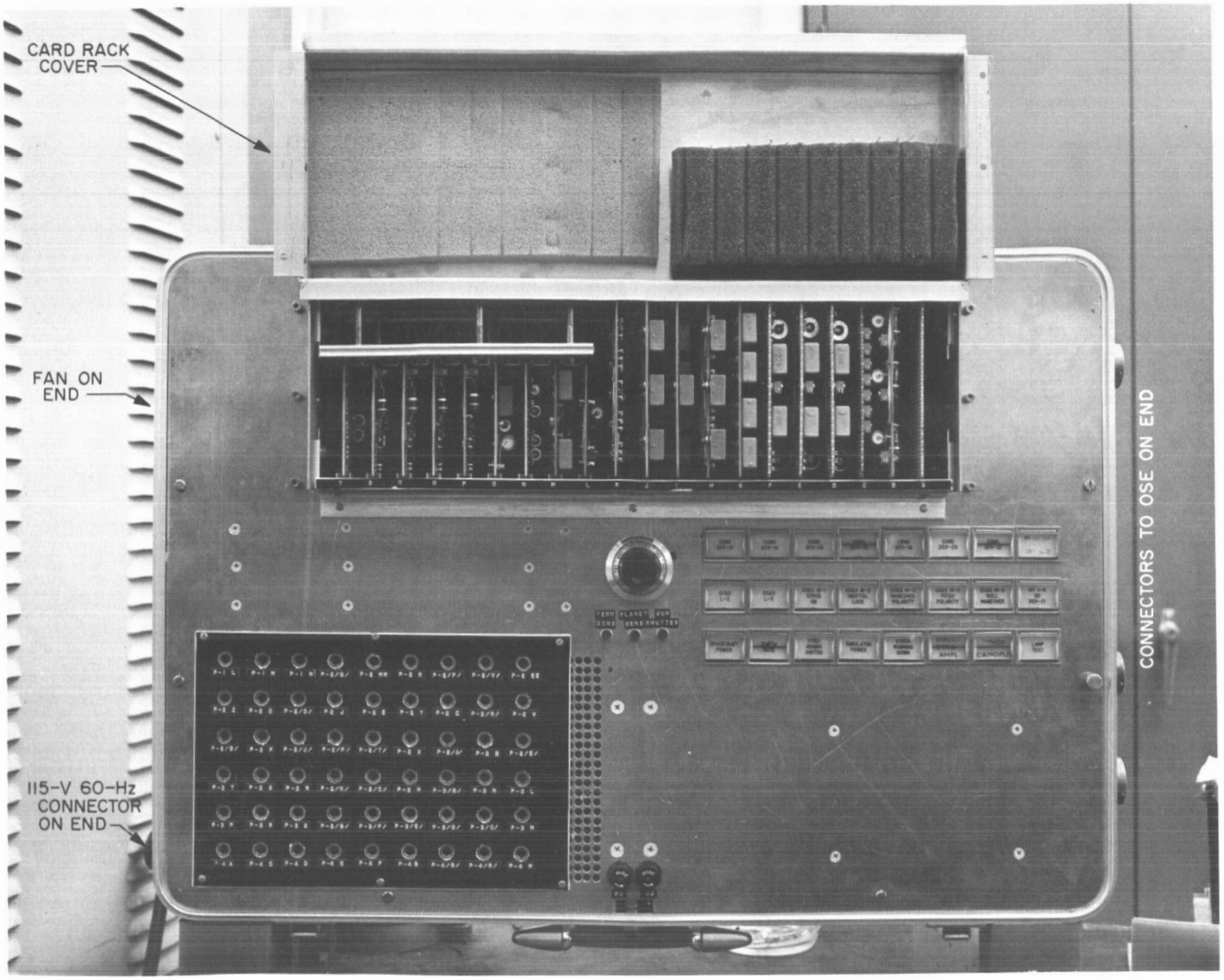

Fig. 2. Attitude control simulator front panel

were designed to consume the same power as the devices used in system test, so that the stimulus control can be verified and adjusted under load. The detectors were designed to provide the same voltages and currents to the test sets as the ancillary OSE does.

The AC flight subsystem simulation is an analog of the flight subsystem. All functions and logic are simulated so that, when the simulator is used as a training aid, the trainee must operate the OSE and the simulator correctly to get the correct indications on the OSE. The method used to simulate the AC subsystem was to derive the transfer function for the flight submodules, then instrument the function with operational amplifiers and passive components.

Where required, the ancillary OSE and the AC subsystem were simulated as a unit. An example is the Canopus sensor and Canopus sensor hood. A dc motor is used to simulate a load for the OSE command functions. The motor drives two potentiometers; one potentiometer simulates the Canopus sensor roll error output, while the second simulates the Canopus sensor hood position signal.

When used for verification or calibration of the OSE, the output voltages and currents of the simulator can be measured at test points and the OSE adjusted for proper operation. When used for training, a complete AC subsystem test can be performed, and the trainee will see

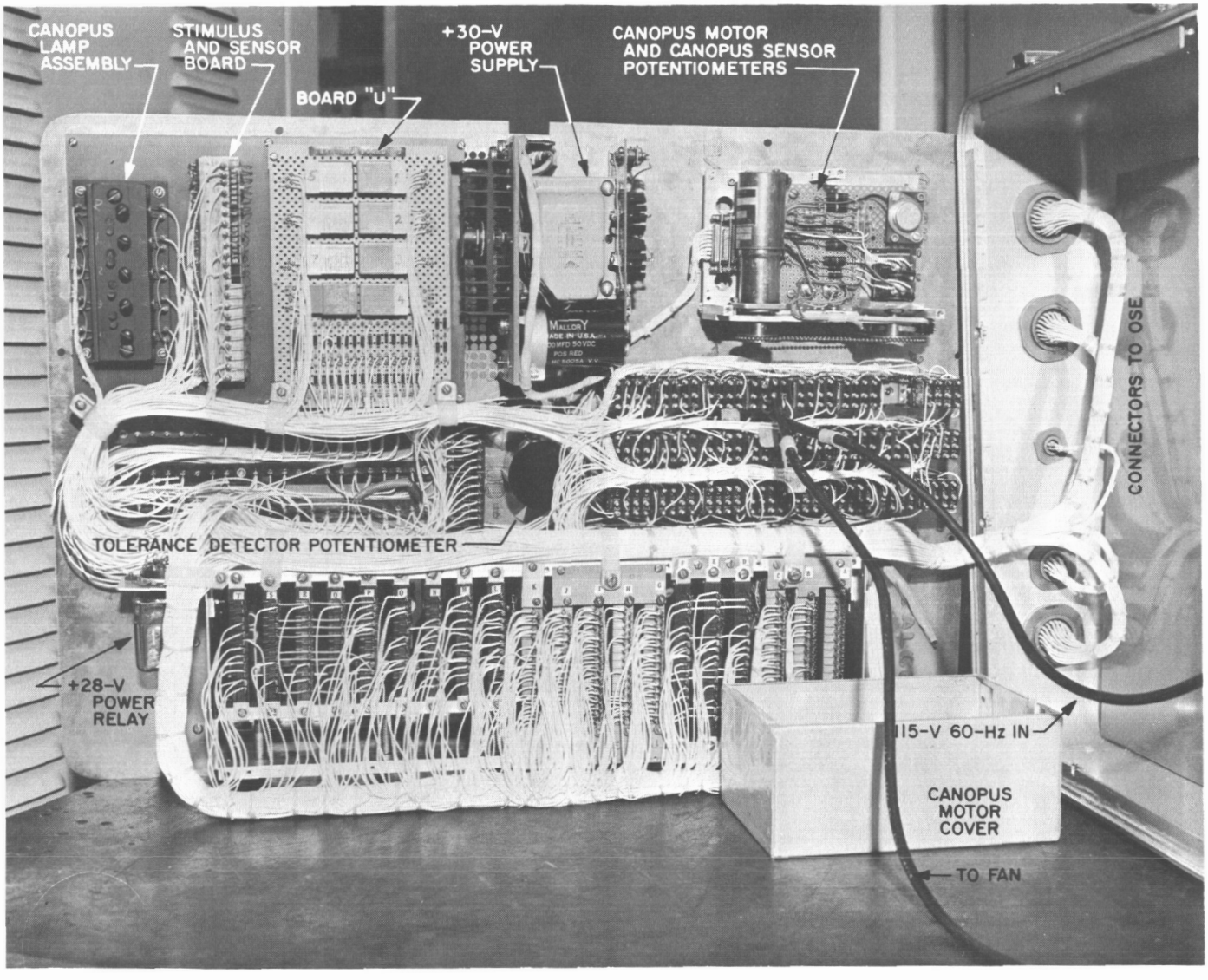

Fig. 3. Attitude control simulator inside view

the same OSE response that will occur during the spacecraft subsystem and system tests.

It is planned to modify the simulator to correspond to the *Mariner* Mars 1969 AC subsystem configuration, and to use it in test team training and in OSE acceptance testing.

4. Operational Support of Canopus Acquisitions

The SIPM was developed to support operations for *Mariner V* during Canopus acquisitions. This support was essentially the same as that provided for the *Mariner* Mars 1964 mission (Ref. 1). A few changes were made to improve support for the *Mariner V* mission.

These changes were based on experiences gained during the *Mariner* Mars 1964 mission. For example, *Mariner IV* attempted to acquire reflected light from the earth during its initial attempt to acquire Canopus. Because the Canopus sensor's response to this type of light had not been modeled, this attempted acquisition was not predicted. As a result, the spacecraft analysts were not able to provide an estimate of what had been acquired until some time after the acquisition. To correct this, a model of the Canopus sensor's response to this type of reflected light was constructed, from tests made on the *Mariner V* Canopus sensor, and incorporated into the SIPM. The estimated Canopus sensor intensity output could then be used to indicate when these acquisitions might occur. During the mission, this model allowed

the analysts to predict that *Mariner V* would acquire reflected light from the earth if roll search started when the clock angle of the Canopus sensor was between 225 and 357 deg (as was the case during flight).

The map-matching technique was made somewhat more efficient for this mission. Instead of being hand plotted, the estimated, telemetered intensity output of the Canopus sensor was plotted to a specified scale by the SIPM. This made it possible to vary the size of this plot to match the real-time strip chart plot of telemetry data. It also became practical to make new versions of this plot as the knowledge of *Mariner V*'s actual trajectory improved.

A new technique to support operations for *Mariner V* was the use of the intensity output of the *Mariner V* earth sensor during the roll spin (used to calibrate the helium magnetometer) prior to Canopus acquisition. By observing the times at which the earth passed through the earth sensor's field of view, the clock angle of the Canopus sensor at the time *Mariner V* started its Canopus acquisition attempt was estimated. These times were correlated with the clock angles of the Canopus sensor to obtain an indication of how the sensor clock angle varied with time. This technique proved very useful in estimating what would be acquired and allowed the acquisition of reflected light from the earth to be predicted.

This estimated clock angle was also useful in making an estimate of the clock angle of the Canopus sensor at the time of acquisition. Two methods were used. The first method was to determine the amount of roll between the start of roll search and acquisition, and add to it the clock angle of the Canopus sensor at the start of roll search. This method provided a quick estimate of the sensor's clock angle at acquisition. The second method consisted of matching the estimated intensity output of the Canopus sensor with the intensity output telemetered from *Mariner V*—the map-matching technique.

The estimated clock angle of the Canopus sensor at the start of roll search was used to indicate which part of the estimated output plot should match best with the telemetered output. Because the plot of the estimated output vs clock angle covered 360 deg in clock angle, and the telemetered output usually covered something less, the estimate of the clock angle at the beginning of roll search was quite useful. The map-matching technique was more accurate because it was not affected by uncertainties in the estimated clock angle of the Canopus sensor at the start of roll search, and most of the variations in the roll rate of *Mariner V* could be taken into account.

Preparations for this operational support were made more efficient for this mission by another modification to the SIPM computer program. Prior to the launch of *Mariner V*, it was desirable to make the plots of the estimated intensity output for different times during the mission (e.g., for the initial attempt to acquire Canopus and for the reacquisition of Canopus after the midcourse maneuver). At other times during the mission, it was desirable to have these plots for several different locations of the probe along the trajectory (usually for planning purposes). During the *Mariner* Mars 1964 mission it would have taken many runs of the SIPM to produce these plots, because the earlier version of the program could only consider one point on the trajectory per run. A single run of the modified program may now consider up to 31 points along a trajectory.

Reference

1. *Mariner Mars 1964 Project Report: Spacecraft Performance and Analysis*, Technical Report 32-882. Jet Propulsion Laboratory, Pasadena, Calif., Feb. 15, 1967.

III. *Mariner* Mars 1969 Project

PLANETARY–INTERPLANETARY PROGRAM

A. Introduction

The *Mariner* Mars 1969 Project was initiated in late December 1965 and formally tasked on February 1, 1966. The primary objective is to conduct two Mars flyby missions in 1969 to make exploratory investigations of the planet which will set the basis for future experiments—particularly those relevant to the search for extraterrestrial life. The secondary objective is to develop Mars mission technology.

The spacecraft design concept is based on the configuration of the successful *Mariner IV* spacecraft, with considerable modifications to meet the 1969 mission requirements and to enhance mission reliability.

The launch vehicle is the *Atlas/Centaur* SLV-3C as used for *Surveyor* missions. This vehicle, developed under contract for and direction by the Lewis Research Center by General Dynamics/Convair, has a single- or double-burn capability in its second stage and a considerably increased performance rating over the *Atlas D/Agena D* used in the *Mariner IV* mission.

Mariner Mars 1969 missions will be supported by the Eastern Test Range launch facilities at Cape Kennedy, the tracking and data acquisition facilities of the Deep Space Network, and other NASA facilities.

Six planetary-science experiments have been selected by NASA for the *Mariner* Mars 1969 missions; they are listed in Table 1.

During the period, flight equipment fabrication proceeded at the various subsystem contractors, with the emphasis on proof-test-model flight hardware, since most proof-test-model equipments are scheduled for delivery to the spacecraft assembly facility in the next period. Many prototype assemblies are scheduled for delivery to the spacecraft assembly facility in time to permit an earlier beginning of spacecraft assembly and testing. A number of prototypes underwent environmental testing during the period. With few exceptions, the operational support equipment units were delivered to the spacecraft assembly facility in December, and began their functional tests. The system test complex data system also began

Table 1. *Mariner* Mars 1969 scientific investigations

Experiment	Scientific investigator	Affiliation
Television	R. B. Leighton[a]	CIT
	B. C. Murray	CIT
	R. P. Sharp	CIT
	N. H. Horowitz	CIT
	J. D. Allen	JPL
	A. G. Herriman	JPL
	R. K. Sloan	JPL
	L. R. Malling	Massachusetts Institute of Technology
	M. E. Davies	Rand Corporation
	C. Leovy	Rand Corporation
Infrared spectrometer	G. C. Pimentel[a]	UCB
	K. C. Herr	UCB
Ultraviolet airglow spectrometer	C. A. Barth[a]	University of Colorado
	W. G. Fastie	Johns Hopkins University
Infrared radiometer	G. Neugebauer[a]	CIT
	G. Munch	CIT
	S. C. Chase	Santa Barbara Research Center
S-band occultation	A. J. Kliore[a]	JPL
	D. L. Cain	JPL
	G. S. Levy	JPL
Celestial mechanics	J. D. Anderson[a]	JPL

[a]Principal investigator.

operations. All subsystem contracts had been definitized by the end of the period. Unit and compatibility testing of the TV subsystems, verifying design capability and compatibility of the spacecraft television camera and data-storage equipment and the ground-based image processing laboratory, were also conducted.

Flight plan approval, subject to certain detail assurances regarding range safety, was obtained from the Air Force Eastern Test Range early in December. Preparation of documents covering planetary quarantine, near-Mars trajectory and geometry, trajectory accuracy capability, and flight path characteristics began during the period; these documents will be published early in 1968. The launch vehicle system design review was conducted late in November 1967; the design was found to be generally satisfactory. The high-rate telemetry design of the tracking and data acquisition system was reviewed in December 1967. Modifications to the mission operations system, to simplify the equipment utilization configuration for enhanced reliability and economy, were studied during the period. The seventh quarterly project review will be conducted in the next period.

B. Project Engineering

1. Launch Vehicle Integration

During this report period, the launch vehicle integration effort continued to maintain the interface between the spacecraft system and the *Atlas/Centaur* launch vehicle system. First revisions of the hardware interface control document and the interface schedule together with additions and changes to the interface control drawing were prepared and released. A number of specific detail technical agreements were also negotiated.

2. Spacecraft System Design

a. Reliability. The availability of *Mariner* Mars 1964 spacecraft flight experience has been recognized as a source of potentially significant data in the reliability analysis of the *Mariner* Mars 1969 spacecraft. Data compiled on component failures on the *Mariner* Mars 1964 spacecraft are being used in the development of a failure rate multiplier. The failure rate multiplier derived from the 1964 experience will be used to factor-in the effect of the interplanetary space environment and thus modify the failure rates of the *Mariner* Mars 1969 spacecraft components.

b. Sequential turn-on of the science instruments. Sequential turn-on of the science subsystems has been studied to reduce the turn-on transient, which might become a problem for the power subsystem. When the approach guidance experiment was deleted, an additional power switching relay was left in the power distribution module. This additional relay could be used to energize part of the science payload separately. The capability would also exist to turn off an instrument if it developed a problem which might cause failures in other spacecraft subsystems.

The UVS and IRS operate only in the near encounter period. These two subsystems could be switched independently of the other science subsystems. However, the division of the science payload into these two units, DAS, TV, and IRR, and IRS and UVS, did not reduce the turn-on transient. For this reason, and because of the cost and schedule implications, the approach guidance power switching relay will not be used for sequential science turn-on. Instead it will be used to optimize the TC of the scan platform. The transient problem is being solved

by redesigning the power supplies of those instruments with large turn-on transients.

c. Optimization of temperature control. The first series of scan platform TC test results shows that the present spacecraft TC design should be optimized by employing additional electric heaters switched by ground command. The performance of the thermal blanket was better than anticipated, which made the scan platform more sensitive to any power variations. Design changes had to be made to compensate for any power variations to the platform.

The final TC design recommended by the TC cognizant engineer and the spacecraft system design group is as follows:

(1) Changes to reduce power variations

  (a) Polish the platform support structures.

  (b) Incorporate a plastic insert in the clock angle drive tube. This will minimize the temperature gradient across the platform bearings.

These changes, which reduce the radiation and conduction ties to the bus, have been implemented.

(2) Changes to compensate for power variations

  (a) Adapt a louver assembly to the thermal blanket.

  (b) Use the approach guidance power switching relay and ground command DC-34 to turn on a heater in the event of an IRS heater failure.

The louvers will be fitted in the thermal blanket and mounted to an adapter plate, which is located on the UVS. The operation of the louvers is such that they will be normally open and constantly radiating about 10 W overboard. In the event of an instrument or heater failure under the blanket, the louvers will provide in-flight adjustment to maintain a constant platform temperature.

Figure 1 shows the required TC heater circuitry changes to the present design. The earlier use of relocated heaters is shown in parentheses. From Fig. 1 (top to bottom), the explanation for each change is as follows:

(1) Platform heater 2 is located in the IRS. A failure of either the ac or dc heater before encounter may result in a failure of the IRS. Because the instrument is located outside of the thermal blanket, a loss of 4.0 W would cause the IRS preamplifier electronics temperature to exceed the lower operating temperature limit. A heater failure can be monitored by engineering telemetry data, and DC-34 would be sent to correct a failure mode.

(2) The UVS heater and bay 5 heater will be interchanged, one for one. The original design philosophy of mutually exclusive instruments and heaters can now be accomplished; i.e., the UVS and UVS heater cannot both be off during playback and the data storage subsystem and bay 5 heater cannot both be on during playback.

(3) The original intent of the DC-50 power relay was twofold. One was to provide two levels of TC power to the platform (solar panel level and battery level controlled by DC-50), and the other was to provide battery test capability. Because of the blanket louver assembly, two TC power levels are no longer required. Platform heater 1, IRS 1 and TV-narrow heaters will be connected to the dc bus. Platform heater 1 is presently located in the UVS. It will be relocated experimentally during the second series of platform TC tests. An alternate location for this heater is on the platform structure. Test results indicated that the wide angle TV temperatures were sufficiently high without the use of the dc heater. This heater will be deleted. To provide test capability of the battery, a test load will be switched on and off by DC-50.

d. Mission operations. Because of the late manning of the SSAC area during the *Mariner* Mars 1969 mission the need for science representation in the SPAC area has been reviewed. In the past the SPAC team included a science liaison representative who provided the communications link between the SPAC and SSAC teams. Since present planning calls for the manning of the SSAC area in May 1969, the SPAC organization has been changed to include a data automation subsystem analyst in addition to the science liaison representative. The DAS analyst will be responsible for monitoring the engineering and real time science telemetry and providing information on the performance of the DAS as a functioning subsystem of the spacecraft. This additional analyst will be particularly necessary during system test and prelaunch operations when SPAC is monitoring both engineering and real time science telemetry.

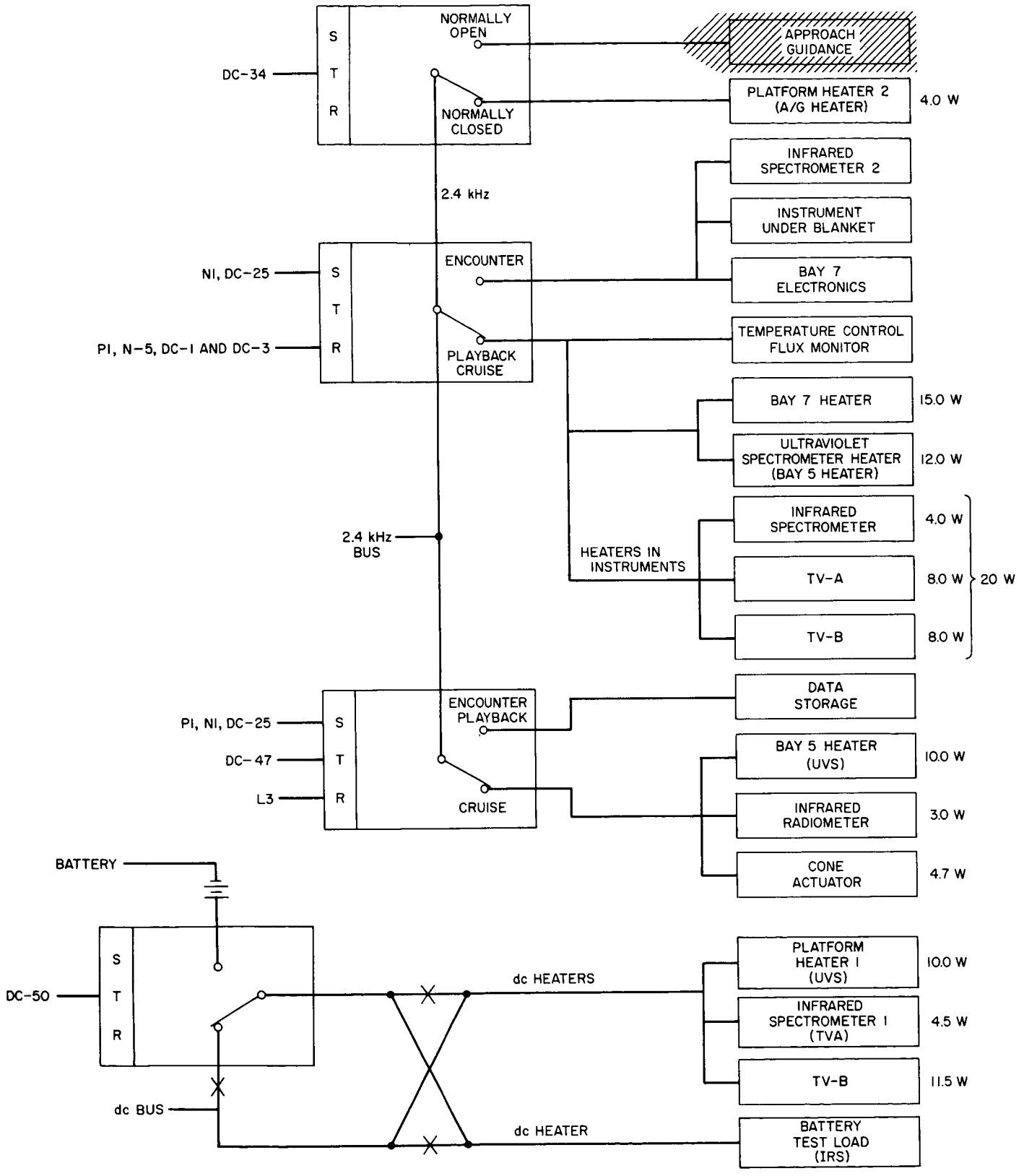

Fig. 1. Heater circuitry changes to present TC design

C. Systems

1. Trajectory Design

The PEGASIS computer program (SPS 37-47, Vol. I, p. 26) has been checked out, and production runs have been submitted for generation of an encounter science scan data package. This data package is being prepared for transmittal to the experimenter teams by mid-January, 1968. The data package will present both graphic and tabular data for approximately ninety different fly-by cases. The ninety cases comprise fifteen different launch date/arrival date combinations, and six different aiming points per launch date/arrival date combination.

2. Near-Earth Mission Design

The *Mariner* Mars 1969 near-earth mission design effort is concerned with the phase of each flight between launch and initial control of the spacecraft by the mission operations system after DSN acquisition. The objectives of the near-earth mission design are to:

(1) Establish the final launch windows and launch period for the project.

(2) Establish mission launch-hold criteria.

(3) Establish tracking and data acquisition support requirements for the near-earth phase which will enable early and continuing evaluation of the status of the flight for the conduct of mission operations.

In order to achieve these objectives it is necessary to perform analyses of the capabilities of the elements of the project to utilize the desired launch windows, identify any resultant limitations to the windows, and make tradeoffs, as necessary, between these limitations and the project requirements in order to insure a high probability of launching both spacecraft. Near-earth mission design activities also require participation in the *Centaur/Mariner* performance and trajectory working group, the lunar and planetary projects tracking panel, telemetry and communications panel, the mission operations design team, and near-earth tracking and data system planning meetings.

Several milestones have occurred in the development of the near-earth mission design. One of these milestones was the publication of Preliminary Near-Earth Trajectory and Station View Characteristics. This document provides information concerning near-earth tracking data system coverage capabilities and limitations. This information is used in the development of the mission design and in identifying problem areas requiring further analysis. For example, launching very early in the launch period will result in a significant reduction in the coverage capabilities of the DSN. Thus, analyses are under way to determine the earliest launch date which will provide acceptable DSN coverage of the spacecraft.

Another milestone in the near-earth mission design which has been achieved was the submittal of the *Mariner* Mars 1969 flight plan approval request to the range safety officer of the AFETR. The proposed flight plan represents the best compromise between meeting range safety criteria and providing acceptable launch windows for the project. The plan was developed as a consequence of several working meetings between the project and range safety personnel. Approval of the flight plan was conditional upon two points:

(1) That most southerly 3 σ right impact point locus does not violate the Bahama Island and Leeward Island destruct lines.

(2) That certain additional impact locus and *Centaur* malfunction probability data be provided for evaluation and approval.

Item (1) will be met by restricting the maximum *Centaur* yaw index to the region of 29, and the data requested in item (2) were shipped to the range authorities in December 1967.

3. *Mariner* Mars 1969 System Test Complex Data System

As reported in SPS 37-47, Vol. I, p. 43, the STCDS is a computer-based data acquisition and processing system primarily intended to support system-level testing of the proof test model and flight-model *Mariner* Mars 1969 spacecraft.

During this reporting period, the STCDS Policy and Management Document, which describes a general management plan for the development of the STCDS and its operation in support of science subsystem tests and spacecraft system tests, was released. A procurement specification was completed for the low-speed analog modules which are intended to scan analog voltages, digitize the values, and transmit them to the controller module for computer entry. The high-speed analog module used in the *Mariner* Venus 67 STCDS will be incorporated in the *Mariner* Mars 1969 STCDS and used to support all autopilot tests. Only one such module will be used for test support at all the system test complex locations. The

high-rate controller module which, like the analog modules, is also a part of the data input subsystem, was delivered and accepted. This module provides for entry, via the CDC 3300 computer channel interface, of the block-coded 86.4 k bits/s telemetry from the flight telemetry system OSE, as well as the 113.4 k bits/s digitized analog video data originating in the science OSE.

In the early part of the reporting period, the capability was demonstrated to acquire and provide standard processing, recording, and display for the 66⅔ bits/s real-time science DAS hardline telemetry data stream.

Timing studies on the CDC 3300 processing of the 16.2 k bits/s DAS hardline data stream indicated that about 46% of the total available computer time was required to accomplish anomaly detection on each data word, and the necessary time tagging, decommutation, and identification functions, and, additionally, that about 26% of the computer time was needed for data formatting. This 72% loading factor combined with a 56% timing requirement for the software system executive function and data moving loaded the computer to about 130% of capacity, thus preventing real-time operation of the program. The video decommutation and some special processing functions are, therefore, presently limited to nonreal time operation, using input data reproduced from the digital log tape of the actual test as the data source for processing.

Improvements have been made in the software efficiency of the executive and data moving functions; however, these improvements are still insufficient to permit accomplishment of all the special processing functions and message formatting requirements in real time. There are at least three alternatives being considered for accomplishing further reduction in the usage of processing time, as follows:

(1) Eliminate the anomaly test prior to decommutation, 9%.

(2) Utilize simplified UVS processing, similar to the IRS processor, 11%.

(3) Provide an external hardware module to time tag the high-rate data prior to computer entry, 18%.

Total potential savings are 38%. Utilization of the first two solutions may be sufficient. Actual timing studies on software system operation are being conducted, and will continue.

4. *Mariner* Mars 1969 DAS Automatic Functional Checkout System

The DAS checkout system employs a general-purpose digital computer for performing real-time simulations of the spacecraft experiments in addition to providing flight-type commands. The system contains three major subsystems: the test unit, data channel and PDP-7 data processor (Fig. 2).

The test unit contains equipment which simulates, by computer control, the spacecraft TV, IRR, IRS and UVS science instrument data output bit streams, feeds the simulated data to the DAS, and waits for responses. Interface circuitry, event registers and decode networks are contained within the test unit for conditioning, recording, and transferring the DAS responses to the general-purpose computer. The computer selected for data simulation and on-line data processing of test data is a Digital Equipment Corporation PDP-7 data processor, containing 16 k words of core memory.

The high density of information and relatively short word length (18 bits) of the computer requires recording test data in an information format containing two 18-bit words each time the DAS responds to test inputs. For this reason, the data channel subsystem was designed to control and receive test data from the test unit and place it directly into a 6000-word block of core memory located within the computer. Therefore, the normal input/output function of recording test data using the accumulator is eliminated, and the accumulator can focus its efforts on issuing commands and test data.

The PDP-7 data processor controls the signal patterns of the science instruments which are sent to the DAS, and, based on the simulations, determines the expected DAS data output for comparison against the observed data output. The computer system monitors the DAS event signals to see whether they occur at the proper time. If an event fails to occur, or occurs outside the acceptable time range, or if an unexpected event occurs, an error message is printed. The parameters used in the simulation algorithms can be easily changed.

The functional design was established in August 1967, and in September the detailed logic design was completed to a point where fabrication had started. Over 800 control gates, 400 flip-flop circuits, and 90 DAS interface circuits for signal conditioning between the DAS and the test system were used. Four hundred Computer Control Company 1- and 5-MHz cards were utilized in the construction of the system.

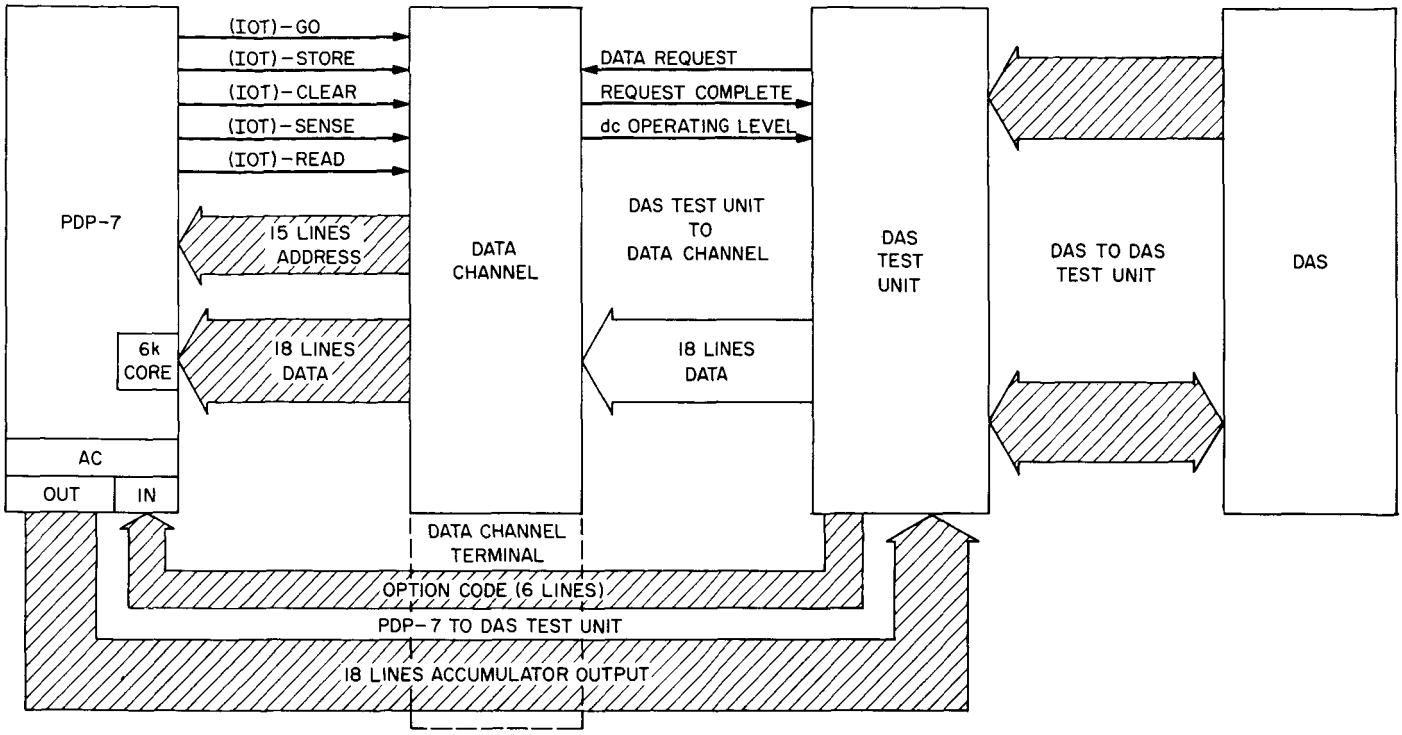

Fig. 2. Block diagram of DAS PDP-7 test unit

During this reporting period the three major subsystems (data channel, PDP-7 data processor, and test unit) were tied together and an end-to-end system checkout was started. System documentation (circuit diagrams, wire lists, and cable lists) was developed to serve as hardware instructions and trouble-shooting aids. Detailed software information was also provided as an operator guide in understanding the functional requirements of the system.

5. Mission-Dependent Data Processing System Design

During this reporting period a study was conducted of a number of design recommendations in the areas of tracking, telemetry, and command data processing, which was intended to simplify the configuration of the mission operations system and to reduce the costs of development and operation. The study considered the following major simplifications or reduction of capability in the mission dependent areas of the existing MOS design. (The DSN/NASCOM hardware elements of the original data processing system design for telemetry and command are shown for information purposes in Figs. 3 and 4.)

(1) No use of the high-speed data transmission capability between the TCP located in the DSIF, and the 7044 processor in the SFOF.

(2) No use of the SFOF 7044 processor for any telemetry data processing. Accomplishment of the real time MOS telemetry processing previously planned for the SFOF 7044 by analysis of the TTY data, supplemented by use of the STCDS described previously in SPS 37-47, Vol. I, pp. 43–47. The STCDS is a data processing system (based on CDC 3300 computers) which is used to support spacecraft system tests and science subsystem tests at the JPL spacecraft assembly facility, environmental test laboratory, and launch complex facility at AFETR.

(3) No use of the 7044 for command transmission and verification purposes, and removal of all command handling and verification functions from the TCP. All communications processors for command data transmission to be bypassed by TTY command lines.

(4) Use of the 7094 processor in SFOF in a stand alone configuration only for the operation of selected SPAC programs. In the stand-alone configuration, no connection is established between the 7094 and 7044 computers, and thus no capability exists to control from the SPAA the 7094 program being executed.

(5) Minimized number and simplified capability of the 7094 SPAC programs.

(6) Minimized development of new FPAC program capability and freeze, i.e., place under immediate change control, most of the FPAC programs in their existing configuration.

(7) Reduced programming effort for data simulation to only that required for program checkout and the provision of "canned" or constant-value data for operational training purposes.

The previously planned capabilities of the data processing system were reviewed in detail. The functions which had been requested in existing functional requirements documents, RFPs, and memoranda for performance in the TCP and 7044 were reviewed, and each function was assigned a priority category of mandatory, highly desirable, desirable, or least desirable. Detailed reviews of the requirements for 7094 FPAC and SPAC programs were also conducted. The guidelines also specified delaying development of the SSAC nonreal time 7094 programs until FY69; and, consequently, the detailed review of these program requirements has been postponed pending completion of RFPs and decisions by the project management on the details of encounter science data handling. The latter function includes the production of science master data records and experimenter data records.

As a consequence of the reviews, the original data system design was modified as follows:

(1) High speed data transmission from the DSIF to SFOF was reinstated as the prime means for transmitting telemetry to the SFOF. This transmission will not be interrupted by a failure in the NASCOM teletype telemetry transmission circuits, communications processors, or in the telemetry processing function in the TCP which produces teletype formatted output. Note that the high-speed data do not pass through any communications processors. A list of the TCP processing functions is contained in Table 2.

(2) The use of the 7044 as a telemetry processor was continued, primarily because of the need to maintain near-continuous automatic alarm monitoring capability during the long cruise-phase operation of a two-spacecraft mission. Although this capability might be accommodated in the DSIF TCPs, such an arrangement poses logistic problems with respect to transmission, modification, and verification of the limits to be used during operations. Since the DSN planned to continue the use of the 7044 for recording teletype tracking data on magnetic tape or disk file (in 7044/7094 shared mode), for transmission of tracking data predictions, and for monitoring purposes,

Table 2. Data processing functions of the DSIF TCP

Item	Function	Description
1	Bit synchronization	Determines timing of A/DC samples and bit decision timing on demodulator output.
2	Bit detection	Integrates demodulator output samples over bit time interval and makes bit identification decision.
3	Frame synchronization	Searches for and recognizes pseudo-noise codes defining start of engineering or science data frames.
4	Decommutation	Separates and identifies science and engineering data words within a frame.
5	TTY formatting	Formats and encodes decommutated data for TTY transmission.
6	HSDL formatting	Formats raw data bits into ADSS blocks for high-speed data line transmission, including SNR parameters. Provides separate data blocks for ground receiver AGC/SPE data.
7	Data recording	Produces a digital log tape of received data, SNR base parameters, ground data acquisition system status, bit sync status, time, identifiers, and AGC/SPE.
8	Operator messages	Provides TCP system status to operator, allows program control inputs by operator.
9	SNR base parameters	Calculates demodulator analog signal output sample sums and sum of squares for SNR calculations at SFOF.
10	Ground data acquisition system status	Provides ground receiver lock and demodulator lock status to TTY and HSDL formatter, AGC and SPE data to HSDL formatter.
11	Bit sync status	Provides loop-lock status of demodulator bit sync loop to HSDL output.
12	Status to DSS operators	Provides spacecraft telemetry data to DSS operators. Spacecraft AGC, SPE, command lock, events, and VCO offset.
13	Status to DSN monitor	Provides operational mode, configuration, and sync status, tape recording status, ADSS block status, to DSIF digital instrumentation subsystem.
14	Data playback	Reads digital log tape, retransmits data via HSDL to SFOF.
15	Test mode	Receives canned data via demodulator interface, calculates performance statistics.

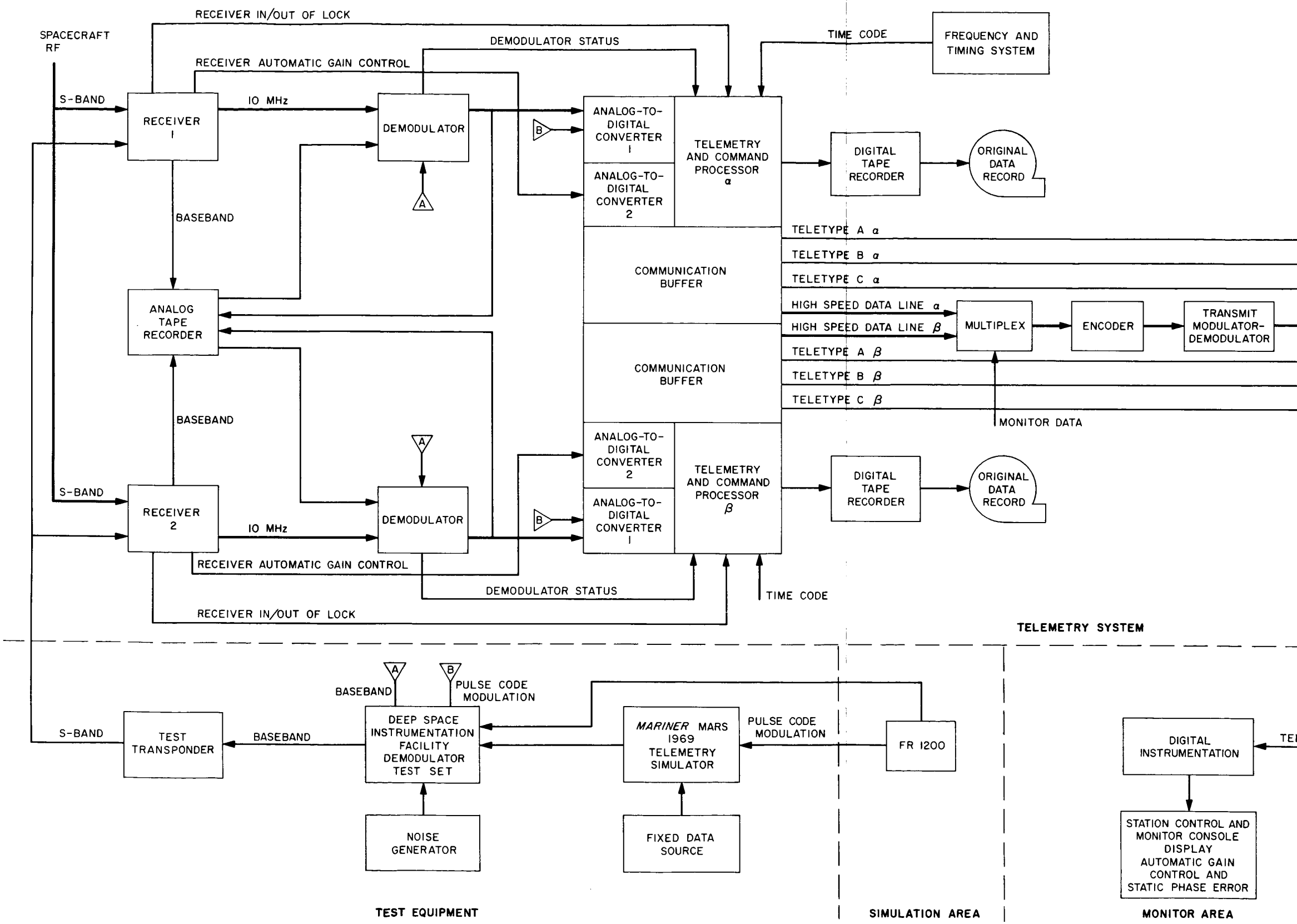
RECEIVER IN/OUT OF LOCK
SPACECRAFT RF
DEMODULATOR STATUS
TIME CODE
FREQUENCY AND TIMING SYSTEM
RECEIVER AUTOMATIC GAIN CONTROL
S-BAND
RECEIVER 1
10 MHz
DEMODULATOR
ANALOG-TO-DIGITAL CONVERTER 1
ANALOG-TO-DIGITAL CONVERTER 2
TELEMETRY AND COMMAND PROCESSOR α
DIGITAL TAPE RECORDER
ORIGINAL DATA RECORD
BASEBAND
TELETYPE A α
TELETYPE B α
TELETYPE C α
COMMUNICATION BUFFER
HIGH SPEED DATA LINE α
HIGH SPEED DATA LINE β
MULTIPLEX
ENCODER
TRANSMIT MODULATOR-DEMODULATOR
ANALOG TAPE RECORDER
TELETYPE A β
TELETYPE B β
TELETYPE C β
COMMUNICATION BUFFER
MONITOR DATA
BASEBAND
ANALOG-TO-DIGITAL CONVERTER 2
ANALOG-TO-DIGITAL CONVERTER 1
TELEMETRY AND COMMAND PROCESSOR β
DIGITAL TAPE RECORDER
ORIGINAL DATA RECORD
S-BAND
RECEIVER 2
10 MHz
DEMODULATOR
RECEIVER AUTOMATIC GAIN CONTROL
DEMODULATOR STATUS
TIME CODE
RECEIVER IN/OUT OF LOCK
TELEMETRY SYSTEM
BASEBAND
PULSE CODE MODULATION
S-BAND
TEST TRANSPONDER
BASEBAND
DEEP SPACE INSTRUMENTATION FACILITY DEMODULATOR TEST SET
MARINER MARS 1969 TELEMETRY SIMULATOR
PULSE CODE MODULATION
FR 1200
DIGITAL INSTRUMENTATION
STATION CONTROL AND MONITOR CONSOLE DISPLAY AUTOMATIC GAIN CONTROL AND STATIC PHASE ERROR
NOISE GENERATOR
FIXED DATA SOURCE
TEST EQUIPMENT
SIMULATION AREA
MONITOR AREA

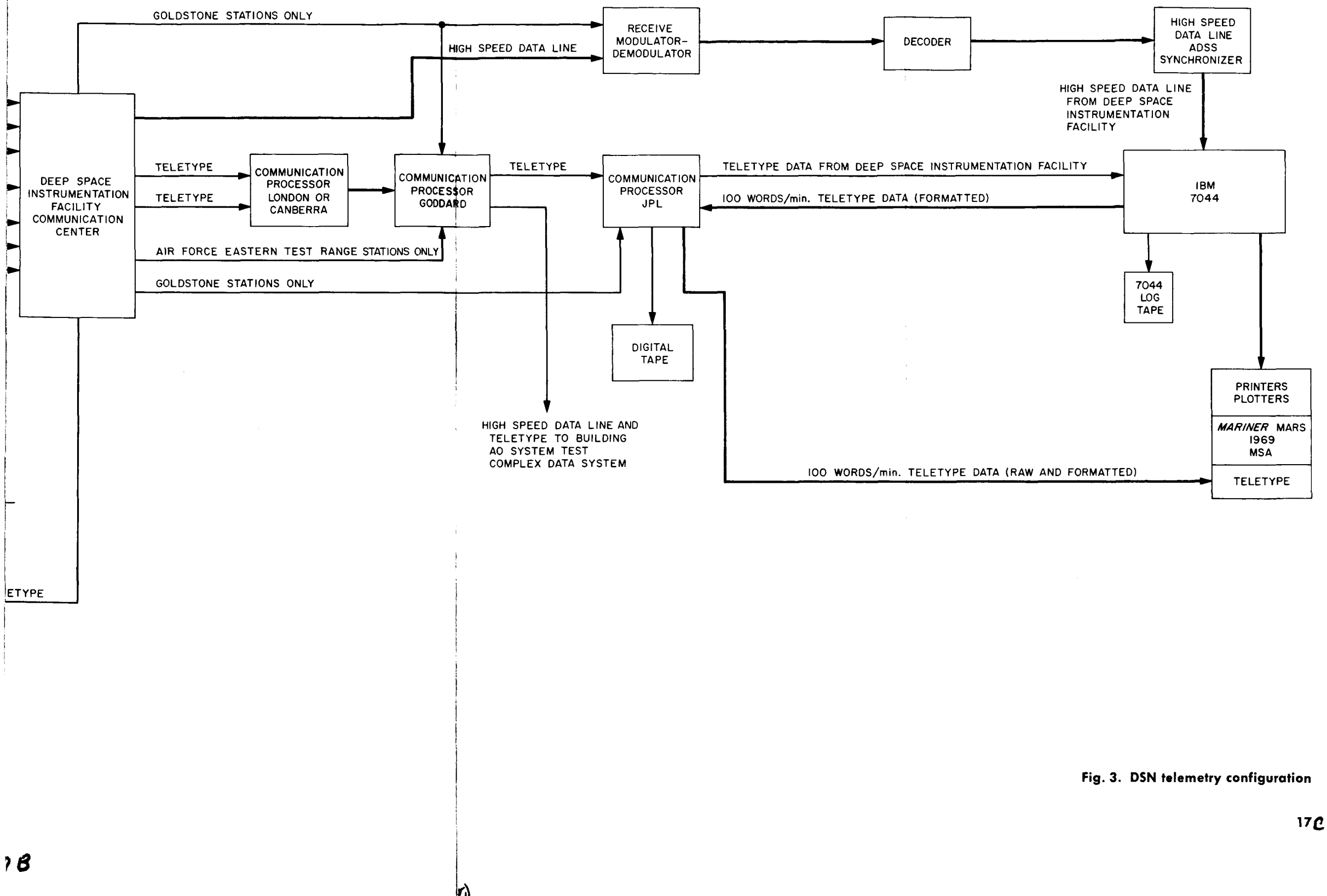

Fig. 3. DSN telemetry configuration

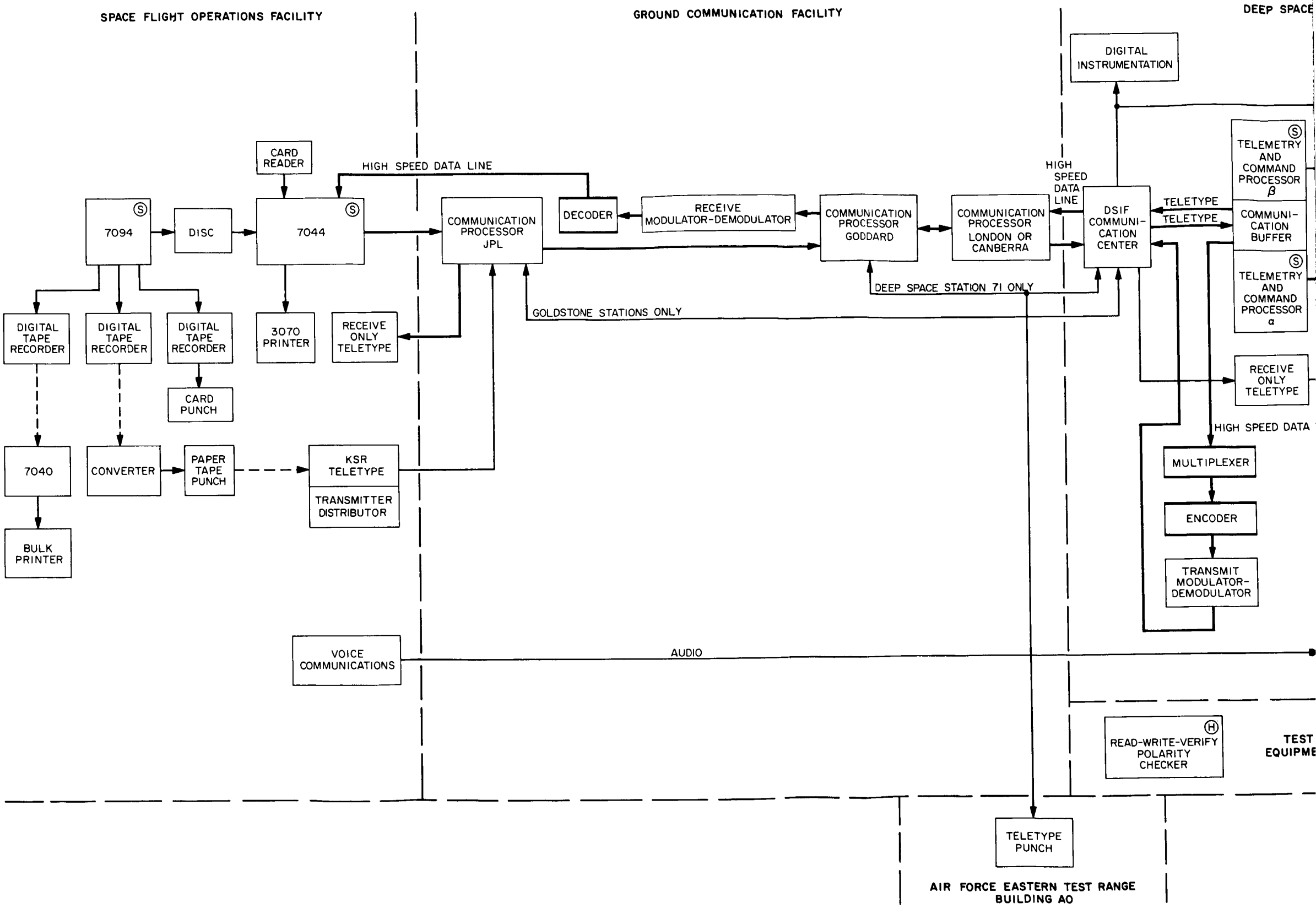

Fig. 4. DSN command configuration

INSTRUMENTATION FACILITY

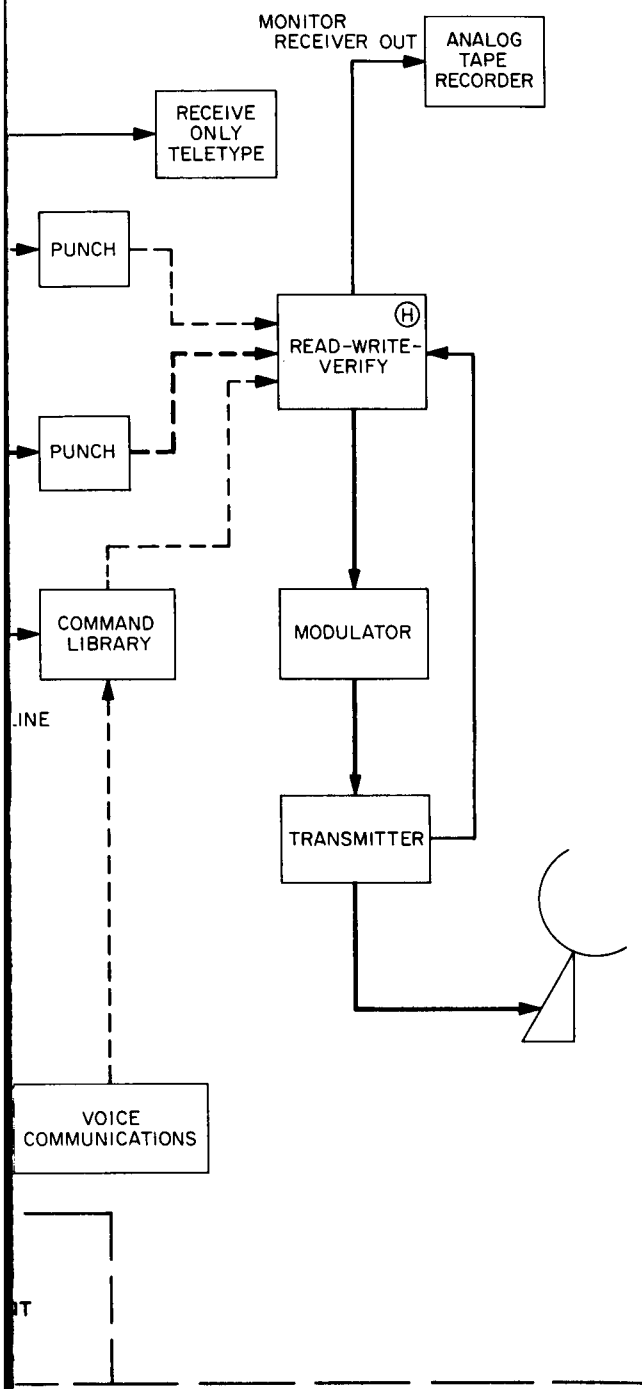

including tracking pseudoresidual plotting, the telemetry alarm monitoring function did not require significant additional hardware or operations costs.

Once the 7044 mission-dependent function of telemetry decommutation is performed, which is a prerequisite to alarm monitoring, certain processing and display capabilities of the DSN 7044 mission independent processor can be utilized at low cost by modification of portions of the *Mariner* Venus 67 mission-dependent engineering data processor. Such usage is possible because of the similarity to *Mariner* Mars 1969 data rates, telemetry frame size, and formats. The additional processing functions and capabilities which become available are included in Table 3 and detailed in the block diagram, Fig. 5. Figure 5 also indicates a phased development plan for the 7044 mission-dependent processor, which results in minimum development costs for the engineering processor in FY-68, and delays work on the more unique (relative to *Mariner* Venus 67) science processor until FY-69.

An important secondary requirement of the 7044 processor is the preparation of telemetry-frame-synchronized log tapes for use by offline processors. Engineering quick-look processing is simplified by use of such a tape, and a 7094 program called RECORDS is planned which will accept these tapes as input and will provide tabular lists and S-C 4020 plot tapes as an output. The frame formatted tapes will also provide the means for video data transmission to the JPL IPL and may be part of the MDR for the TV science data.

Note that there is no project requirement for an engineering MDR in an archival sense, except during critical mission phases or spacecraft failure modes. Gaps or deficiencies in the MDR data will be filled in by retransmission of the TCP log tape ODR from the DSIF, or by processing the ODR after its receipt at JPL.

The guideline proposing use of the STC data system (STCDS CDC 3300 computer system) for processing of engineering telemetry data was not applicable following acceptance of the 7044 telemetry processing function. Furthermore, use of the STCDS in the MOS poses operational and logistic problems not present if the SFOF 7094 is used.

One 7044 computer and its associated mission independent software system can accommodate the telemetry data streams from two missions by use of two mission dependent processors operating in one mission independent system, thus permitting the processing of data from both *Mariner* Mars 1969 spacecraft simultaneously. Overlap data, i.e., data from one spacecraft sent from two stations simultaneously can be recorded by the 7044 mission-independent processor, but only one combined engineering/science data stream can be processed in real

Table 3. Data processing functions of the SFOF 7044 mission-dependent processor (excludes tracking data processing, NASCOM functions, and DSN monitoring)

Item	Function	Description
1	HSDL input processor	Receives ADSS data blocks, extracts data and time tag, routes to correct processor.
2	Frame synchronization	Searches for and recognizes PN codes defining start of engineering or science data frames.
3	Decommutation	Separates and identifies science and engineering data words within a frame.
4	Raw data dump	Provides a raw binary science data dump to verify correct receipt of science data (during early TCP-7044 tests).
5	Alarm monitoring	Checks input data samples for violation of upper or lower limit values.
6	Data suppression	Provides output data only when sample value has changed by more than prescribed tolerance.
7	Data history	Stores total frame of latest available engineering data for demand printout.
8	Output processor	Provides interface between mission dependent processors and the mission-independent line print, TTY print, and plotting capabilities of the 7044.
9	Data recording	Provides frame synchronized digital tape of received engineering and science data. Master (tape) data record.
10	SNR calculation	Receives SNR parameters from TCP, calculates SNR periodically.
11	Acquisition system status	Receives and processes ground receiver status data received from TCP.
12	Operator messages	Provides for processing input messages for program control, and alarm and data suppression limits and tolerances.
13	Status to DSN monitor	Provides information on mission dependent processor operation to DSN monitor.

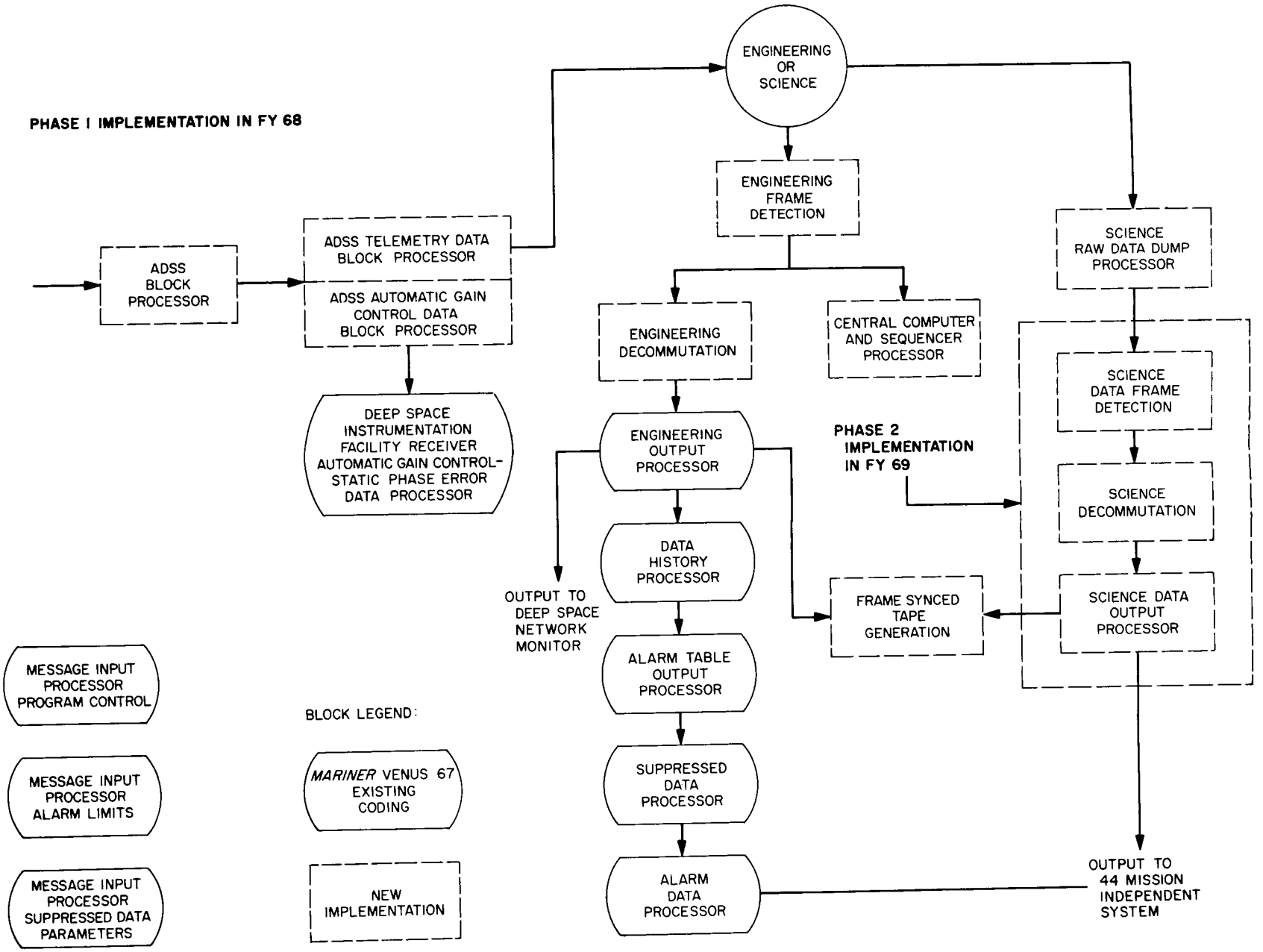

Fig. 5. 7044 mission dependent program

time. It would be possible to process engineering telemetry received from one station and science telemetry from another, from the same spacecraft source.

(3) The configuration for transmission of coded commands will consist of perforated-tape TTY transmission equipment in the SPAA, with transmission to the DSIF by conventional TTY, except during encounter when the command TTY lines are to be hard-wired around all communications processors. A library of direct commands and quantitative commands will be maintained at each deep space station capable of commanding the spacecraft. The detailed plans for preparation and verification of command tapes prior to transmission have not been developed. Teletype commands will be received, printed, and punched at the DSIF RWV operator's position. Thus, no use will be made of the 7044-HSDL-TCP system for commands. The increased time required to prepare commands in the SFOF, transmit them to the DSIF, and verify the punched commands has been accepted by the project.

(4) The planned usage of the 7044 for alarm monitoring also permits the use of the available control capabilities of the 7044, including the use of the SPAA control console to communicate (in 7094/7044 shared mode) with the 7094 computer. This will allow control of 7094 SPAC programs, as well as the capability to change the 7044 alarm limits, select various print and plot formats, etc.

(5) A detailed review of the proposed SPAC programs was made, resulting in plans for development of the programs described in Table 4. The table indicates whether each program is a new development for *Mariner* Mars 1969, is a modification to a *Mariner* Venus 67 program, or is a *Mariner* Venus 67 carryover.

Table 4. List of 7094 SPAC programs

Description	Title of program	New	Mariner Venus 67		Function
			Modified	Existing	
CMDM	Command generation and validation a. Assembly b. Translation c. CC&S memory processor d. CC&S simulator e. OSE formatter f. Command formatter g. Comparator	x			Prepares CC&S programs, generates coded commands, records tape data necessary for punching CC&S OSE tapes to support system test, launch operations, and flight operations. Provides flight operations analysis, simulation of sequences, and modification of the CC&S memory.
RECM	Engineering records	x			Accepts frame synced 7044 log tape, produces tapes for offline listings by a 7040 computer, and for plots.
CP2M	Communications prediction		x		Computes predicted telecommunication channel performance from antenna pattern tape, system characteristics, and SAVE trajectory input, tape data.
CMPM	Communications measurement	x			Provides actual performance data for comparison with predictions (CP2M). Uses real time telemetry MDR tape from 7044 (spacecraft and DSIF system data), CP2M output tape, and predict data cards as input data. Outputs prints and plots.
AGCM	Automatic gain control calibration			x	Processes DSS data acquisition system prepass calibration data to produce look-up tables and plots.
SIPM	Star identification		x		Provides data on in-flight star sensor performance vs clock angle, listings of acquirable objects, etc., from known sensor characteristics and SAVE trajectory tape input.
ATRM	Attitude reference		x		Computes spacecraft attitude relative to sun, planets, or selected stars. Provides cone and clock angles of desired celestial object.
SOEM	Sequence-of-events generator	x			Generates time ordered sequences of events for two missions from card inputs. Provides sort capability by DSS, mission, or "report to or by." Outputs are prints, plots, or sequences sent to DSIF via TTY.

(6) The review of FPAC programs resulted in plans for development of the set of programs listed in Table 5, which also indicates whether the programs are new or have evolved from other projects. In the case of most of the FPAC programs, as well as for those SPAC programs for which some operational version exists, it was shown that it is impractical to "freeze" a program far in advance of its future use, with the intention of leaving it essentially unchanged, and with no cognizant engineering or programming support. Some continuing minimum amount of support of both types is required in order to maintain an understanding of the operational details and functions of the programs and be capable of maintaining the program in the face of hardware or software changes to the system in which it operates.

In almost all cases there are sufficient differences between missions, or sufficient advancement in the state-of-the-art of the technology which the program supports that it is unfeasible or undesirable to lock-up and use some old version of the program. In addition, many programs interface with other programs by interchange of data in some specific format, thus requiring program modifications when the format is changed.

(7) The recommendation for minimizing the project-funded simulation effort was adopted, thus reducing the effort planned for simulation of spacecraft performance, interaction between spacecraft subsystems under simulated failure conditions, etc. Emphasis is being placed on the use of the PTM spacecraft tests, either directly or by use of recorded test data, to provide data inputs to the MOS for operational tests and training purposes.

Plans are now being proposed to operate a DSIF compatible analog magnetic tape recorder in the SAF during system tests to permit continuous recording of the PCM engineering and science data, sync, and time. Selected portions of these data could then be entered at a later time into the data processing system for simulation purposes. At present, it does not appear that the wow and flutter compensation of the DSIF tape reproducers is sufficiently good to permit entry of the data recorded by FTS OSE (undemodulated subcarrier data) in SAF into the DSIF MMTS (SPS 37-46, Vol. III, pp. 175–243). There currently appears to be no way to enter system test data into the SFOF without incurring additional software development costs to provide digital input data in SFOF-compatible format.

Requests for programming have now been received for all FPAC programs, and for 5 of the 8 SPAC programs. The real time SSAC requirements appear in the RFPs for the TCP and 7044. Requests for programming reviews

Table 5. List of 7094 mission-dependent FPAC programs (excludes DSN predictions and tracking data processor programs)

Description	Title of program	New	Mariner Venus 67 (modified)	Function
ODGX	Orbit data generator		x	Prepares orbit data file from TDP master file using selection and editing criteria to correct or average the data.
ODPM	Single-precision orbit determination		x	Calculates orbit from ODG file using weighted least-squares method. Solves for orbital elements, physical constants, encounter statistical errors, etc.
MOPM	Midcourse maneuver operations		x	Calculates maneuver capabilities, maneuver values, and commands, subject to mission constraints. Optimizes maneuver.
PEGM	Planetary encounter geometry and science instrumentation sequence	x		Computes Mars-centered coordinates of instrument traces, event times such as limb or termination crossings, etc., using assumed approach asymptote and pointing directions.
ICGM	Injection condition generator	—[a]		Computes injection time, velocity, radius, coordinates, azimuth using launch time and a polynomial equation.
TRJM	Trajectory		x	Integrates equations of spacecraft motion from epoch to desired point. Input from ODP, ICG, or nominal values. Provides listings or trajectory SAVE tape output of position, velocity, and DSIF view.
FLYM	Flyby fine print		x	Calculates details of encounter geometry (angles, times, etc.) and timing of backup commands.

[a]This is a modified Surveyor program.

were conducted on the FPAC programs, command generation program, and the TCP and 7044 engineering telemetry processor (including science telemetry processor, phase 1). A detailed design review of the TCP software was also conducted during this report period.

D. Engineering Mechanics

1. Delamination of Solar Cell Back Contacts

The first production lot of *N* on *P* solar cells for *Mariner* Mars 1969 use subjected to the type-approval thermal cycle was found to exhibit cracking and delamination at the edges and corners of the back contacts on almost 50% of the cells. The test consisted of five cycles from +135 to −196°C at not less than 50°C/min (actually more than 200°C/min). Reducing the rate of temperature change and elevating the minimum temperature reduced the incidence and severity of delamination, but under conditions meeting mission requirements considerable delamination and cracking occurred.

The cells are constructed from silicon, with silver over titanium vacuum-deposited to form contacts, and coated with solder to facilitate attachment of connections. The front side has a network of thin contact strips; the back contact covers the entire surface except for a narrow border. It was the back contact which suffered delamination.

It was observed that solder coverage on the lot of cells tested was uneven and heavy near the edges. Studies were conducted on thermal expansion of the materials involved, stress-strain properties, solder composition anomalies, and mechanical properties of the silicon blanks.

The failure mechanism was found to be differential thermal expansion between the silicon cell and the solder-backed silver-titanium contact strips. Separation occurred in the silicon and was aggravated by thickness variations in the solder coating.

Conclusion of the studies was that the critical factor in preventing delamination under type-approval-level thermal cycling is the maintenance of a thin, uniform solder layer, a control operation within the capability of the solar-cell manufacturer.

E. Guidance and Control

1. Power Subsystem

The *Mariner* Mars power subsystem is entering the flight hardware fabrication stage, and documentation to support this phase is virtually complete. The type approval solar panel assembly is in progress, and the prototype units of the power conditioning equipment have been delivered, as have portions of the power subsystem test equipment. A temperature survey is in progress in thermal vacuum for the prototype power conditioning equipment units to establish temperature boundaries for the type approval and flight acceptance thermal vacuum tests.

a. Battery test load. In the previous design some of the spacecraft heaters could be switched from the dc power bus to the battery (SPS 37-47, Vol. I, p. 51). In this manner, the battery voltage regulation may be sampled under load near Mars to determine its capability to share the spacecraft load with the solar array, if required. Moreover, this load conditions the surface of the battery plates to enable the battery to respond to a sudden load with minimal terminal voltage decline. In the present configuration, these heater loads are supplied solely from the dc power bus, but an additional fused battery test load will be maintained on the spacecraft for this purpose.

b. Power conditioning equipment. A number of modifications have been made to the power conditioning electronics to limit noise generation and to increase noise rejection:

(1) *Noise suppression.* Spiking on the output of the booster regulator was caused by transistor switching with fast rise times, and to base drive imbalance that caused an imbalance of the duty cycle of the regulator. The spiking was reduced with despiking capacitors, and with matching SCR transistor gate currents to equalize duty cycles.

Increased stability was obtained for the 2.4-kHz inverter synchronization circuit with the elimination of spikes in the power stages by despiking capacitors.

Filtering. Noise suppression networks are located in the fail sense circuitry in the power control, and the relay circuits in the heater and dc power distribution and power distribution modules.

Transducer outputs are filtered to reduce noise.

Wire routes. Wiring routing and grounding networks in the power conditioning equipment have been modified to reduce noise pickup and generation.

(2) *Reduced noise susceptibility.* Line input filters are located in the inputs to the booster regulators, to the

2.4-kHz inverters, and to the single and three phase 400-cycle inverters.

The possibility of miscounting has been reduced in the three phase ring counter located in the 400-cycle three phase inverter. This was accomplished by increasing the time delay in the feed back loop, and by decreasing the susceptibility to noise of the integrated circuits by increasing their dc supply from 3.3 to 4.3 V.

F. Space Sciences

1. Data Automation System

The data automation system, described in SPS 37-47, Vol. I, pp. 71–77, was developed and is being built by Litton Systems, Inc. The prototype unit and bench check-out equipment were delivered in October. Both breadboard and prototype unit tests were conducted during this reporting period.

The DAS breadboard (which has the same electrical characteristics as other DASs) has been extensively tested and verified over a temperature range from $-25°$ to $+90°$C with voltage variations from -15 to $+40\%$ of nominal operating voltage. In addition, the DAS breadboard has been successfully integrated with all four science instrument breadboards or engineering models. Tests have also been successfully completed with the data storage subsystem breadboard and the narrow angle Mars gate-2 (NAMG-2) engineering prototype. The DAS breadboard is presently interfacing with the OSE and individual science instruments. Initial DAS/OSE/instrument tests have been completed except for the ultraviolet spectrometer.

The DAS prototype is presently undergoing voltage and temperature tests and has, to date, been verified as operating satisfactorily over $\pm 10\%$ voltage variations from $-25°$ to $+90°$C. All these tests were performed with the DAS prototype mounted on a special test fixture, as shown

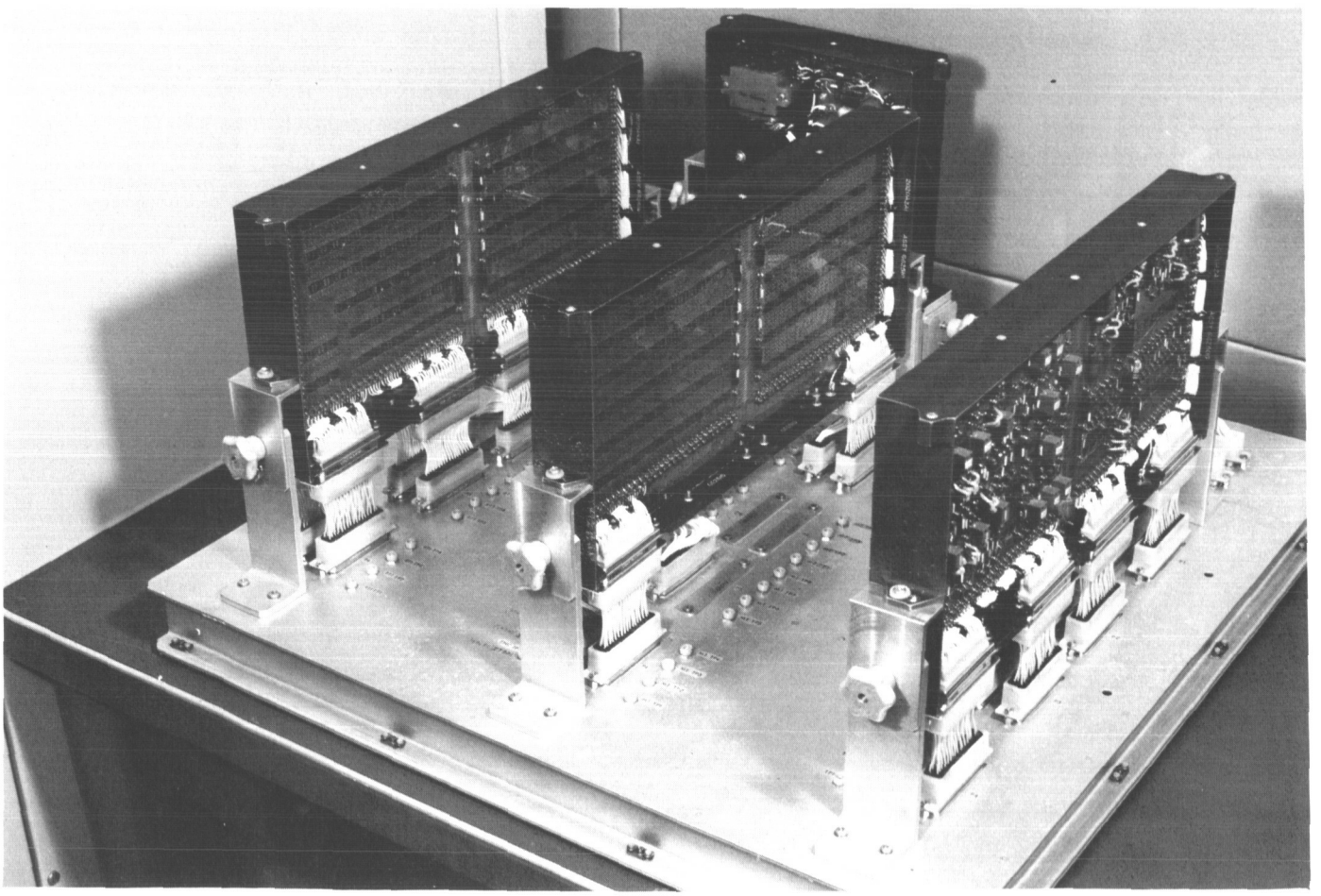

Fig. 6. Prototype DAS mounted in subsystem test fixture

in Fig. 6. Figure 7 shows the bench checkout equipment with the prototype. A test flight harness and case should be available shortly for use with the DAS prototype. A complete interface with a full complement of science instrument prototypes, the DAS prototype, and science OSE was conducted in December 1968.

Extensive testing with BCEs and interface tests with the various subsystems have verified the DAS logic design as functionally correct and compatible with the other subsystems. A change has been made in the DAS logic to accommodate a timing change in the Lyman alpha portion of the ultraviolet spectrometer spectrum.

Future testing of DASs will include further testing with the BCEs and automatic checkout of the DASs with a PDP-7 computer programmed to simulate all the subsystems with which the DAS interfaces. This checkout system is described above, in Subsection C,4.

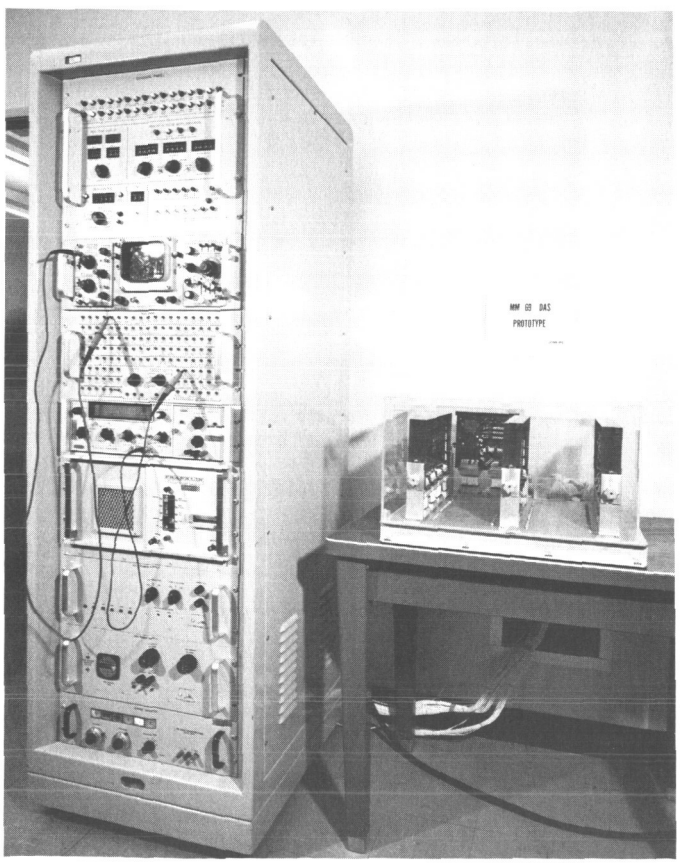

Fig. 7. Prototype DAS connected to bench checkout equipment

The DAS first article (SPS 37-47, Vol. I, p. 77) has been designated for life test. The test plan has been generated and is in the approval cycle. The plan requires the contractor to run the first article in a vacuum environment at 125°C. Electrical tests on all output functions will be performed on a daily basis. A final report with findings and conclusions will be published at the end of the test. The first article has completed a 250-*g* shock test with no electrical or mechanical damage.

The third BCE is complete, and preliminary checkout is under way. The BCE will be delivered to JPL for interface tests with the breadboard and prototype DAS upon completion of the appropriate calibration and acceptance test procedures.

The first BCE was the breadboard unit and does not include all of the required test capabilities. Number 1 BCE was returned to Litton Systems, Inc. to be reconfigured to the same mechanical and electrical configuration as BCEs 2 and 3.

2. Scan Platform Instrument Alignment Verification

The scientific instruments and planet sensors aboard the *Mariner* Mars 1969 spacecraft are mounted on a scan platform which can be rotated about two axes to point the instruments toward the planet during encounter. The instruments are: ultraviolet spectrometer; infrared radiometer; infrared spectrometer; wide angle TV camera; narrow angle TV camera. And the sensors: far encounter planet sensor; narrow angle Mars gate; wide angle Mars gate.

Their pointing directions (in a celestial coordinate system) depend on their relative positions on the platform, the position of the platform with respect to the *XYZ* reference coordinates of the spacecraft, and the attitude and position of the spacecraft in space.

A method has been developed to verify the angular relationships of the instruments relative to one another and to the reference plane of the scan platform without removing them from the platform. The procedure is known as "alignment verification." The necessary instrumentation is presently being designed and purchased to implement this method. The tests shall be performed at the JPL spacecraft assembly facility and at the Air Force Eastern Test Range. Misalignments shall be noted, allowing them to be corrected where required.

The instruments are initially positioned on the platform by assuming a reference pointing direction for the platform (that of TV camera B) and by mounting each instrument on the platform in such a manner that its respective pointing direction will bear the correct angular relationship to the reference. This involves: (1) an instrument alignment calibration, in which the pointing direction of each instrument is aligned to its reference mounting plane; and (2) a mechanical alignment in which the mounting plane of the instrument is aligned to the platform with alignment pins. Alignment verification is intended to detect errors and changes both in the instrument alignment and in the mechanical alignment.

The method developed uses an autocollimator supported in a transit base equipped with azimuth and elevation scales, and a reference reflecting surface attached to the scan platform. The collimator is positioned in front of the scan platform and used to stimulate the instruments. The angular position of the collimator can be accurately adjusted to bring its optical axis into alignment with the pointing direction of the instrument. If the beam from the collimator is assumed to be incident on the entrance aperture of the instrument, any ray of the beam will define an angle θ with a line parallel to the pointing direction of the instrument. The collimator is said to be in alignment when this angle is equal to zero. Alignment (or minimum θ) is detected by monitoring the output of the instrument.

G. Propulsion

1. Propulsion Subsystem

The *Mariner* Mars 1969 propulsion subsystem generally resembles that employed in the *Mariner IV* and *V* missions. It is a constant-thrust liquid-monopropellant rocket engine with associated tankage, tubing and valves. Jet vanes actuated through the spacecraft attitude control subsystem provide for thrust-vector-control attitude stabilization during the burning period. A dual-start (and -stop) capability provides for two trajectory correction maneuvers in the mission.

Principal subsystem components consist of a high-pressure gas reservoir, a pneumatic pressure regulator, a propellant tank and propellant bladder, and a rocket engine. The pressurizing gas is nitrogen; the monopropellant is anhydrous hydrazine. The engine contains a quantity of spontaneous catalyst to initiate and maintain the decomposition of the propellant. Two parallel sets of start and shutoff explosively-actuated valves in the nitrogen and fuel lines provide the two-maneuver capability. Welded and brazed tubing and fittings are used wherever possible to minimize leakage during the relatively long (maximum 250 days) storage period, as are metal seals, rather than elastomer seals, where welding and brazing are impossible. The subsystem is being manufactured under contract by TRW Systems, Inc.

a. Status and progress. During this report period the DTM was delivered to JPL. The model is presently being used in a series of vibration tests to determine the dynamic response characteristics of the propulsion subsystem for various pressurization levels in the propellant tank. It was noted in previous programs that the level of pressurization in the propellant tank had an affect on the damping characteristics of the propellant. This phenomenon had a major affect on the amplification of the vibration levels in the propulsion structure.

All of the components for the proof test model were received at TRW Systems, Inc. The last components to be received were the squib-actuated valves and the pressure transducers. These items are now in the acceptance test cycle. The rocket engine, fabricated by TRW, was subjected to flight acceptance vibration and hot fire tests early in this report period. Assembly of the pressurization gas regulator was also completed. Acceptance testing of the regulator is now being conducted. Fabrication of the regulator was a difficult task, complicated by the loss of several assembly details during the time between the buildup of the *Mariner* Mars 1964 system and this present buildup. To expedite the proof test model schedule, assembly of the subsystem has been initiated in parallel with some of the component acceptance tests.

Reduction of the data from the prototype rocket engine tests was completed. The test and results are described in subsection 2 below.

2. Assembly and Test of Prequalification Engines

a. Introduction and summary. Two propulsion subsystem engines, conforming to the current *Mariner* Mars 1969 flight design except for certain minor details, were fabricated and subjected to a prequalification test program. This program was intended to verify the engine design prior to committing it to the formal contractor-conducted type-approval program.

Two engines were utilized. Engine 1 was briefly fired at JPL for calibration purposes then sent to the JPL Edwards Test Station for a series of firings in a vacuum environment. Engine 2 was similarly calibrated at JPL

then subjected to vibration and acceleration tests at the JPL environmental laboratory. These tests were followed by a postenvironmental firing and a high chamber pressure firing.

b. Engine description. The *Mariner* Mars propulsion subsystem engine utilizes a liquid monopropellant, anhydrous hydrazine. The engine construction is shown in Fig. 8. It consists of an orifice-filter assembly, a showerhead injector, a catalyst bed, and a *Mariner* C type nozzle assembly. A cavity in the face of the injector contains granulated Shell 405 catalyst (20 mesh), which is retained by 60-mesh screens. The chamber is packed with a homogeneous mixture of $\frac{1}{8} \times \frac{1}{8}$ in. cylindrical pellets consisting of 75% (by weight) Shell 405 catalyst and 25% (by weight) JPL type H-A-3 catalyst.

When hydrazine is injected into the Shell 405 catalyst, a spontaneous decomposition results. The nominal chamber pressure developed by the reaction is 189.0 psia, resulting in a vacuum thrust of about 50.0 lbf at a propellant flow rate of 0.220 lbm/s.

The engines were assembled in accordance with the flight design, except for some minor deviations primarily in fabrication methods. Particular care was taken to pack the catalyst materials as firmly as possible to prevent their breakdown during vibration.

c. Calibration firings. Engines 1 and 2 were test fired in JPL test cell "J" for 30 s duration each to determine their general performance at ambient conditions.

Thermocouples were attached to the engine to measure surface temperatures at the mounting flange, at the top and bottom of the chamber, and at the throat section. The chambers were insulated by a ½-in. layer of micro-quartz covered with aluminized tape. A 40-μm (nominal) screen-type filter and a 0.121-in. diameter orifice were installed in the injector inlet.

Table 6 outlines the test program. The test results are given in Table 7. Oscillographic records indicated acceptably smooth chamber pressures with satisfactory start and shut down transients.

d. Vacuum firings. Engine 1 was shipped to JPL's altitude test facility at Edwards Test Station for vacuum performance testing. Results of the six tests conducted, using the *Mariner C* thrust stand, are listed in Table 7. As anticipated, the measured specific impulse was approximately 2½% lower than the previous nonspontaneous design engine of the *Mariner* C type.

Table 6. Prequalification test program

Engine 1	Engine 2
Assembly	Assembly
Calibration firing	Calibration firing
Vacuum ignition	Sinusoidal vibration
Firings at Edwards Test Station	Random vibration
	Static acceleration
	Postenvironmental firing
	High chamber pressure firing

Table 7. Prequalification engine firing test results

Test	Engine	Duration, s	Chamber pressure P_c, psia	Flow rate $\dot{w}$, lbm/s	Specific impulse I_s, $\frac{\text{lbf-s}}{\text{lbm}}$	Roughness ΔP_c, psi peak-to-peak
Calibration	2	30	182	0.207	—	5.6
Postenvironmental	2	100	180	0.203	—	12.0
Hi-pressure	2	200	242	0.271	—	8.4
Calibration	1	30	186	0.206	—	4.0
Vacuum 1	1	60	188	0.217	226.7	10.5
Vacuum 2	1	20	188	0.218	226.5	12.3
Vacuum 3	1	60	188	0.216	227.7	12.3
Vacuum 4	1	20	190	0.217	228.0	14.3

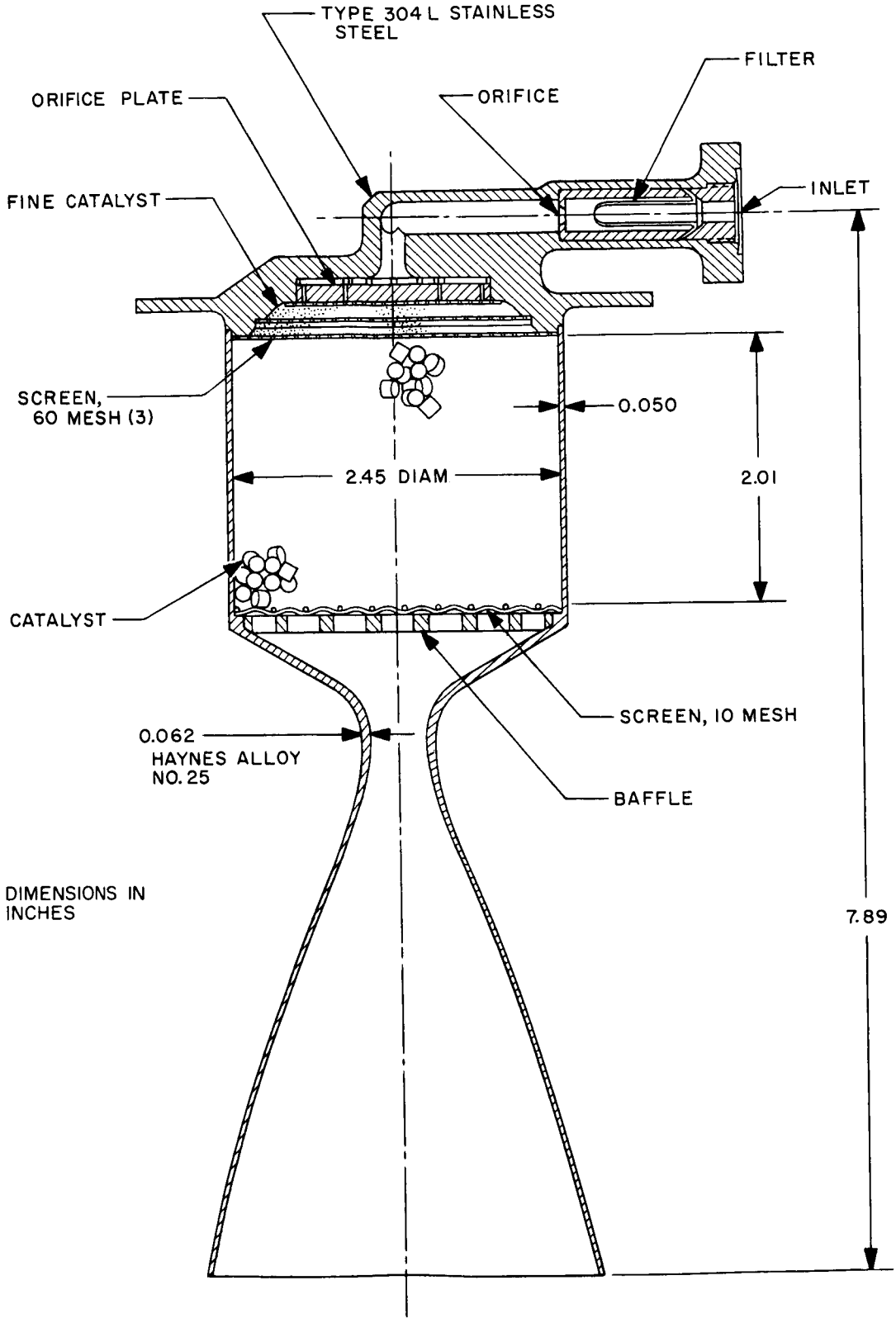

Fig. 8. *Mariner* Mars 1969 engine configuration

e. Environmental tests. Engine 2 was mounted into a test fixture and subjected to the following type-approval level environmental tests:

Sinusoidal vibration. Constant sweep rate of 1.0 octave/min from 5 to 2000 Hz and back to 5 Hz along three orthogonal axes.

Frequency, Hz	g's, rms
5–30	0.75
30–250	7.5
250–600	4.5
600–2000	13.5

Random vibration. The engine was subjected to a shaped spectrum of random Gaussian vibration for 60 s duration along each of three orthogonal axes. The shape was as follows: (1) flat power spectral density of 2.25 g^2/Hz from 50 to 150 Hz, decreasing linearly from 150 Hz to 0.065 g^2/Hz at 225 Hz; (2) flat from 225 to 750 Hz at 0.065 g^2/Hz. The wideband level was approximately 18.1 g rms.

Static acceleration. An acceleration of 9 g's was imposed at the engine center of gravity in both directions along an axis perpendicular to the engine centerline and also in each direction along two other orthogonal axes for a total of 6 tests. Duration of each test was 5 min.

f. Postenvironmental firing. Engine 2 was fired again in test cell "J" to determine any changes in performance caused by the environmental tests. Duration of the firing was 100 s. Engine performance appeared nominal, except for an increased roughness. The average peak-to-peak values in chamber pressure during the postenvironmental firing were ±12 psi, as compared to the ±5.6 psi obtained during the calibration firing. This roughness is still acceptable.

g. High chamber pressure firing. Engine 2 was fired at 1.25 times the nominal chamber pressure for a duration of 200 s. No adverse effects were noted. The peak-to-peak chamber pressure values averaged ±8.4 psi.

h. Results. These results indicate that the new engine design can pass forthcoming type-approval tests and will adequately perform the *Mariner* Mars 1969 mission. This design appears to be life-limited, however, since chamber pressure roughness values appear to increase after repeated operations. This limitation does not impose any restrictions upon its use in the relatively short burns required by the *Mariner* Mars 1969 mission (~100 s). Future tests will be required to accurately predict engine performance during nonstandard operating conditions.

3. Pyrotechnic Subsystem

The *Mariner* Mars 1969 pyrotechnic subsystem is involved in the performance of the following flight events:

(1) Spacecraft separation.

(2) Solar panel deployment and scan platform unlatching.

(3) Propulsion thrust initiation and termination.

(4) Infrared spectrometer cooldown and motor start.

Separation is effected through two mechanically redundant 2-squib release devices which are actuated by the launch vehicle firing unit. Solar panel deployment is accomplished by four 2-squib pinpullers. The scan platform is unlatched by a squib valve, the propulsion system contains eight squib valves (start and shutoff for nitrogen and fuel for two maneuvers), and the infrared spectrometer is started by two squib-valves. The squib-operated valves each contain one dual-bridgewire squib.

The squib-firing power storage and switching and command control are performed redundantly by two identical pyrotechnic control units, which also provide for prelaunch analytic testing and inflight diagnostic telemetry. Squib-firing energy is accumulated by charging capacitor banks. Simple redundancy is provided in the duplication of pyrotechnic control units and the use of either dual-bridgewire squibs or dual-squib pinpullers.

A simplified schematic of the subsystem is shown in Fig. 9, except for the spacecraft release devices. This shows the sources of command input and the outputs to the squibs, infrared spectrometer subsystem motor and flight telemetry subsystem. The pyrotechnic control unit is being developed and manufactured under contract by Electro-Optical Systems, Inc. The valve squibs are manufactured by Hi-Shear Corp.

a. Status and progress. During this period the two prototype pyrotechnic control units were utilized for the firing of live squibs. The pyrotechnic control units were at −20°C, the pinpuller squibs at −60°F, and the valve squibs at −100°F, simulating worst case conditions. The

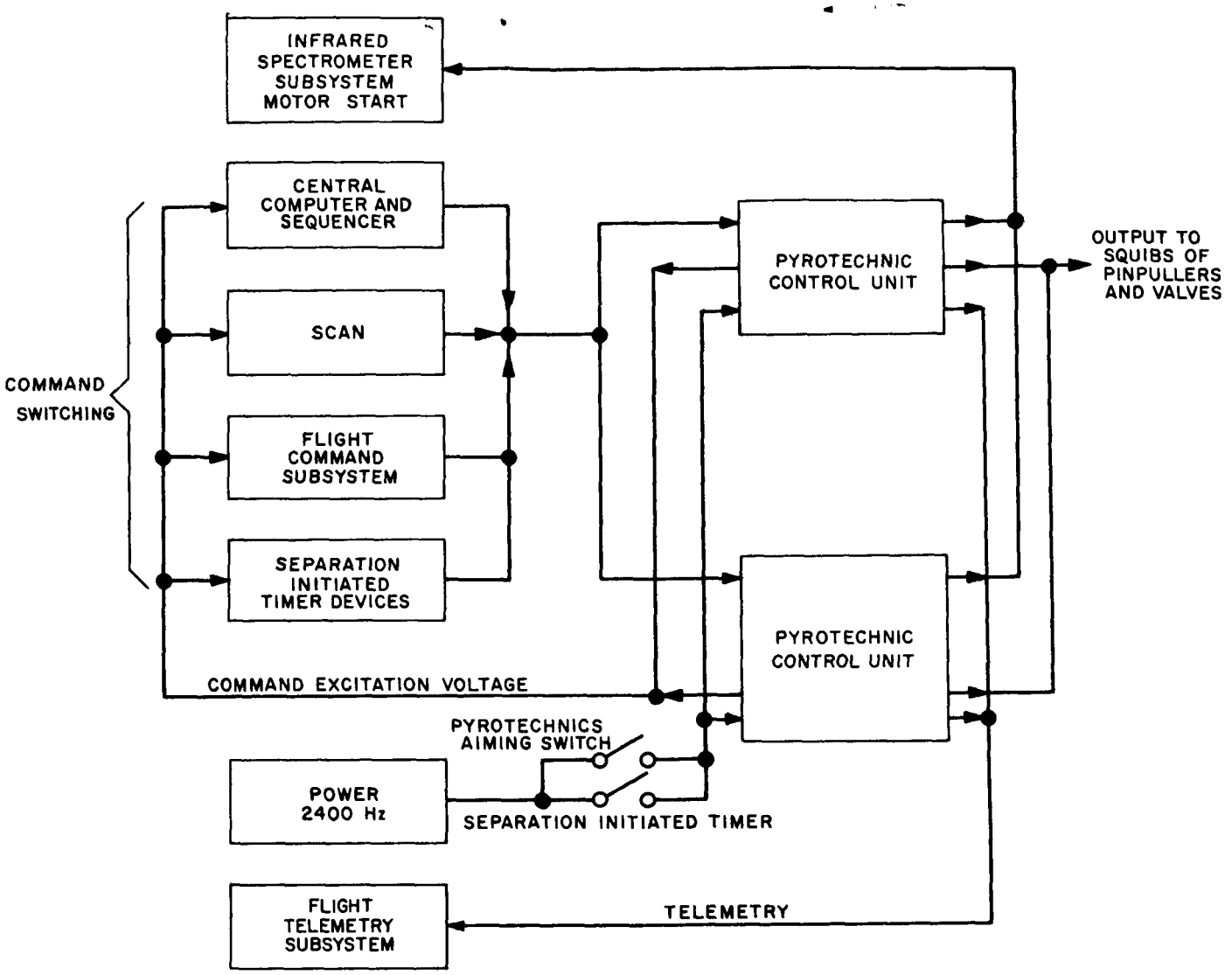

Fig. 9. Pyrotechnic control subsystem

energy to fire and time to ignition were nominal and indicated that an adequate margin existed for reliability purposes. No anomalies occurred.

Redesign and rework of the prototype units to modify the narrow angle Mars gate circuit were accomplished, and prepot functional tests were performed. One unit was subsequently vibrated as a subassembly at the type-approval test level. No visual damage occurred and functional testing of the unit is presently scheduled.

Fabrication and functional tests on the proof test model pyrotechnic control units has been accomplished and completion of type approval testing is anticipated to meet a February 22, 1968 delivery to the spacecraft assembly facility. This delivery date is subject to qualification of vibration fixtures, availability of a case with dummy mockups, environmental test facility scheduling and availability of detail test procedures.

The start of fabrication of the second lot of 71 valve squibs is imminent, pending direction to Hi-Shear Corp. of the pin header source. Only one of three possible sources now appears capable of supplying these parts.

Detail drawings of the V-band release device assembly and squib, and of the pinpuller squib have been released. Negotiations are in process for these procurements. The pinpuller detail drawings are approximately 70% complete and these procurements are yet to be placed. No special difficulties are envisioned.

IV. Surveyor Project

LUNAR PROGRAM

A. Introduction

The object of the *Surveyor* project was to soft land a series of spacecraft on the Moon to obtain information to support the Apollo manned lunar landing program. Seven missions were planned. The first mission with *Surveyor I* was carried out with complete success beginning with launch on the *Atlas-Centaur* booster on May 30, 1966. *Surveyor I* survived its first night on the moon and returned additional television pictures during its second lunar day. The second flight spacecraft, *Surveyor II*, was launched on September 20 and failed during the midcourse maneuver due to a probable vernier propulsion system malfunction. *Surveyor III* was launched on April 16 and successfully touched down on April 19, 1967. The spacecraft landed in a crater 1.6 mi from the planned target area. *Surveyor III* was responsive to commands throughout the lunar day, which ended May 3. Surface sampler operation was excellent throughout the mission.

Surveyor IV was launched on July 14, 1967. The spacecraft performed all in-flight functions without significant anomalies, and well within the predicted limits, until just prior to main retroengine burnout on July 16. All telemetry signals were abruptly lost when the spacecraft was 49,000 ft from the moon. Subsequent ground activities aimed at reestablishing RF contact were unsuccessful.

Surveyor V was launched on September 8 and successfully soft landed in a crater 18 mi from the planned target area on September 10, 1967. A total of 18,006 TV pictures was received before lunar sunset on September 24, and 93.5 h of lunar surface data were accumulated by the alpha-scattering experiment. The spacecraft was successfully revived on October 15.

Surveyor VI was launched on November 7, 1967, and soft landed approximately 4 mi from the planned landing site on November 10. A total of 30,037 TV pictures was received, and 19 h of alpha-scattering data were accumulated before shutdown on November 25. A successful translation of 8 ft was performed on November 17. Over 10,000 of the total pictures were taken from the post-translation position, providing valuable stereo views of surface objects.

B. Structures, Mechanisms and Spacecraft Integration

1. Engineering

a. Structures.

Dynamic analysis. The shipping container containing the alpha scattering sensor head and roll actuator for

SC-7 was dropped from a fork lift truck at Cape Kennedy and fell to the ground. An analytical simulation of this fall showed the maximum loads to be 7 g on the roll actuator and 15 g on the sensor head. These loads were below the 18-g fragility level of these units; and, therefore, it was considered that the units sustained no structural damage.

Surveyor V—postmission analysis. Prior to the first lunar night, the 0636 lock-landing gear command was transmitted five times to *Surveyor V*. On entering lunar night, legs 2 and 3 were observed to deflect, indicating a failure in the shock absorber locking system. Subsequently, both legs were observed to re-extend during the second lunar day and, at the onset of the second lunar night, leg 3 again deflected. The observed sequence of events and leg deflection are summarized in Table 1.

Table 1. *Surveyor V* leg deflections: sequence of events

Event	Leg deflections, deg			Shock absorber temperatures, °F		
	Leg 1	Leg 2	Leg 3	Shock 1	Shock 2	Shock 3
Touchdown	0.6	0.7	0.6			
Touchdown plus 11 days	0.8	0.6	0.6	127	−20	145
0636 lock gear commands						
1 sent				103	−55	107
4 sent				100	−58	100
First lunar night	0.9	4.2	6.5	−265	−265	−265
Second day: 0636 command sent 82 times	1.3	0.3	0.8	177	198	154
Second night	1.2	0.6	8.2	−124	−193	−175

Locking failure could occur in the lock mechanism itself or in the associated telemetry and electronic circuits. Possible mechanism failure modes are summarized in Table 2. Other than the possibility of premature firing, no failure mode listed is considered a plausible reason for failure. If premature firing occurred, the shear-out loads incurred at touchdown would be small relative to total shock absorber load levels and, because of their short duration, would not be detectable on the shock absorber strain gage time histories.

It is considered that the nondeflection of leg 2 in the second lunar night (following its deflection during the first lunar night) is attributed to the unit characteristics at low temperatures and is not an indication that leg 2 may have locked during the 0636 command transmissions during the second day. It is probable that leg 1 is also unlocked, but did not deflect because of the lower static shock absorber load (80 lb) compared with the 120-lb load in the shock absorber on downhill legs 2 and 3.

Table 2. Possible shock absorber locking mechanism failure modes

Mode	Comment
No pistons installed	National Water Lift data; AFETR visual inspection precludes this.
Premature firing	A possibility.
Mechanism failure:	
(1) Piston shears under static load.	During 12 flight unit tests, no shear load less than 292 lb occurred. Static load = 130 lb.
(2) Excessive squib output (housing rupture).	No housing damage visible on TV pictures. Tests of high output squibs into low volume yielded good performance.
(3) Low squib output (piston fails to penetrate).	Tests of 450-psi squib in 150% of maximum volume yielded good penetration. Flight squib is 500-psi type.
(4) Excessive interference between housing and piston.	Differential thermal expansion will not cause interference with worse manufacturing tolerances.
(5) Cold welding of piston to housing.	Stainless steel piston, aluminum housing is not favorable for cold welding.
(6) Piston breaks through diaphragm, or diaphragm not included.	Diaphragm installed per National Water Life Quality Control data. If diaphragm was not there, lock mechanism would still function (see item 3 above). Premature piston shearing against rack not possible.

Surveyor VI—postmission analysis. No anomalies occurred in the *Surveyor VI* landing gear during mission F. Initial assessment of the shock absorber strain gages after touchdown indicated a landing at approximately 12 ft/s vertical velocity on a slope of 2 to 3 deg. Shock absorber strain gages indicated touchdown velocities during the hopper experiment of approximately 13 ft/s vertical and 1.5 ft/s lateral. Table 3 shows the peak forces experienced by the shock absorbers during these two events. Computer studies are being performed to more accurately determine the landing conditions for these events.

Table 3. Peak shock absorber force, lb

Event	Leg 1	Leg 2	Leg 3
Initial touchdown	1560	1760	1410
Hopping maneuver	3000	1650	1670

The landing velocities attained during the hopping maneuver were higher than the velocities previous analysis had shown to be tolerable (*Bimonthly Progress Summary*, October 23, 1967). However, a hard landing surface was used to establish the allowable hopping velocities, whereas *Surveyor VI* actually encountered a soft surface. A subsequent analysis considering a 5-psi static bearing pressure has resulted in maximum solar and roll moments of 393 and 331 in.-lb, respectively in the top assembly of the ASPP for the touchdown velocities indicated above. These are well below the 500 in.-lb allowable for deflections in the elastic range.

Stress analysis. A stress analysis has been performed which demonstrates the structural integrity of the stereoscopic mirror installation on SC-7. Adequate margins of safety exist for the critical load conditions during launch, boost, transit, and landing. In addition, all items were investigated for the predicted thermal and fatigue environments and found to be satisfactory.

The stereo mirror will utilize an existing 9.5 by 3.5-in. mirror which was procured for *Surveyor IV*. It has a beryllium base which is nickel plated and aluminized, and has a protective coat of silicone monoxide. The mirror is polished to 12 wavelengths (4000 to 7000 Å) over its reflective surface. The finished mirror has an average specular reflectivity of greater than 80% (within 60 deg of normal) and an average diffuse reflectivity of less than 0.25% between 4000 and 7000 Å.

The mirror is mounted on the lower portion of the A/SPP mast by a two-piece clamp and adapter made of 7075-T6 aluminum. The mirror normal line is depressed 14 deg from horizontal and is 22 deg clockwise from the −Y-axis. The clamp segments are bonded to the mast to prevent movement. The bolts that connect the clamp segments are preloaded to a controlled value to prevent high stresses from developing in the mast tube wall.

The machined yoke-tube joint (Fig. 1) is the principal means of attaching the various substructure tubes to the basic spaceframe tubes. Standard stress analysis methods for predicting the strength of these yokes have produced allowable load values which are far below actual test

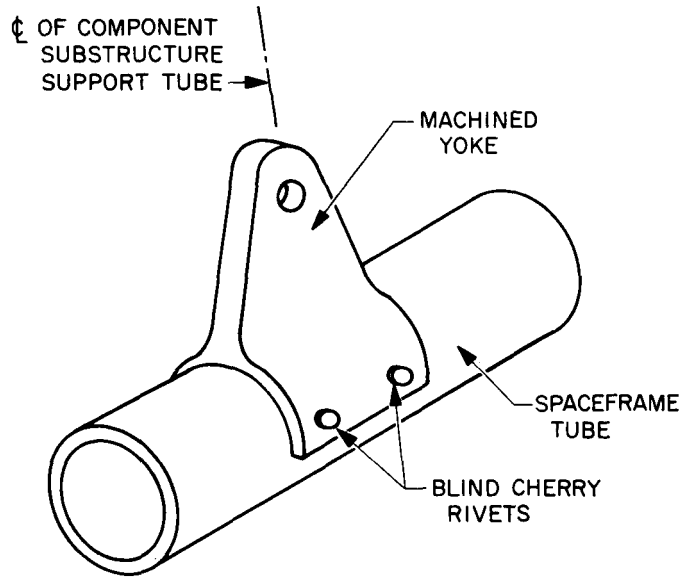

Fig. 1. Machined aluminum yoke mounted on spaceframe tube

values. It is necessary, therefore, from a design point of view, to be able to accurately predict the strength of various yoke designs.

To aid in arriving at an empirical means of computing the strength of these yokes, a test was performed, the purpose of which was to determine the direction and magnitude of the stresses at many points on the yoke. The photostress technique of experimental stress analysis lends itself perfectly to this application since it yields these results directly.

Although three different loading conditions were imposed upon the yoke, the case of a large vertical load is by far the most critical condition for the yoke. The yoke was coated with a birefringent plastic and attached to a fixed tube in the same manner as would be used on the spacecraft. As the vertical load was applied in increments, color photographs were taken through a polariscope to record the fringe patterns produced. The test setup, with specimen and polariscope, is shown in Fig. 2. These photographs (an example of which is shown in Fig. 3) can be superimposed to yield the directions and magnitudes of principal stresses. Typical results of this superposition are shown in Fig. 4. The lines shown are derived from the fringe lines and represent the trajectories of the principal stresses.

The results yield a series of figures such as that shown in Fig. 4. Each figure represents a different load level.

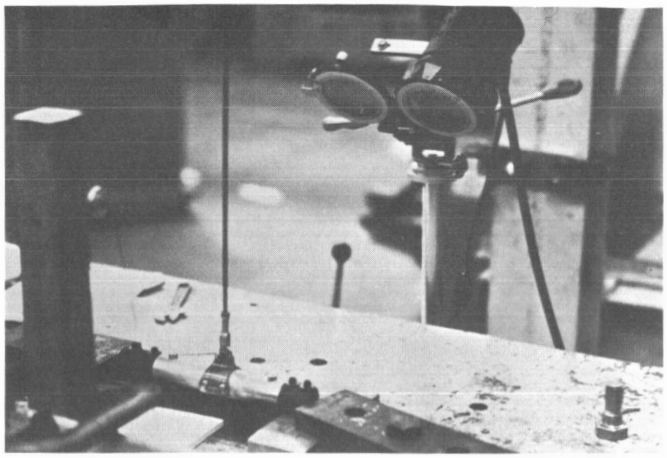

Fig. 2. Test setup

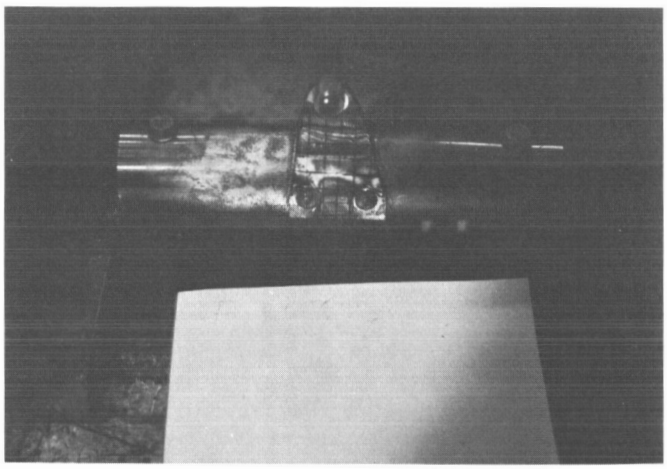

Fig. 3. Typical fringe pattern produced

The magnitudes of the principal stresses are obtained in an identical manner and check closely with results obtained in previous tests where the yokes were instrumented with strain gages.

b. Integration. Engineering has been generated, released, and implemented for the development and installation of eight additional mirrors on SC-7 in compliance with JPL action directive, change order 177. The objectives of the mirrors are as follows:

(1) Stereo mirror (1 required).

(a) To obtain stereoscopic photographs of a portion of the lunar surface within the SM/SS operational area. The coverage obtainable is approximately 17% of the SM/SS operational area.

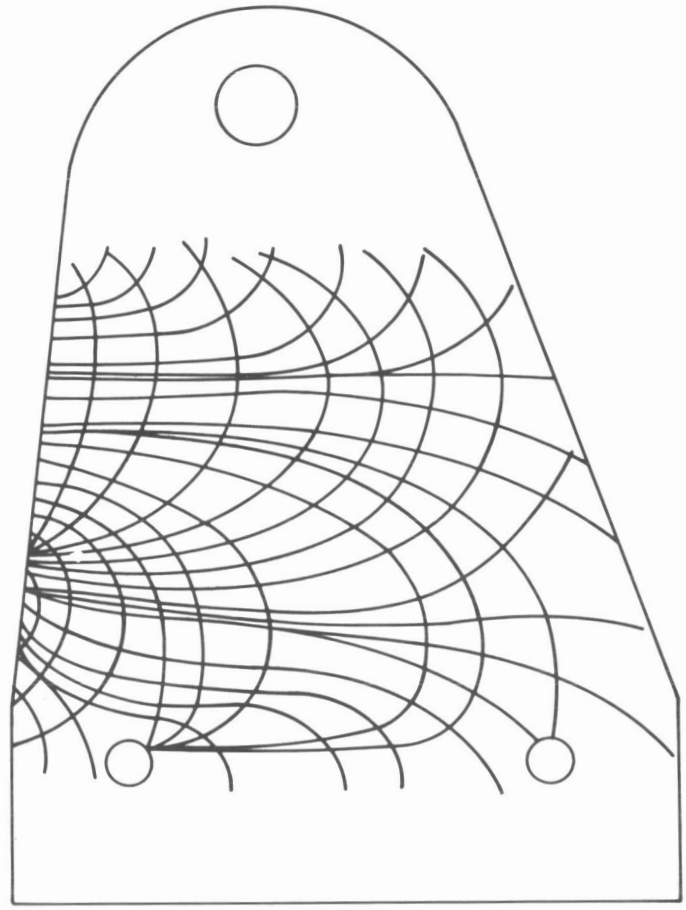

Fig. 4. Stress trajectories for vertical load of 1000 lb

(b) To provide imagery for photogrammetric study of a portion of the lunar surface near the spacecraft for the TV experiment.

(2) Particle viewing mirror.

(a) To study the adhesion of small particles flung up from the lunar surface.

(b) To determine the effect on adhesion of distance and height from the subvernier points.

Six mirrors, PN 3050959-1, are used for the objectives in item 1. The mirrors are aluminum alloy 2024-T4 material, with a ½-in. hexagonal surface, polished and coated with a protective coating of silicon monoxide (Fig. 5).

(c) To determine the effect on adhesion of different material surfaces.

(d) To differentiate between adhesion and erosion.

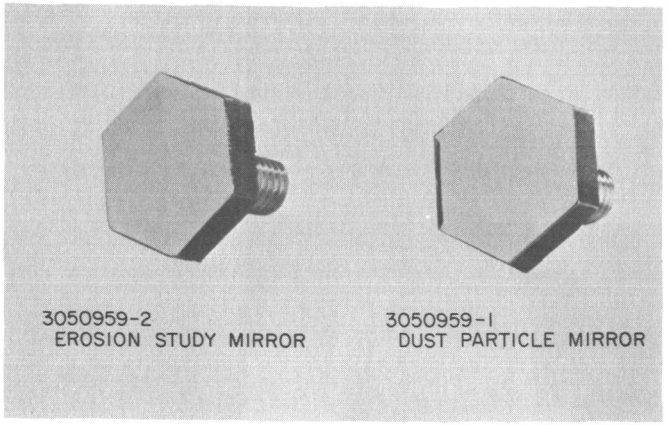

Fig. 5. Particle viewing mirrors

One mirror, PN 3050959-2, is used for the objectives in items (c) and (d) above. The mirror is aluminum alloy 2024-T4 material with a ½-in. hexagonal surface, polished, and only half of the surface coated with a layer of silicon dioxide. The remaining half of the surface is to remain bare polished metal (Fig. 5).

JPL action directive, change order 180, dated November 29, 1967, requested the installation on SC-7 of an additional photometric TV chart and a magnetic experiment. The chart will be located on the omnidirectional antenna A boom. The general installation will be the same as on omnidirectional antenna B. The magnetic experiment will be located on the leg 3 footpad in accordance with the requirements established for the leg 2 footpad magnetic experiment by change orders 151 and 163 wherever applicable. In compliance with change order 180, engineering has been generated, released, and implemented for both items.

Flight vehicle status. SC-7 was shipped from El Segundo and arrived at AFETR November 5, 1967. The vehicle has completed PVT-5 and propellant loading phases of the preflight preparation on schedule.

c. Mechanisms.

Antenna/solar panel positioner. The A/SPP provides mounting, positioning, position indicators, and launch and landing locks for the planar array antenna and solar panel. The antenna support structure includes controllable axes for roll, elevation, solar, and polar rotations. The drive for each axis uses a solenoid stepper motor for power and a wirewound potentiometer for position indication.

The *Surveyor VI* A/SPP performed in a normal manner during transit and after touchdown. The roll and solar axes were unlocked immediately after touchdown. The elevation axis was unlocked after the lunar liftoff and translation experiment was completed. All locks responded normally. Throughout the lunar day, A/SPP stepping efficiency appeared to be 100%

The elevation and polar drives were inadvertently stepped with these axes locked and at the limit of travel, respectively. Subsequent elevation and polar axis drive operation appeared normal.

Liftoff and translation were performed with the solar and roll axes unlocked, the elevation axis locked, and the A/SPP positioned to minimize landing moments on the unlocked axes. Telemetry position indications varied less than 1 deg after the hop. The elevation axis was then unlocked, and the A/SPP functioned normally.

At the end of the first lunar day, the total mission step count for the A/SPP axes was:

Solar	8,283
Polar	2,779
Elevation	196
Roll	14,290
Total	25,548

Active elements of the *Surveyor* compartment thermal control are nine thermal switches on compartment A and six thermal switches on compartment B. These bimetallically-operated units either make or break a conductive path to fixed radiators as a function of compartment temperatures to maintain temperature within a narrower band than the external temperature excursions.

One of the thermal switch contact faces is bare aluminum, and the other is coated with RTV-11 and MoS_2, vacuum baked for 48 h at 300°F.

Surveyor VI postmission analysis indicated that several thermal switches opened at lower than expected temperatures and that a number of switches had not opened when last monitored going into the first lunar night.

Figure 6 presents a summary of thermal switch mission experience for *Surveyors I* through *VI*, showing the quantity of switches which appeared to operate normally, stick temporarily, and stick permanently. Figure 7 indicates the number of months during which the thermal switches were continuously closed prior to reaching their normal opening temperature during the lunar mission.

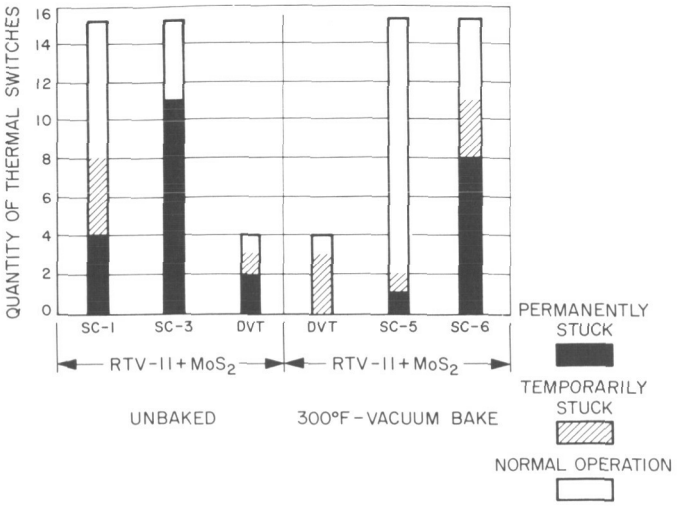

Fig. 6. Thermal switch performance

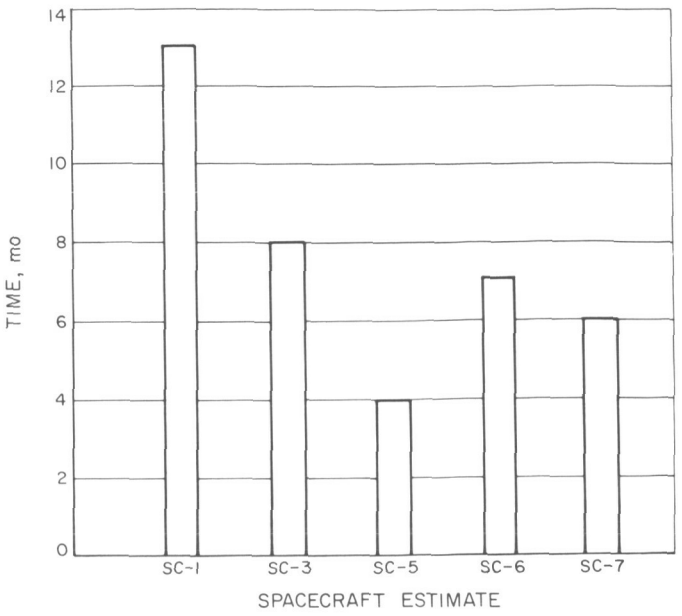

Fig. 7. Thermal switch period of continuous closure on spacecraft prior to lunar opening temperature exposure

Conductance and actuation tests were performed in December 1967 on four spare thermal switches of the *Surveyor VI* and SC-7 type to determine their performance as a function of time since they were last open. Table 4 summarizes these test results.

It can be concluded from these tests that the sticking switches on SC-6 were normal for this design. It shows that 25% of the switches will function normally, 50% will open below the normal opening point and 25% will never open. These conclusions are based on a very small sample so they are not too accurate but do indicate the trend of switch opening tendencies for this design.

2. Manufacturing

Approximately 99.9% of the manufacturing effort has been completed. The remaining tasks encompass primarily the repair or upgrade of spares and the implementation of change orders 177 and 180.

Principal activities for this reporting period are:

(1) Completion and delivery of the last three flight pin-pullers.

(2) Rework and upgrading of the SP-1 landing leg 3 assembly and TV auxiliary harness to SP-2 configurations.

Table 4. Thermal switch special test results

Test date	Switch number	Conductance, Btu/h-°F		Opening temperature,[b] °F			Time since last open, mo
		85° to 95°	60° to 70°	Test 1	Test 2	Original FAT (date, opening temp, conductance)	
Dec 6, 1967	PN 3028200-2, SN 1	0.725	0.68	+12	30	April 4, 1967 33°F (0.61 at 90°F)	8
	PN 3028200-3, SN 12	0.55	0.56	+12	35	May 15, 1967 38°F (0.56 at 90°F)	6
Dec 7, 1967	PN 3028200-2, SN 5			36	40	April 5, 1967 39°F (0.64 at 90°F)	8
	PN 3028200-3, SN 22			[a]	—	February 20, 1967 35°F (0.54 at 90°F)	10

[a]Contacts were still closed at end of test, +3°F.

[b]Opening temperature should be 35° ±10°F.

(3) Completion of particle viewing and stereo mirrors (change order 177). These items were shipped December 4.

(4) Initiation of the manufacturing of an additional magnet and control bar (change order 180). This item was delivered December 8.

(5) Shipment of the T-21 vehicle to California Institute of Technology.

C. Propulsion

1. Main Retroengine

a. Surveyor VI. The retroengine was successfully fired on October 9, 1967. Preliminary data indicate that the total impulse based on spacecraft ΔV was within 0.1% of prediction and the T_{3500} variation was less than 0.1%. of prediction. The prediction requirement is 1% for both items.

b. SC-7. Engine A22-13, fabricated for use as the SC-7 flight engine, was rejected by Thiokol Chemical Corporation on October 27, 1967. X-rays taken of the engine at ambient temperature and after thermal conditioning to the flight thermal gradient revealed extensive separation in the propellant near the aft boot-to-insulation terminus. The X-rays also revealed that the release terminus was located approximately 1½ in. aft of its design location, prompting another review of the X-rays on engine A22-11. A22-11 was rejected for the same reason as A22-13. The X-rays of A22-11 also revealed a mislocated release terminus. Separation on A22-11 and -13 occurred in the unreleased area that, by design, should have been released. Based on this review, it was concluded that the mislocated release terminus is the major cause of the separation and that the design modification as incorporated in A22-13 did not tend to reduce the separation.

The investigation next centered on the cause of the mislocated release terminus. The suspected cause was insufficient release material being applied during the insulation bonding and curing operations. The insulation processing procedure has been modified and additional in-process inspection points have been added. The changes are as follows:

(1) The quantity and number of applications of "Surfak" (release agent) to the release area is being doubled.

(2) Depth of release is being measured from several points before and after vulcanization of the insulation installed in the case.

(3) The insulated case is being X-rayed after vulcanization.

Another anomaly associated with A22-13 was the data obtained from the 5-in. motor firings used to check the propellant batch. Conflicting data were obtained on performance and π_k. A careful review of the data acquisition and data reduction revealed the cause to be improper calibration of a pressure transducer.

Engine A22-14 was fabricated to replace A22-13. The insulation processing changes mentioned above were successfully incorporated and the engine was shipped to AFETR December 8, 1967. The engine is currently being prepared for flight and will be mated with the spacecraft on December 19.

2. Vernier Propulsion System

a. System analysis.

Consent documentation. Current effort is directed toward closure of B action items generated at the SC-7 consent-to-ship and *Surveyor VI* consent-to-launch meetings. Currently, three vernier propulsion system, one retro, and one propulsion aerospace ground equipment B action items are open. Effort has been initiated on preparation of inputs for the SC-7 consent-to-launch meeting to be held at El Segundo in December.

Mission support. The successful *Surveyor VI* mission was supported by the SPAC propulsion team on a continuous basis from launch on November 7 until the lunar liftoff and translation on November 17. Additional support on a single-shift basis was provided until November 22. Propulsion performance during midcourse, terminal descent, and liftoff and translation was highly satisfactory. No propulsion anomalies were noted until November 20 when oxidizer pressure began to decay. Analysis of the pressure loss is currently under way.

b. Spacecraft servicing—El Segundo.

SC-7. Deservicing of the propulsion system during this period included the following:

(1) Leak test at flight pressures.

(2) Propellant tank off loading, using referee fluids.

(3) Removal of flight thrust chamber assemblies.

(4) System flow test after referee fluid loading.

(5) Propellant tank off loading.

(6) Installation of VEV engines.

(7) Vacuum drying of system.

(8) Check and relief valve function test.

(9) Helium regulator functional test.

(10) Bladder leak test.

Following vernier engine vibration, the vernier pressurization assembly was installed and the helium tank pressurized to shipping pressure.

c. Spacecraft servicing AFETR.

Surveyor VI. Following the vernier propulsion system functional test, engine installation and phasing test, and high/low pressure solvent leak test, the system was loaded with propellants and the high pressure leak test and the bladder integrity tests were performed with no leakage noted in the system. Continuous monitoring of the propulsion system for propellant leakage was maintained until shortly before launch.

SC-7. During the functional test at AFETR, the leg 1 fuel tank bladder leak rate was 71 cc/h, and the leg 3 fuel tank bladder leak rate was approximately 100 cc/h. Although the leg 1 tank leak rate was within specification limits, both tanks were replaced and returned to El Segundo for disassembly and inspection. The helium tank had a leak rate of 1.1 psi/day above the specified limit, based on data acquired during the high pressure decay test. The leak was observed to be at the transducer O-ring seal. The seal was replaced, and a high pressure leak check after replacement showed no visible leakage.

d. Helium regulator tests. A test program was performed on a flight-type helium regulator to determine the effects of a Freon flush of the regulator. Testing included three Freon flushes, each followed by 8-h vacuum dry and gas purging, and a functional and leakage test; a 10-day ambient storage test, a 5-day N_2O_4 vapor storage test, three-axis sine wave vibration test, an 88-h vacuum test, and a squib firing test. Functional and leakage tests were performed following each environmental test with no out-of-specification values noted.

3. Pressure Vessels[1]

a. General description. The *Surveyor* spacecraft uses seven pressure vessels for its vernier propulsion feed system. The helium pressure vessel is used as the pressurization source and six propellant pressure vessels are used for storage, three for oxidizer and three for fuel. The oxidizer is 90% nitrogen tetroxide and 10% nitric oxide, while the fuel is monomethylhydrazine monohydrate. In addition, the *Surveyor* uses a pressure vessel containing gaseous nitrogen for its attitude control system.

In order to insure a soft landing on the moon, a number of drop test vehicles were tested at Holloman Air Force Base, New Mexico. The drop test vehicle used a modified nitrogen pressure vessel for helium pressurization and two propellant pressure vessels, one for fuel and one for oxidizer. A gaseous carbon dioxide pressure vessel was also required to inflate a bag to cushion this special vehicle upon landing.

The original propellant pressure vessel shell was fabricated from 7178-T6 aluminum alloy. The rejection rate on the tanks was quite high due to problems associated with machining and welding. These problems coupled with the possibility of stress corrosion, led to the use of 6Al-4V titanium. Both the aluminum and the titanium propellant pressure vessels have spherical ends with about a 3-in. cylindrical section and a volume of 736 $in.^3$.

The helium and nitrogen pressure vessels were originally fabricated from 7Al-4Mo titanium alloy. The design was fully developed and qualification tested, but the generally poor history of 7Al-4Mo pressure vessels, together with the desire for better ductility, led to the development of a helium and nitrogen pressure vessel shell fabricated from 6Al-4V titanium alloy.

The spherical gaseous carbon dioxide pressure vessels, 32 $in.^3$ of volume, were developed for the T2 drop test vehicle. These were also fabricated from 6Al-4V titanium.

Table 5 presents data for each of the four different types of pressure vessels.

b. Reliability requirements. It was required that three pressure vessels be subjected to a bulk yield and burst test. The burst pressures of the three vessels must not exceed a spread of 5% when normalized. Normalizing is the

[1]Prepared by JPL Technical Section 351 and HAC Space Systems Division, Propulsion Department.

Table 5. Pressure vessel description

Shape	—	Spherical	Spherical	Spherical
Length of cylinder, in.	3.23	—	—	—
Ends	Spherical	—	—	—
Working media	Monomethylhydrazine	Gaseous He	Gaseous N_2	Gaseous CO_2
Radius (internal), in.	4.915	6.770	4.560	1.980
Thickness, in.				
Membrane	0.023–0.018	0.276–0.270	0.186–0.181	0.056–0.052
Weld	0.048–0.044	0.316–0.310	0.225–0.220	0.069–0.065
Volume, $in.^3$				
Required	736	1291	395	32
Actual	742	1298	398	33
Weight, lb				
Required	2.28	27.80	9.98	0.65
Actual	2.11	27.04	9.10	0.54
Safety factor	1.25	2.20	2.20	2.20
Pressure, psig				
Operating	840	5175	5000	3181
Proof:				
Room temperature	960	8684	8400	6050
−320°F	1325	12158	11725	8500
Burst:				
Required	1050	11385	11000	7000
Actual	1403	12665	13925	9383
Normalized	1235	11670	12250	8730
Units	139	38	31	14
Material	← 6Al-4V-Ti →			
Supplier	TMCA; Reactive metals	TMCA; Reactive metals	TMCA; Reactive metals	Reactive metals
Heat treat, kpsi	155–170	145–160	145–160	145–160
Vehicle use	A-21, T-2	A-21	A-21, A-24, T-2	T-2
Fabricator	FMC, Airtek Div.	FMC, Airtek Div.	SI, Airite Div.	FMC, Airtek Div.

process of relating the ratios of actual thickness to minimum required thickness and the actual tensile strength to minimum required tensile strength to give a minimum burst pressure.

Three reliability requirements (Table 6) were:

(1) A minimum spread of burst pressures on the initial three burst vessels.

(2) Ductile type bursts.

(3) Satisfactory completion of TAT program by three pressure vessels selected at random.

It was required that every tenth production pressure vessel be subjected to a bulk yield and burst test. The burst pressure of that pressure vessel after normalizing must be equal to or greater than 95% of the normalized average pressure of the three initial burst vessels.

The reliability requirements resulting from the one-in-ten burst test were:

(1) Normalized burst pressure $\geqq$ 95% of the average of the three initial burst vessels. The burst must be of a ductile type.

(2) Required minimum vessel volume with a minimum spread.

(3) Less than the maximum weight required with a minimum spread.

Table 6. Reliability requirements

1. **Manufacturing and process control**
   a. Forging:
      (1) Chemistry.
      (2) Beta transus evaluation.
      (3) Macro structure.
   b. Heat treat and aging:
      (1) Thermal model control.
      (2) Aging development testing.
   c. Welding:
      (1) Preproduction weld development.
      (2) Preproduction weld qualification.
      (3) Postproduction weld confirmation.
   d. In-process chemistry check for hydrogen.
   e. Hardness check:
      (1) Machining.
      (2) Welding.

2. **Initial burst**
   a. Three vessels tested to destruction:
      (1) Determine bulk yield pressure.
      (2) Determine actual burst pressure.
      (3) Determine normalized spread.
      (4) Determine proof pressure.

3. **TAT**
   a. Three vessels to be tested:
      (1) Examination of product.
      (2) Inspection of welds.
      (3) Capacity test.
      (4) Weight test.
      (5) Proof test:
         • Three cycles at K_1% bulk yield at room temperature.
         • One cycle at K_2% bulk yield at room temperature using LN_2 at −300° to −320°F.
      (6) Leak check.
      (7) Pressure cycle.
      (8) Leak check.
      (9) Pressure hold.
      (10) Leak check.
      (11) Vibration:
         • Shock (1 unit)
      (12) Leak.
      (13) Burst.

4. **Acceptance testing**
   a. All delivered hardware:
      (1) Examination of product.
      (2) Inspection of welds.
      (3) Capacity test.
      (4) Weight test.
      (5) Proof test:
         • Three cycles at K_1% bulk yield at room temperature.
         • One cycle at K_2% bulk yield at room temperature, using LN_2 at −300° to −320°F.
         • Leak test.
      (6) Cleaning test per HAC 262613.

5. **One-in-ten burst test**
   a. Every tenth production vessel:
      (1) Determine bulk yield pressure.
      (2) Determine actual burst pressure.
      (3) Determine normalized burst pressure.
      (4) Determine normalized burst pressure is ≥ 95% of the average of the three initial burst tests.

6. **Postburst test evaluation**
   a. Low burst of one-in-ten:
      (1) Metallurgical evaluation for reason for low burst.
      (2) If (1) is unsatisfactory, burst three additional vessels to establish a new average normalized burst pressure.
   b. All vessels tested to destruction:
      (1) Microhardness survey:
         • Parent metal surfaces.
         • Weld section.
      (2) Tensile properties:
         • Membrane.
         • Weld.
      (3) Micro structure:
         • Parent metal.
         • Weld metal.
      (4) Fracture:
         • Origin.
         • Appearance.

Vessel type	K_1	K_2
He, N_2, CO_2	85	119
Propellant	90	126

c. Design requirements. The design of the pressure vessels starts with a definition of its function, life and its environment. Its environment may have long term storage, cyclic loading, vibration, temperature variations, corrosion, dust, vacuum or impact loading to name a few. A material must be selected to survive the environment. Then, a safety factor should be chosen and the test requirements defined.

Once the total environment has been established, only the material and safety factor need be selected to design the vessel, unless one is forced to design the vessel to the test requirements.

In the design of *Surveyor* pressure vessels, the material selected had to possess low density, good ductility and toughness, ease of fabrication, and consistent metallurgical, physical and mechanical properties. To obtain these properties in Ti-6Al-4V, controls were established on chemistry, forging temperature, heat treating profile, and prewelding and weld schedules, etc.

Surveyor pressure vessels are designed to a 2.20 safety factor with an ultimate tensile strength of 145,000 to 160,000 psi. With an ultimate tensile strength range of 155,000 to 170,000 psi, a safety factor of 3.0 is required. Nonman rated pressure vessels have a safety factor of 1.25.

An alternate solution to an arbitrary safety factor is to qualify the vessel to ten times the number of expected environmental pressure cycles with prudent quality controls on production vessels. *Surveyor* pressure vessels have met the pressure cycling qualifications as well as the arbitrary safety factor.

d. Results.

Mechanical properties. The 5% spread allowed for the initial three-burst tests, and the one-in-ten burst test requirements emphasize the need for adequate representation of the mechanical properties of each pressure vessel. From the forging cut chart, the forging at each end of the bar is cut up to provide tensile coupons, as shown in Fig. 8. This provides a minimum of eight and a maximum of twelve tensile coupons to ascertain the properties of that bar and the forgings within the bar. A summary of some of the results for propellant pressure vessels for tensile ultimate, tensile yield, elongation, and reduction of area

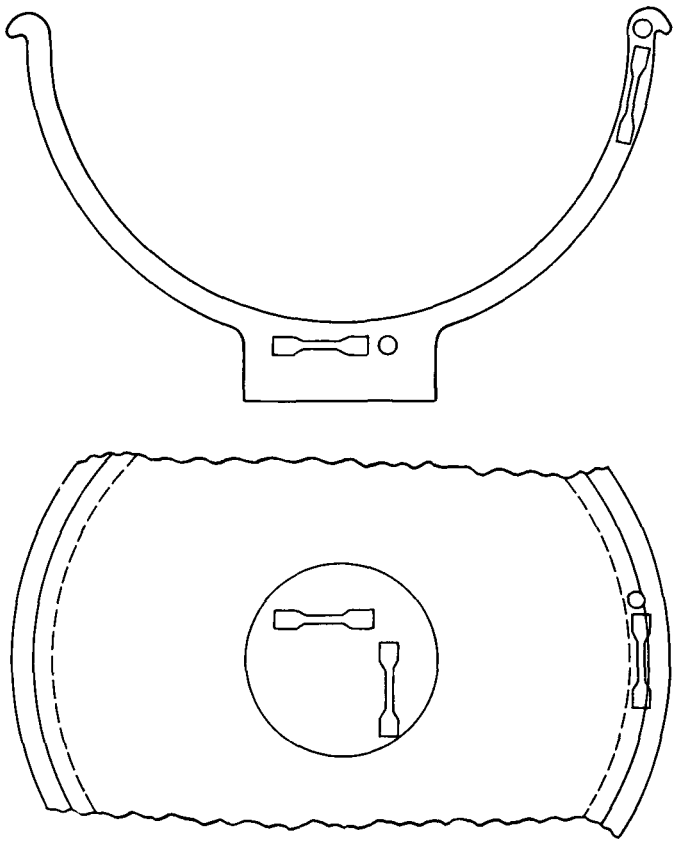

Fig. 8. Forging tensile specimen location

are shown in Table 7. Similar data are available for all of the *Surveyor* pressure vessels, but are not included in this discussion. Weld joint efficiency was determined from preproduction and postproduction weld test data to be 94%. In actual burst tests of pressure vessels, there were no instances of initiation of burst in the weld area.

Burst tests. Table 8 gives a summary of all burst tests to date, including the actual burst test pressure, the normalized burst test pressure, and the ratio of the normalized burst pressure for the one-in-ten production units divided by the minimum required pressure. The minimum spread achieved was 0.80%, while the maximum was 3.89%, well within the required maximum of 5%. The 0.80%, it is felt, was obtained due to the use of high energy forgings; disregarding this case, the average spread was 3.27% with a minimum of 2.74 and a maximum of 3.89%, showing an approximate variation of less than ±0.6%.

Table 7. Summary of mechanical property values[a] of propellant pressure vessel

Pressure vessel		Ultimate strength, psi	Yield strength, psi	Elongation, %	Reduction of area, %
Required	min	155,000	145,000	10	30
	max	170,000	160,000	—	—
Boss	Average	165,250	153,870	13.50	45.36
Rim	Average	164,210	153,040	13.92	46.03

[a]Based on the test results of approximately 80 specimens from both the boss and rim areas.

It is required that all one-in-ten burst test pressure vessels burst in a ductile manner and that the normalized pressure exceed 95% of the average of the normalized pressure of the three initial burst vessels. All pressure vessels burst in a ductile manner. The ductility was achieved by the control of the chemistry of the material, forging technique, heat treating and aging procedure and the control of the welding procedure.

The one-in-ten burst test results are also shown in Table 8. The normalized burst pressure was divided by 95% of the average normalized pressure of the initial three-burst tests or the minimum required burst pressure, whichever is the larger. If that ratio is less than 1.000, then a lot of ten vessels is rejectable. See the right hand column under each pressure vessel.

The data indicated that all of the burst tests meet the requirements with a maximum spread of less than 10% and the lowest ratio was 1.006. If, in the event one of the one-in-ten pressure vessels burst low, a failure analysis would be performed to determine the cause of failure. If the cause of failure was determined to be unsatisfactory, three additional pressure vessels would be burst to establish a new average and qualify that group of pressure vessels, providing the minimum normalized burst met or exceeded the minimum burst requirement and the maximum normalized spread did not exceed 5%.

Special stress corrosion tests. Special stress corrosion tests were performed on some selected propellant tank pressure vessels. Four propellant pressure vessels were exposed to MON-10 at temperatures ranging from 110° to 270°F with pressures ranging from 840 to 1079 psig, and exposure times from 7 to 16 days. Two vessels, SNs 28 and 61, were proof-tested after completing exposure tests and subjected to sectioning and metallurgical examination. Two others, SNs 66 and 68, were burst at temperature after completing the exposure test bursting at 1375

Table 8. Burst test pressure data

Pressure vessel	Propellant pressure, psi			Nitrogen pressure, psi			Helium pressure, psi			Carbon dioxide pressure, psi		
	Actual	Normalized	Normalized 1173	Actual	Normalized	Normalized 11638	Actual	Normalized	Normalized 11385	Actual	Normalized	Normalized 8296
Initial burst tests:												
1	1400	1237	—	14475	12360	—	12790	11761	—	9500	8690	—
2	1370	1258	—	13500	12000	—	12215	11465	—	9400	8750	—
3	1380	1210	—	13800	12390	—	13000	11785	—	9250	8760	—
One-in-ten burst tests:												
1	1370	1180	1.006	11850	12050	1.035	12475	11711	1.029	9450	8800	1.061
2	1370	1285	1.095	13050	12570	1.080	12000	11544	1.014	—	—	—
3	1350	1202	1.025	12850	12360	1.062	12900	12054	1.059	—	—	—
4	1405	1205	1.027	—	—	—	—	—	—	—	—	—
5	1405	1268	1.081	—	—	—	—	—	—	—	—	—
6	1415	1246	1.062	—	—	—	—	—	—	—	—	—
7	1559	1243	1.060	—	—	—	—	—	—	—	—	—
8	1434	1193	1.017	—	—	—	—	—	—	—	—	—
9	1560	1270	1.083	—	—	—	—	—	—	—	—	—
10	1340	1193	1.017	—	—	—	—	—	—	—	—	—
11	1440	1197	1.020	—	—	—	—	—	—	—	—	—
12	1383	1195	1.019	—	—	—	—	—	—	—	—	—
Average of initial three normalized burst tests		1235			12250			11670			8733	
95% of average		1173			11638			11087			8296	
Minimum required burst		1050			11000			11385			7000	
Percent spread initial burst		3.89			3.18			2.74			0.80	

and 1300 psig, respectively. The minimum required burst was 1050 psig. A summary of pertinent data is shown in Table 9.

Type approval tests. All pressure vessels satisfactorily completed the pressure hold, pressure cycle, vibration and leak tests. All pressure vessels, upon completion of TATs, were burst at pressures exceeding the minimum required burst, although this is not a requirement. However, it is a requirement to burst all test pressure vessels. This requirement insures that a tested item will never be assembled into a spacecraft.

Acceptance tests. All delivered pressure vessels successfully passed the 3 cycles of proof pressure and 1 cycle of 1.4 times room temperature proof pressure at a temperature of −300° to −320°F. Even one propellant pressure vessel, 254094, which had been collapsed due to an inadvertent external test pressure of approximately 80 psig and was in a buckled state, passed the acceptance test. The buckles were still in evidence after completion of the acceptance test.

Volume and weight. The minimum volume requirements were met in all delivered pressure vessels. Except

Table 9. Elevated temperature exposure of propellant pressure vessel to MON-10

Tank shell serial No.	28	61	68	66
Exposure test conditions:				
Test media	MON-10	MON-10	MON-10	MON-10
Temperature, °F	110	110	240	270
Pressure, psig	850	850	840	1079, decayed to 309
Time, days	7	14	15 1/2	16
Proof pressure test:				
Test media	H_2O	H_2O	—	—
Temperature, °F	Ambient	Ambient	—	—
Pressure, psig	960	960	—	—
Time, min	5	5	—	—
Prior exposure to MON-10:			S-7 TAT	S-7 TAT
Temperature, °F	Ambient	None	—	—
Pressure, psig	300	—	—	—
Time, days	22	—	—	—
Prior testing				
Type of test	Tank FAT = T-21 FAT	Proof	Pressurized drop/S-7 FAT—tank FAT	Pressurized drop/S-7 FAT—tank FAT
Burst pressure test:				
Burst pressure, psig	—	—	1300	1375
Test media	—	—	H_2O	H_2O
Temperature, °F	—	—	240	270
Results of metallurgical examinations	O.K.	O.K.	O.K.	O.K.
MON-10 compatibility	O.K.	O.K.	O.K.	O.K.
Bladders (Teflon)	No	No	Yes	Yes
Chemical analysis of MON-10, %				
Pretest:				
NO	—	9.85	—	—
N_2O_2	—	90.05	—	—
Ash	—	0.002	—	—
NOCL	—	0.01	—	—
H_2O	—	0.1	—	—
Posttest:				
NO	10.0 ± 0.5	9.40	10.0 ± 0.5	10.0 ± 0.5
N_2O_4	90 ± 1.0	Not taken	90 ± 1.0	90 ± 1.0
Ash	—	0.004	—	—
NOCL	0.08 (max)	0.01	0.08 (max)	0.08 (max)
H_2O	0.1 (max)	Results lost	0.1 (max)	0.1 (max)

in the case of the small pressure vessel with a volume of 32 in.^{3}, examination of the data revealed that the volume spread is approximately 1.0% or less.

The propellant pressure vessels have a weight spread of 0.22 lb in 2.22 lb maximum, while the helium vessel has a weight spread of 0.42 lb out of 37.56 lb maximum or 1.11%. The percent weight spread for the nitrogen and carbon dioxide tanks was 0.98% and 3.64%, respectively. The large variation for the propellant pressure vessel accounted for the fact that wall thickness variation allowed is from 0.018 to 0.023 in. or 21.7%, while the helium pressure vessel thickness is 0.306–0.312 in. or 1.92%.

4. Experimental Investigation of the SC-5 Helium Regulator Failure[a]

a. Introduction. Shortly before the midcourse velocity correction during the SC-5 mission, the vernier propulsion system pressurization squib was fired, admitting high pressure helium to the inlet of the helium regulator and pressurizing the downstream propellant feed system. Following the midcourse maneuver, the high pressure helium supply lost pressure at a high rate, 10 psi/min, and the downstream system pressure was above normal regulator lockup pressure, at a level slightly above the expected relief valve unseating pressure. It was concluded that the regulator had failed to lock up and that helium was leaking through the regulator from the high pressure supply to the downstream system and from there venting through the relief valves to space. Repeated vernier engine firings made in an attempt to lock up the regulator by cycling it were unsuccessful, and helium was vented overboard continuously from midcourse until shortly before the terminal descent maneuver. At this time the high pressure supply pressure level had decayed from approximately 5200 psia to approximately 840 psia. This loss of helium required that a nonstandard, though successful, terminal descent maneuver be performed.

Immediately following the mission an SC-5 review committee was convened. This committee reviewed the design and test history associated with the regulator development, manufacture, and use as a flight component in general, and of the SC-5 regulator in particular. As part of this investigation, an experimental program was performed at Carleton Controls Corporation, vendor of the regulator to HAC.

Following the conclusion of the SC-5 review committee activities a supplemental investigation of the regulator was made in the liquid propulsion gas laboratory at JPL. The purpose of this investigation was to explore the operation of the regulator and to examine its response to nonstandard environmental conditions.

b. Operation of the regulator. Figure 9 shows a cutaway view of the assembled regulator. It can be seen that the upper portion of the regulator consists of a spring package which opposes the motion of a diaphragm. The pressure which moves the diaphragm is the downstream, or regulated, pressure sensed through a port which communicates with the regulator outlet. Also attached to the diaphragm by a pair of aluminum rods (pistons) is a rigid

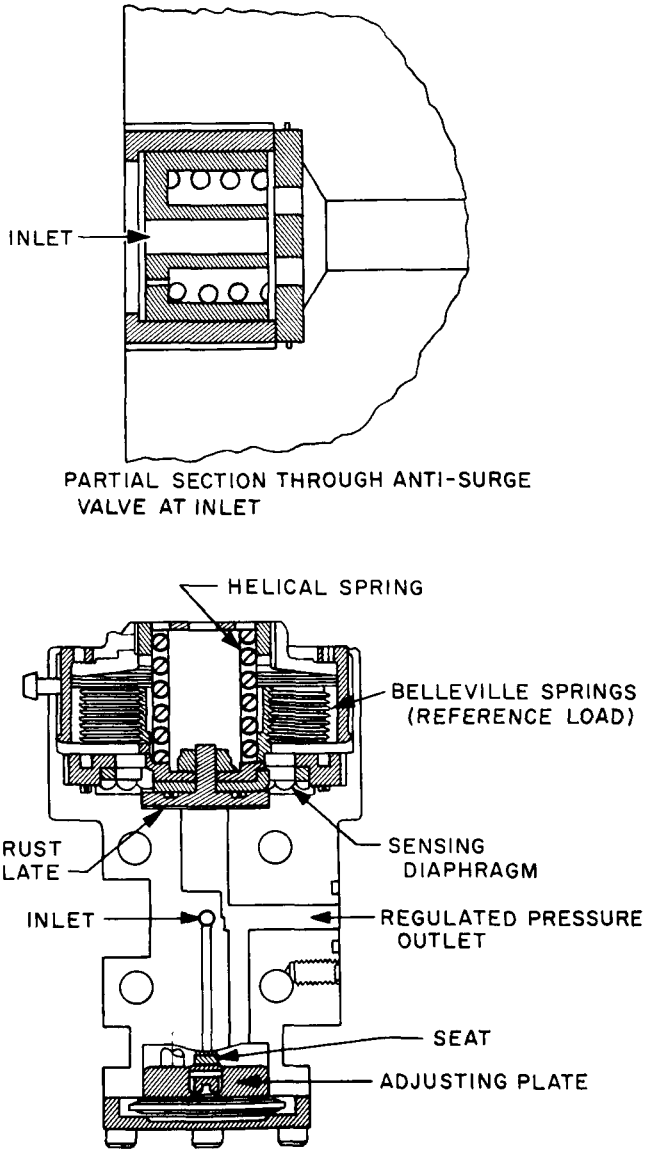

Fig. 9. Helium pressure regulator

[a]Prepared by JPL Section 384.

metal plate which contains the regulator seat. As the diaphragm flexes in response to changes in the downstream pressure, the compression of the springs and the load and location of the regulator seat are changed.

The spring package shown in Fig. 9 is comprised of a Belleville Spring assembly and a helical spring. Typical force/deflection curves of the elements of the spring package, measured before assembly into the regulator, are presented in Fig. 10. Zero deflection corresponds to the free length of the spring; increasing deflection corresponds to increasing compression of the spring. This direction also corresponds to motion of the regulator seat from the open to the closed position. Indicated in Fig. 10 are the spring deflections associated with the full open (preload) and full closed (lockup) positions of the regulator seat.

In the inlet, as shown in a detail of Fig. 9, is the antisurge valve assembly. It is the purpose of this valve to limit the flow rate of helium through the regulator during initial pressurization of the downstream system. The antisurge valve operates only when the pressurization squib is actuated, admitting 5000 psia helium to the regulator inlet. The outlet side of the regulator is at a pressure level < 250 psia before pressurization. Since this is well below the regulator lockup pressure, the regulator is wide open. Should no additional restriction be presented to the flow, the helium flow rate through the regulator is very large. The antisurge valve prevents this by closing down, due to the large pressure drop across it, and forcing the helium to flow into the regulator through a 0.039-in.-diam orifice. This is accomplished by the motion of a small piston which is driven by the pressure drop across it to compress a spring, as shown in Fig. 9.

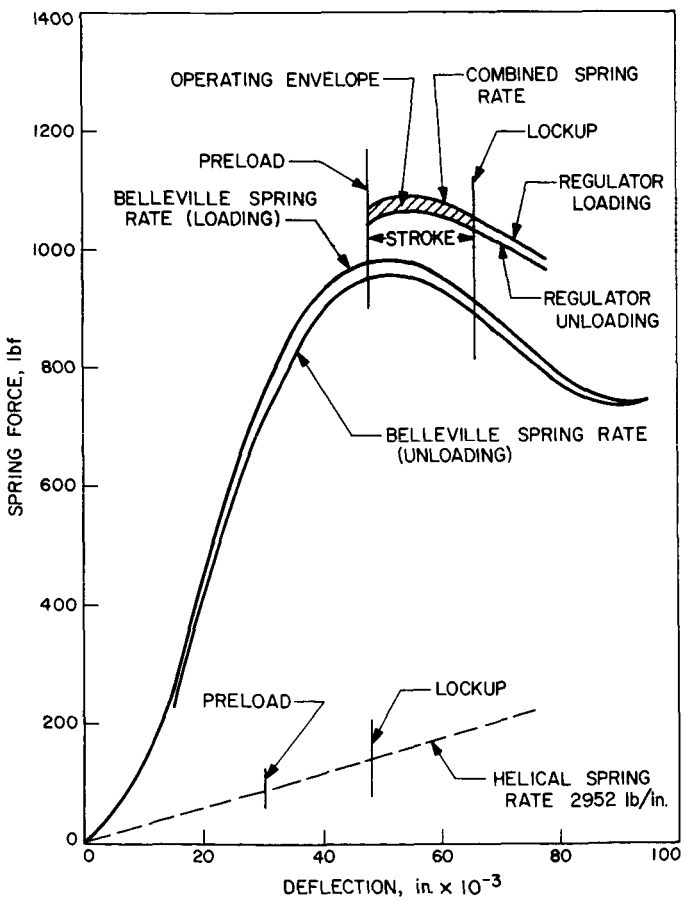

Fig. 10. Regulator spring force regulator seat travel

c. Prelaunch test experience with the SC-5 helium regulator. The SC-5 helium regulator was exposed to the same tests and environment as all previous flight helium regulators up to the check and relief valve tests performed as part of the VPS functional test at Cape Kennedy. During the VPS functional test the regulator lockup pressure is determined, and the ability of the regulator to maintain adequate downstream pressure while flowing is verified. Following this the oxidizer check valve is tested for leakage, and the oxidizer relief valve unseat pressure is then determined.

While performing the leakage test on SC-5 the check valve was found to leak at relatively low pressures (4 and 50 psig) and not at high pressures (300 and 800 psig). The relief valve unseating pressure was then determined to be 838 psig. The check valve was then again leak checked at 4 and 50 psig, and the leakage had increased by a factor of two and an order of magnitude, respectively. The valve leakage was not determined at 300 and 800 psig. The valve leak rates measured after the relief valve test, if extrapolated to higher pressures, indicate the possibility of leakage past the check valve, during the relief valve portion of the test, of sufficient magnitude to have applied as much as the full 838 psig to the downstream side of the regulator.

This 838 psig is 85 psi above the regulator lockup pressure of 753 psig, and is equivalent to a seat loading of 117 lbf. This seat loading is adequate to permanently deform the regulator seat, it is estimated, to a depth of approximately 0.005 in. Changes to the SC-7 VPS functional test have precluded the possibility of a similar occurrence on the SC-7 vehicle.

d. Test results. The testing was organized into two groups. One group of tests examined the influence of contamination, coining of the regulator seat, and blocking of

the antisurge valve. Five regulator seats were used in this group of tests: the original seats in the SN-2 and SN-63 regulators and three seats of JPL manufacture (seats 1, 2, and 3) used in the SN-2 regulator. The second group of tests used the SN-2 regulator and JPL seats 4, 5, and 6 to investigate the effect of surface imperfections on the regulator seat.

The SN-2 regulator was first tested with its original seat in the "as received" condition. It was then tested with the seat coined. Coining of the Kynar seat of the regulator was achieved by applying to the downstream side of the regulator a pressure 85 psi greater than the regulator lockup pressure. This was done to examine the effects of a leaking check valve in the helium system downstream of the regulator on the behavior of the regulator. Investigation of this condition was prompted by the data taken during the VPS functional test performed on SC-5 at Cape Kennedy. The antisurge valve was then blocked, and the seat failed.

The antisurge valve was blocked to simulate one stuck open on a flight spacecraft. This was accomplished by removing the antisurge valve from the regulator, inserting a 0.030-in. annular shim between the piston and the seat, and threading the antisurge valve assembly back into the regulator body.

Figure 11 shows the data taken during this test and the data taken at VPS pressurization during the SC-5 mission. Note the strong similarity between the pressure rise rates seen in the flight and test data. Figures 12 and 13 are photographs of the SN-2 regulator seat taken immediately

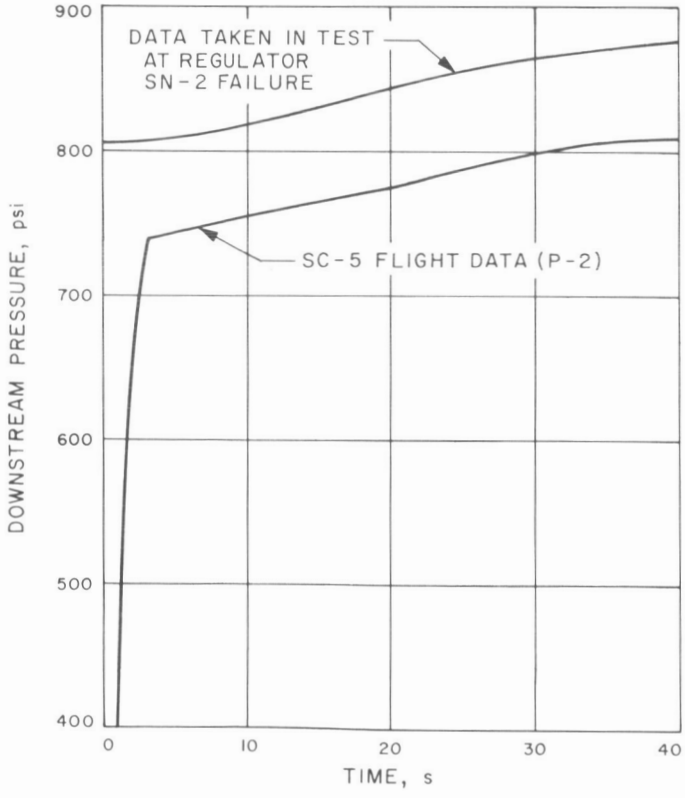

Fig. 11. Comparison of SC-5 pressurization data with test pressurization data

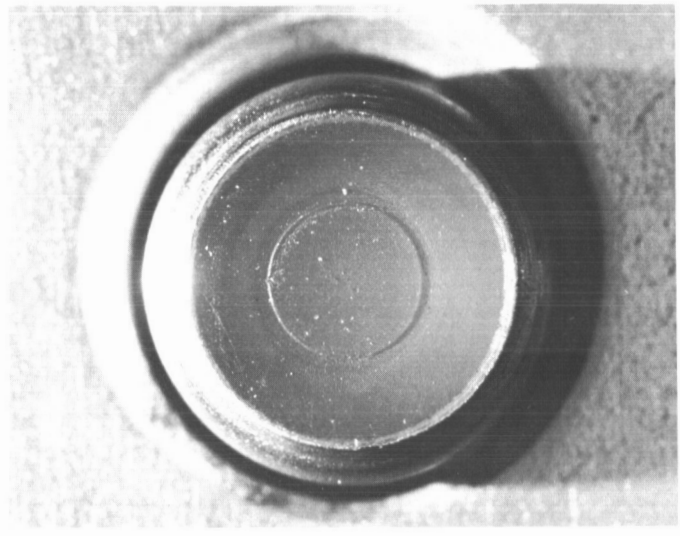

Fig. 12. Original seat furnished with SN-2 regulator, shown after coining

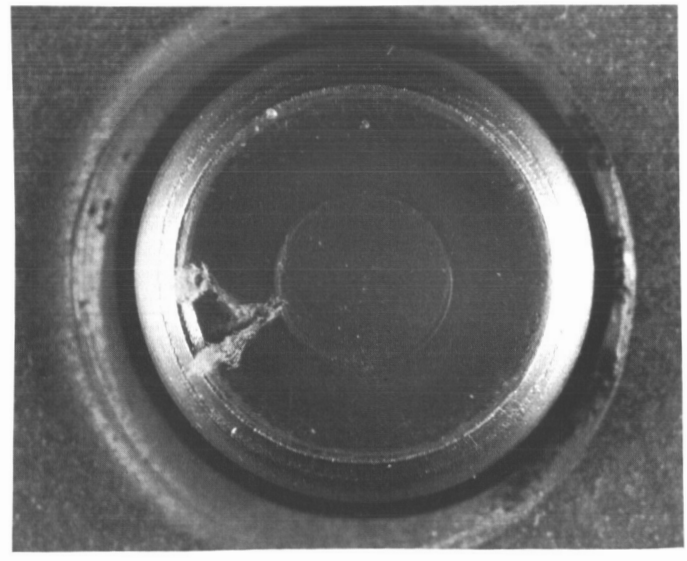

Fig. 13. Original seat furnished with SN-2 regulator, shown after failure

before and after the failure. Figure 14 is a micrograph of the original SN-2 regulator seat before failure showing a region of the seat into which a contaminant had impacted. The absence of "flash" and the "clean" appearance of the impact area can be taken as typical of contaminant impact. Figure 15 shows the innermost region of the failed area of the same regulator seat. The similarities of appearance here indicate that the failure was initiated by the impact of a contaminant into the regulator seat. Following impact a gas-particle-surface interaction caused subsequent massive failure of the seat.

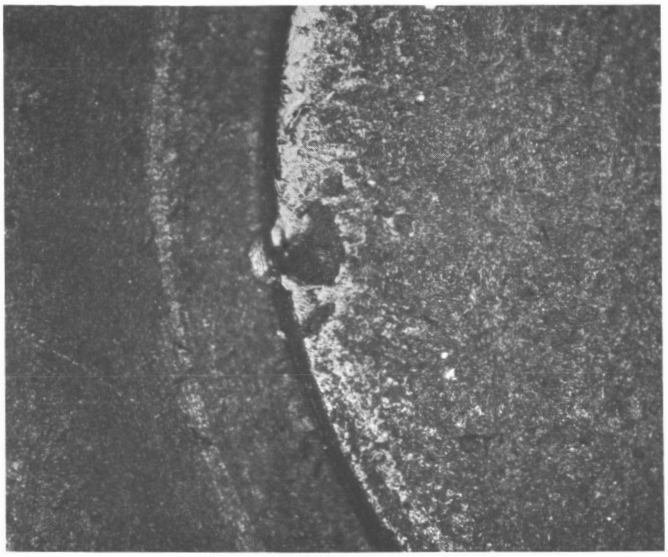

Fig. 14. Micrograph of original seat furnished with SN-2 regulator, shown after coining (region shown includes the impact area of a contaminant particle)

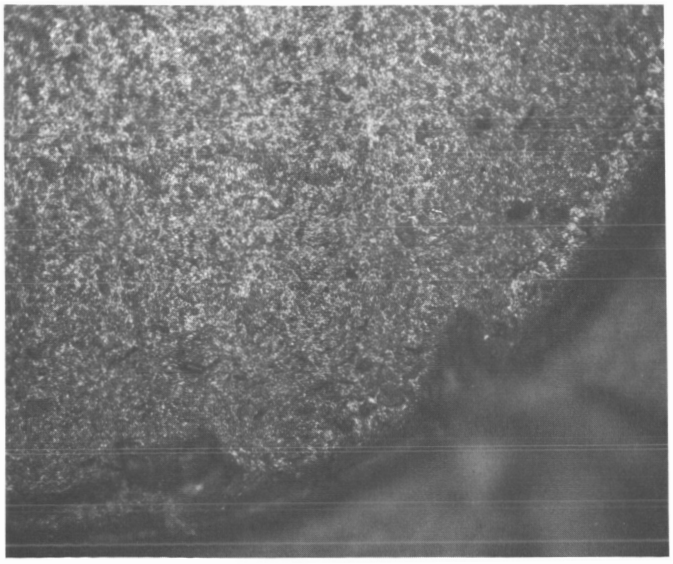

Fig. 15. Micrograph of the original seat furnished with the SN-2 regulator, showing detail of the failed region

The original SN-2 regulator seat was then replaced with JPL seat No. 1. The antisurge valve remained blocked, and the seat was tested with no failure. Figure 16 is a photograph of this seat after testing.

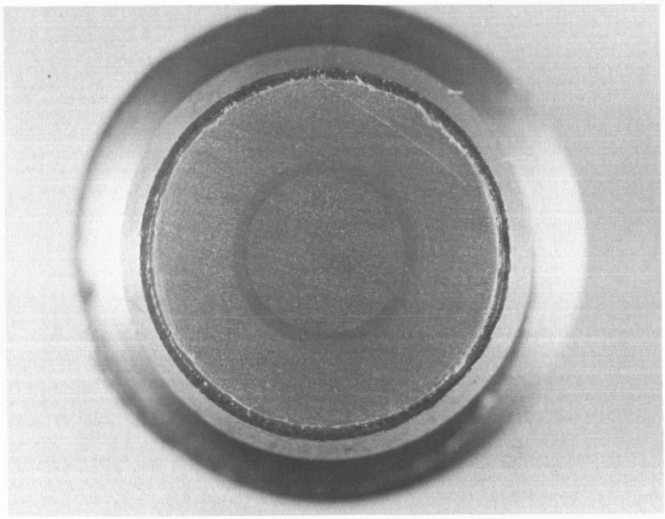

Fig. 16. JPL seat 1 used in the SN-2 regulator, shown after testing

Without changing the condition of the antisurge valve, the seat was replaced with JPL seat 2. This seat was coined, as described above, and the seat tested with no failure. Figure 17 is a photograph of this seat taken following these tests.

Examination of the seat and the millipore filter indicated a very low level of contamination in the system. It was decided to introduce contamination in the 50- to 250-μ range into the system. The regulator was again tested, at which time the seat failed. Figures 18 and 19 are photographs of the regulator seat taken after failure. Note the "clean" appearance of the innermost region of the failure, which can be compared with the impact region shown in Fig. 14.

Again without changing the condition of the antisurge valve, the seat in the SN-2 regulator was replaced with JPL seat No. 3. Contamination was introduced, as above, and the uncoined seat did not fail. Examination of the millipore filter indicated a high level of contamination had passed through the regulator. The regulator seat was

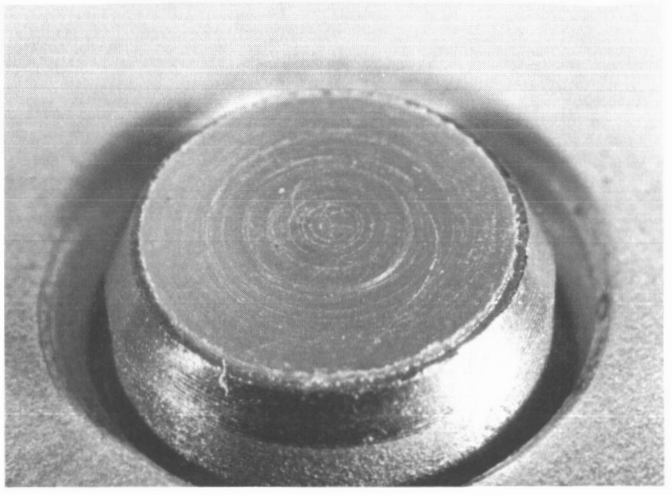

Fig. 17. JPL seat 2 used in the SN-2 regulator, shown after being coined

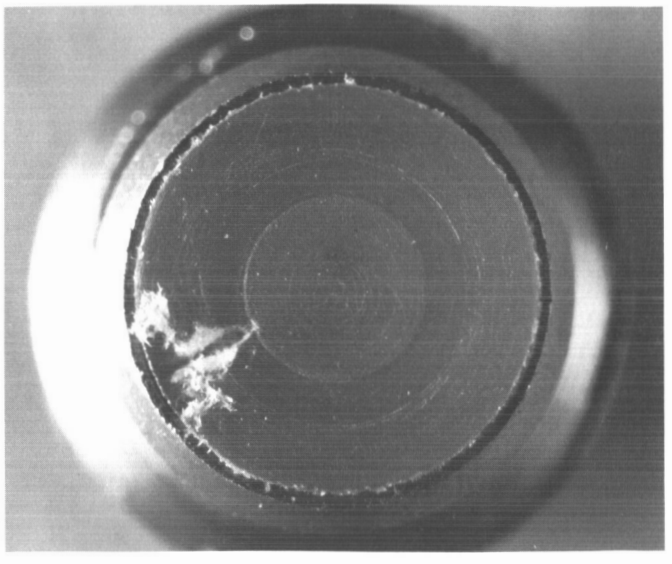

Fig. 18. JPL seat 2 used in the SN-2 regulator, shown after failure

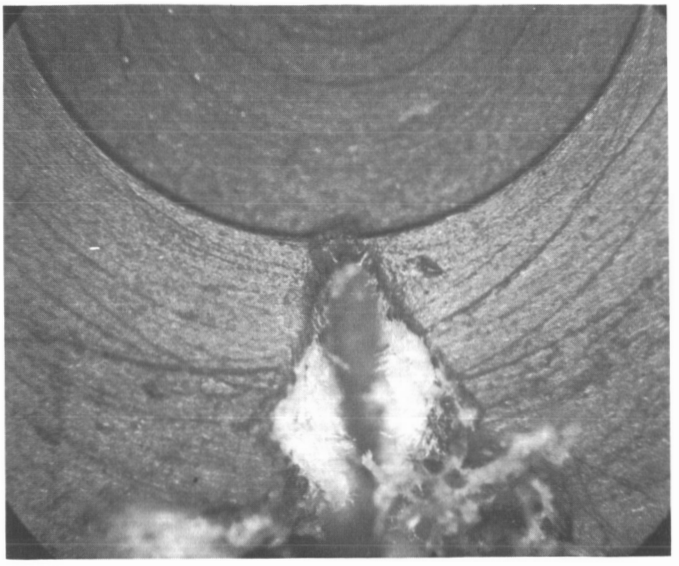

Fig. 19. Micrograph of failed region of JPL seat 2 used in the SN-2 regulator

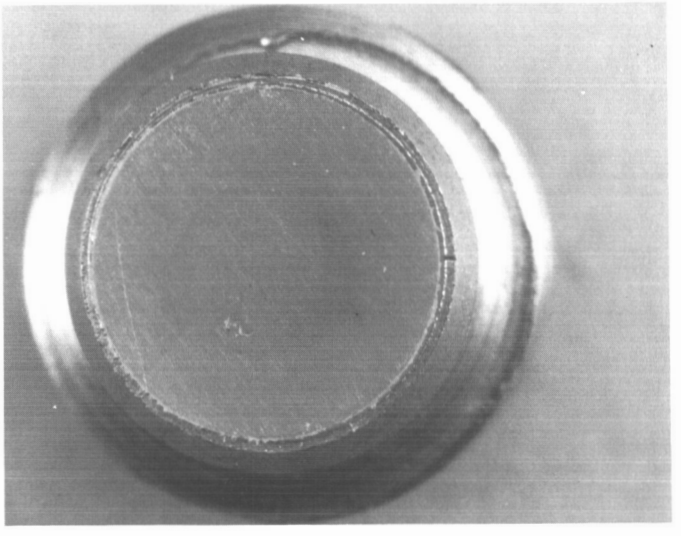

Fig. 20. JPL seat 3 used in the SN-2 regulator, shown after testing

then coined and contamination again introduced. Again the seat did not fail. Subsequent examination of the millipore filter showed little contamination, and examination of the regulator seat again indicated little or no contamination. It can be speculated that the artificially introduced contamination did not pass through the regulator. Figure 20 is a photograph of this seat taken after testing.

The SN-63 regulator was installed in the system and tested in the as received condition with no failure. The seat was coined and the regulator tested again with no failure. The regulator was removed, the antisurge valve blocked in the open position, and the regulator reinstalled. The seat then failed during the next test. Figures 21 and 22 are photographs of this seat taken after failure. Figure 22 can be compared with Fig. 14, and again it can be inferred that the failure of this seat was also caused by the impact of a contaminant onto the seat.

Table 10 presents a qualitative summary of the various conditions under which the one group of regulators and

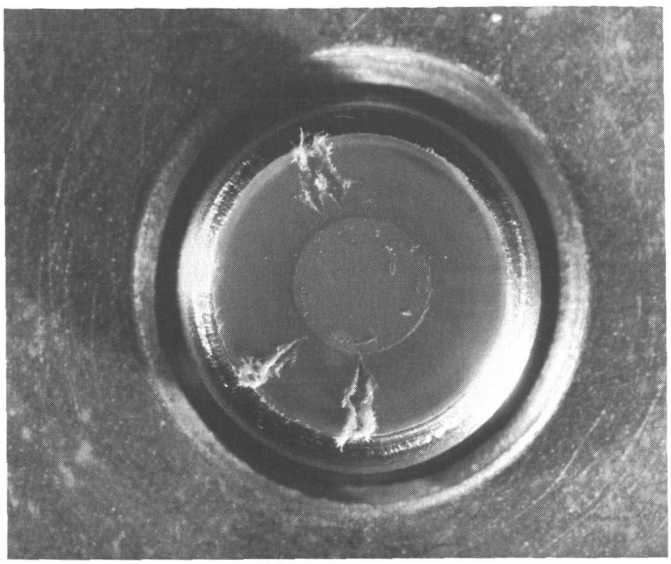

Fig. 21. Original seat furnished with SN-63 regulator, shown after failure

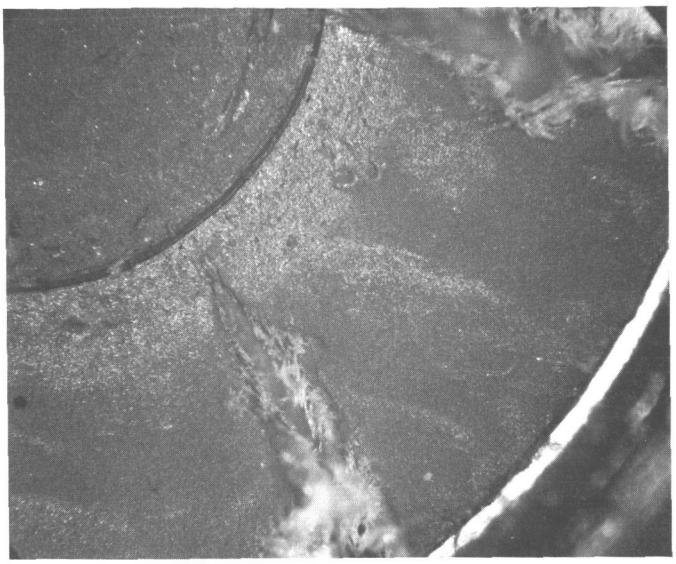

Fig. 22. Micrograph of failed region of the original seat furnished with the SN-63 regulator

seats were tested. Three things are apparent: (1) every seat which had failed had previously been coined; (2) contamination was present; and (3) the antisurge valve had been blocked in all the tests in which a seat failure had occurred.

Based on the photographs and on Table 10 it can be said that the presence of contamination and a previously coined seat were necessary conditions for seat failure in the testing program. Measurements of the failed areas shown in Figs. 15, 19, and 22 indicate that the contaminants which initiated these failures ranged in size from 50 to 150 μ.

At this point it cannot be determined whether the antisurge valve needed to be blocked for failure to occur. Certainly every failure was accompanied by a blocked antisurge valve. However, either the antisurge valve had just been blocked or contamination had just been introduced prior to the failure.

The antisurge valve is a stainless steel component which is threaded into the aluminum body of the regulator. Removing or replacing the antisurge valve probably generates contamination at the regulator inlet. Possibly this contamination is sufficient to cause failure of the regulator seat without also blocking the antisurge valve open.

Table 10. Qualitative conditions of regulator tests

Regulator SN	Seat	Seat coined	Contamination introduced	Antisurge valve blocked	Antisurge valve blocked immediately before failure	Failure
2	Original	Yes	No[a]	Yes	Yes	Yes
2	1	No	No	Yes	No	No
2	2	Yes	No	Yes	No	No
		Yes	Yes	Yes	No	Yes
2	3	No	No	Yes	No	No
		No	Yes	Yes	No	No
		Yes	Yes[b]	Yes	No	No
63	Original	Yes	No	No	No	No
		Yes	No[a]	Yes	Yes	Yes

[a]It was not necessary to artificially introduce contamination into the system because sufficient contamination was already present.

[b]It was not apparent from observations of the millipore filter or of the seat itself that the introduced contamination had passed through the regulator in this test. Such passage was apparent in all other tests where contamination had been introduced.

Thus, it is not possible to determine the necessity of blocking open the antisurge valve without additional testing.

Figures 23 and 24 show the effects on the downstream pressure rise characteristics with the antisurge valve blocked and operable.

For the second group of tests JPL seats 4–6 were used to investigate the effects of surface imperfections on the seat on regulator behavior. Seat 4 had drilled into it a 0.0135-in.-diam hole 0.015 in. deep. This seat failed when tested (Figs. 25 and 26) with a blocked antisurge valve. Contamination was not deliberately introduced.

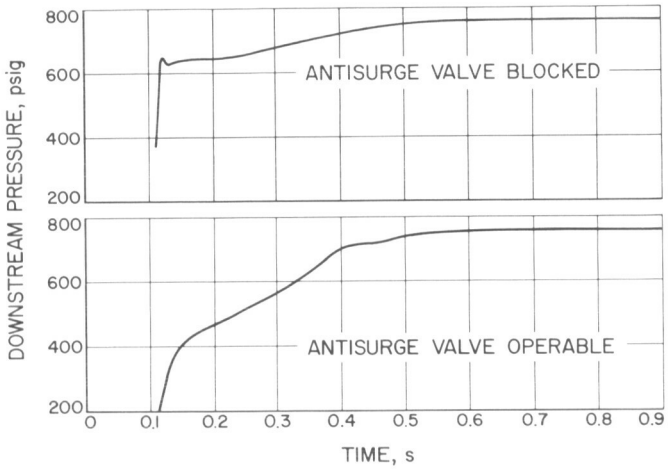

Fig. 23. Pressure response during solenoid actuated pressurization

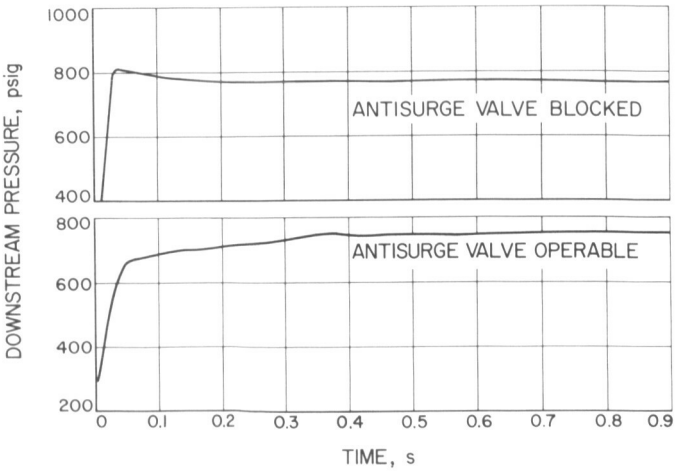

Fig. 24. Pressure response during squib actuated pressurization

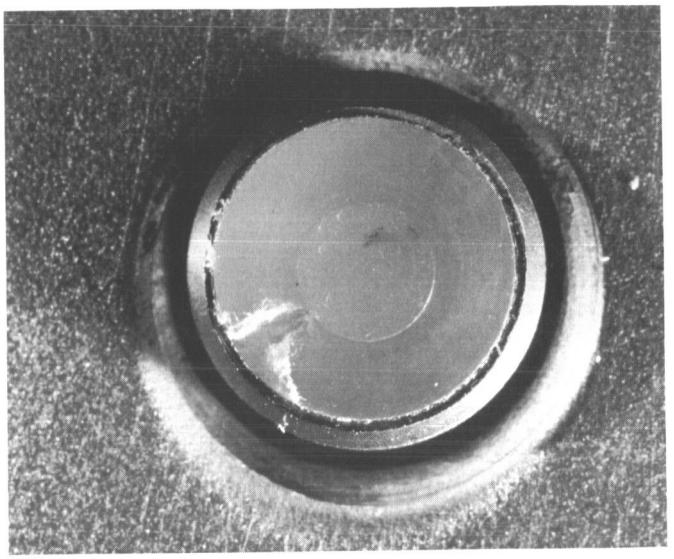

Fig. 25. JPL seat 4 used in the SN-2 regulator (0.0135-in.-diam hole 0.015 in. deep), shown after failure

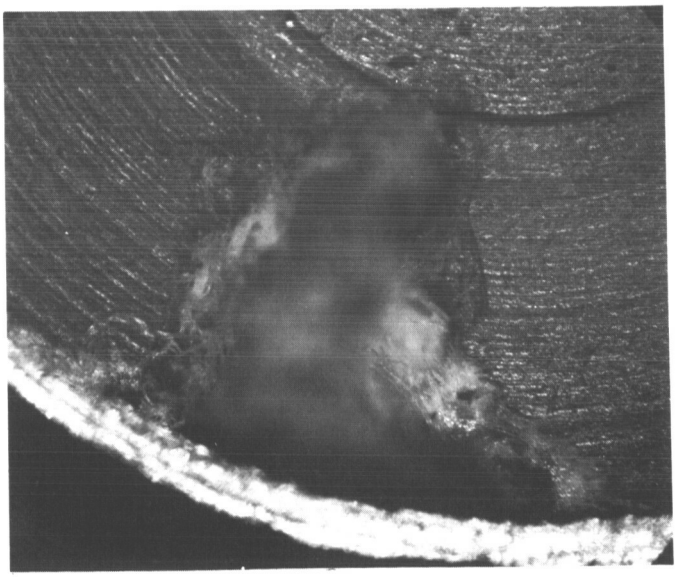

Fig. 26. Micrograph of JPL seat 4 used in the SN-2 regulator, showing detail of the failed region

Seats 5 and 6 (Figs. 27 and 28) each had indented into them with a needle four impressions; each impression was from 0.001 to 0.0015 in. (25 to 38 μ) in diameter and

Fig. 27. JPL seat 5 used in the SN-2 regulator (four 0.001-in.-diam holes 0.003 in. deep, indicated by arrows), shown after testing

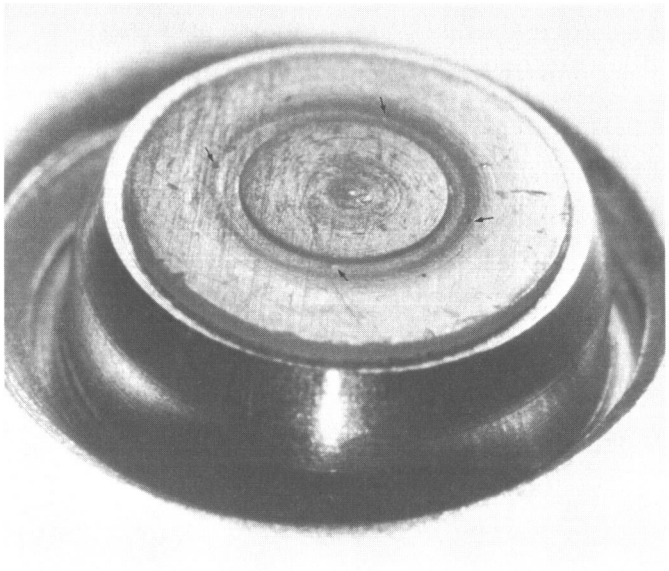

Fig. 28. JPL seat 6 used in the SN-2 regulator (four 0.001-in.-diam holes 0.003 in. deep, indicated by arrows), shown after being coined and tested

0.003 in. (76 μ) deep. Each indentation was placed in a separate quadrant to avoid interference effects; and each was a different distance from the center of the seat: 0.035, 0.040, 0.045, and 0.050 in., respectively. Seat 5 was tested without being first coined; seat 6 was coined before being tested; for each seat the antisurge valve was blocked. Neither seat failed.

Carleton Controls Corporation, manufacturer of the regulator, estimates their inspection procedure capable of resolving and rejecting seat surface imperfections of 5 μ or more.

Since surface imperfections five times the size of the rejection criteria of the manufacturer caused no change in regulator performance, it seems reasonable to conclude that surface imperfections of the regulator seat do not present a major cause for concern.

Table 11 shows the pressure levels at which the four failed seats ceased leaking after failure. Three seats failed due to contamination; the other was JPL seat 4 into which had been drilled a 0.0135-in.-diam hole 0.015 in. deep. Also presented for comparison are the lockup pressures for the particular regulator/seat combination involved and the relief valve unseating pressure. As can be seen, three of the four seats would have ceased leaking at a pressure less than the relief valve unseating pressure and not have resulted in an abnormal loss of high pressure

Table 11. Comparison of postfailure lockup pressures with relief valve unseating pressure

Regulator SN	Seat	Lockup pressure, psig	Postfailure lockup pressure, psig	Force applied to seat at postfailure lockup, lbf	Relief valve unseating pressure, psig
2	Original	800	—[a]	—	885
2	2	809	859	69	894
2	4[b]	806	870	88	891
3	Original	772	798	36	857

[a]Regulator SN-2 with the original seat failed to seal off at a downstream pressure level less than the relief valve unseating pressure.

[b]JPL seat 4 did not fail under the action of contamination. It had drilled into it prior to test a 0.0135-in.-diam hole 0.015 in. deep.

helium. It can be seen that the regulator is capable of healing large scale failures of the regulator seat due to the coining caused by the rise in downstream pressure.

e. Conclusions. As described above, comparison of photographs of the failed seats with a photograph of a contaminant impact on an unfailed seat leads to the conclusion that the seat failures observed in the first group of tests were initiated by the impact on the previously coined seat of contaminants ranging in size from 50 to 150 μ. Thus, it can be deduced that contamination is a necessary condition for failure of a regulator seat.

During testing it was not possible to cause a failure without first having coined the regulator seat. In fact, contamination was artificially introduced into the system and uncoined seats did not fail. Thus, we can infer that contamination alone is not sufficient to cause seat failure.

Tests also were performed on coined regulator seats where inadequate contamination was present to cause failure. Therefore, we can infer that coining of the seat alone is not sufficient to cause failure of the seat. However, since it was not possible to fail an uncoined regulator seat, we can infer that coining of the seat is a necessary condition for failure.

The one exception was in the second group of tests where a seat with a relative large hole drilled into the surface failed without coining or contamination. This is not considered to be a primary failure mode for SC-5, since voids of this size would have been detected during manufacturing inspection.

Sufficient testing has not been done to determine whether blocking of the antisurge valve is a necessary condition for failure or whether contaminants generated by removing and replacing this component were sufficient to cause failure of the regulator seat. Tests were also conducted which showed that surface imperfections on the regulator seat five times larger than allowed by the manufacturer had no effect on regulator performance.

Based on the above observations it seems reasonable to conclude that the failure of the SC-5 helium regulator to lock up was caused by the impact of a contaminant onto a previously coined regulator seat. The contamination could have been introduced during replacement of components in the helium system on the spacecraft. The regulator seat was probably coined during the oxidizer relief valve test phase of the VPS functional test performed at Cape Kennedy.

Changes in the VPS functional test procedure have precluded the use of a coined regulator seat on the SC-6 and -7 flight vehicles, thus removing one of the conditions shown by these tests to be necessary for a contamination failure of the regulator seat. Changes have also been made which reduce the possibility of introducing contamination into the helium system and test to verify system cleanliness after the VPS functional.

5. Thrust Chamber Assembly Solenoid Valves[3]

In November 1967 an experimental investigation was conducted at JPL to determine the effect of temperature on the pull-in voltage required to operate the solenoid valve, which admits helium to the propellant shutoff valve of the vernier engine thrust chamber assembly. Solenoid valve SN J-16, which is representative of the present series of flight valves, was used for these tests. The primary purpose of the investigation was to provide a basis for estimating pull-in voltage requirements for flight valves at temperatures up to 145°F.

The temperature range investigated was from 70 to 165°F. Temperature conditioning was accomplished by placing the solenoid valve in a small thermostatically-controlled oven. A chromel-alumel thermocouple was attached to the solenoid valve case. Helium at 720 to 730 psig was supplied at the valve inlet to simulate minimum pressure available at nominal flight conditions. At each temperature, the minimum required pull-in voltage was determined by gradually increasing the supply voltage until solenoid actuation occurred. The observed temperature change due to electrical heating during each measurement was less than 1°F.

Figure 29 shows the results of two runs conducted on different days. Up to 155°F, the highest voltage required for pull-in was 16 V. When temperature was increased to 165°F, however, the pull-in voltage increased to about 16.3 V.

The shape of the curve of Fig. 29 in the 70 to 150°F range is explained as follows: Increasing temperature increases the resistance of the solenoid coil; thus, the voltage required to provide a given current increases with temperature. However, the current required for this particular type of solenoid valve decreases when temperature increases, because thermal expansion of the nylon inlet valve seat insert in the armature causes a reduction of the magnetic gap of the solenoid.

[3]Prepared by JPL Section 384.

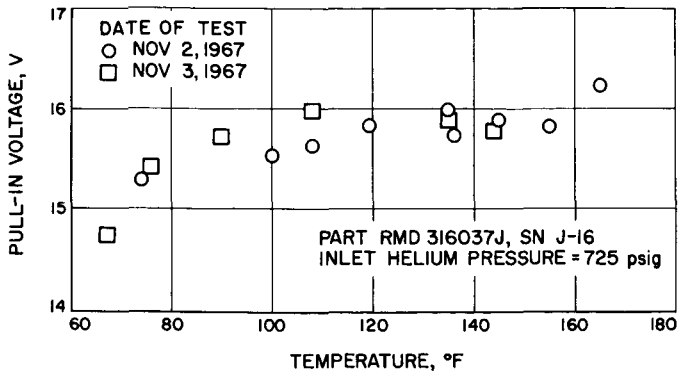

Fig. 29. Vernier engine solenoid valve pull-in voltage as a function of temperature

The slight rise of pull-in voltage at 165°F is attributed to softening of the nylon seat, which permits coining and thus retards the decrease of magnetic gap.

6. Loss of Oxidizer Pressure on *Surveyor V* after Landing on the Moon[4]

a. Introduction. Surveyor V successfully landed on the moon at 00:45:00 September 11, 1967. On landing, the oxidizer pressure was 575 psi rather than the normal 770 psi. The reduction resulted from a leak in the helium regulator valve, which developed approximately 18 h after launch during the first midcourse maneuver.

Helium began leaking through the regulator from a high pressure supply to the propellant tanks downstream. The downstream pressure increased from 770 to 825 psi, causing the oxidizer and fuel relief valves to open and begin venting helium to space. This continued until shortly before terminal descent when the helium tank pressure fell below 840 psi and the relief valves reseated.

During terminal descent, propellant was consumed and the ullage volume increased. The gas pressure fell to 575 psi. After landing, the tanks were heated by the sun for 7 days and oxidizer pressure rose to above 800 psi. On the seventh day, during the tenth hour, *Surveyor V* began to lose oxidizer pressure. The pressure dropped approximately 485 psi in the first 65 h. It continued to fall until it reached the vapor pressure of the liquid oxidizer. An analysis was then conducted to determine the cause of the pressure loss and whether such a failure could occur during the transit phase on future flights.

[4]Prepared by JPL Section 384.

b. Discussion. Surveyor V began losing oxidizer pressure 7 days and 10 h after successfully landing on the moon. The loss was accompanied by temperature drops in elements adjacent to the oxidizer tanks and lines on legs 1 and 2. These temperature changes were studied to determine if they had resulted from the leak. A ⅛ scale model of *Surveyor* and a collimated light source were utilized in the study.

The sun had just risen in the east when *Surveyor* landed on the moon. Leg 2 pointed towards the sun. It was just past noon when the leak started, and the sun was going down facing between legs 1 and 3. On September 18, at 01:57:00 GMT the solar panel was rolled 94 deg counterclockwise, exposing the leg 2 retroengine attach bolt, propellant tanks, propellant lines and vernier engine to the sun. Their temperatures increased. This is seen in Figs. 30(a), (b) and 31. Figures 30(a), (b) and 32 indicate that rolling the solar panel did not alter the shading on the leg 1 bolt, tanks, lines or engine, and that no temperature change is recorded. On the same day at 09:06:00 GMT the solar panel was rolled 123 deg clockwise. The leg 2 bolt, tanks, lines and engines were then shaded, and their temperatures dropped. This is seen in Figs. 30(c) and 31. Also note in Figs. 30(c) and 32 that there are no changes in leg 1 shading or temperatures. At approximately 10:00:00 GMT, the leg 1 retroengine attach bolt, oxidizer tank and oxidizer line dropped in temperature. At this same time the spacecraft began to lose oxidizer pressure. From spacecraft data it is observed that the retroengine attach bolt, located near the base of the oxidizer tank, dropped 20 deg F. The temperature of the oxidizer tank dropped 100 deg. The oxidizer line sensor, located approximately 1 ft from the base of the tank dropped 30 deg. There was no decrease in temperature noted on the leg 1 engine, fuel tank or fuel line.

In assessing the temperature drops it is noted that, if liquid oxidizer is leaking into vacuum, it will vaporize. If helium and oxidizer vapor are leaking into vacuum the helium remaining in the tank will undergo expansion, and the oxidizer vapor will be replaced by liquid vaporizing and permeating the teflon bladder. Vaporizing liquids and expanding gases absorb heat and cool contact surfaces. Since there were no shadows passing over leg 1 during this period, a change in shading could not have caused the temperature drops. They must have been the result of the oxidizer leak.

At 14:42:00 GMT on September 18, the solar panel was rolled 123 deg counterclockwise, reexposing leg. 2. As noted in Figs. 30(d) and 31, the leg 2 bolt, tanks, lines and engine temperatures increased accordingly. After

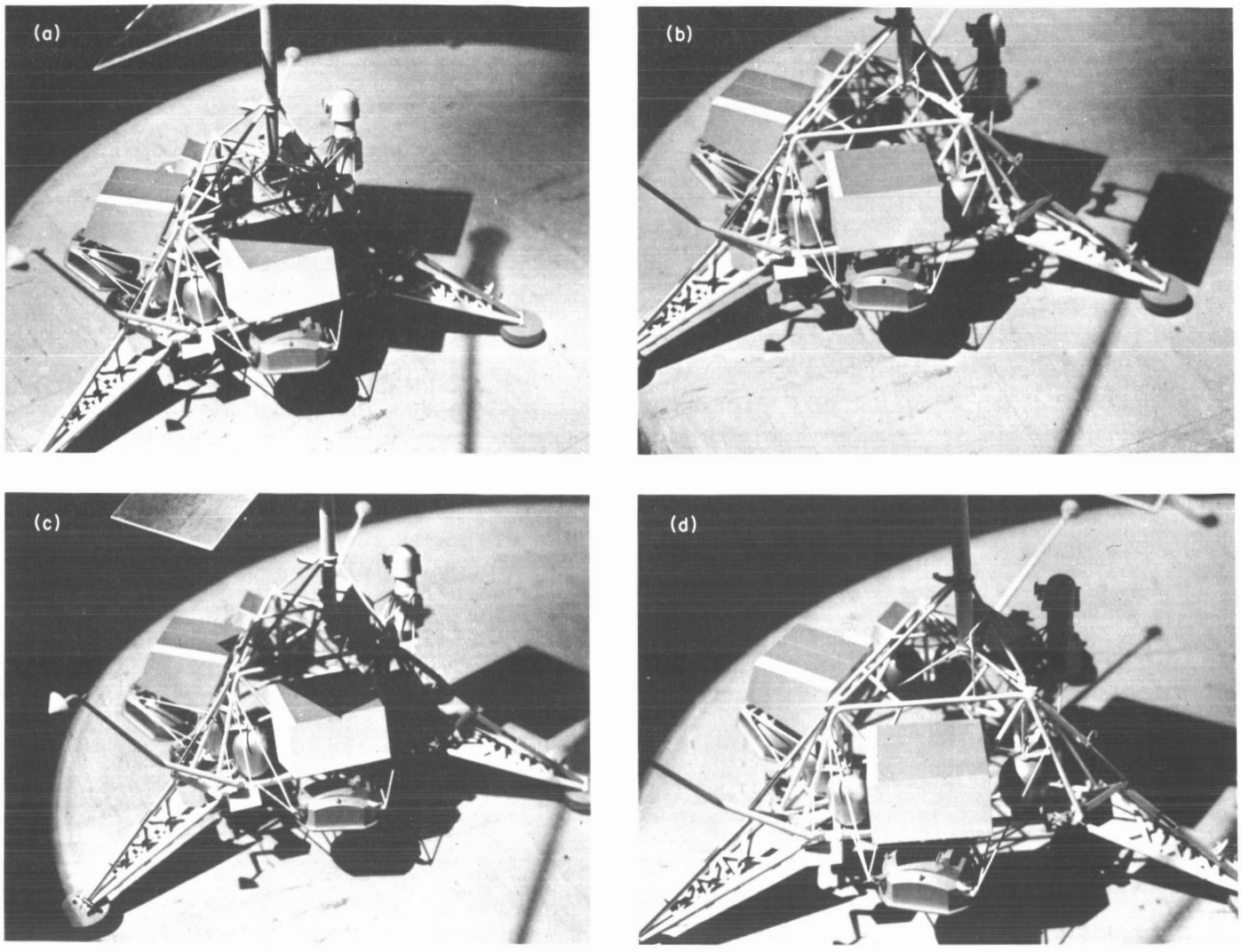

Fig. 30. Shadow pattern on legs 1 (on left) and 2 utilizing a one-fifth scale model, a columnated light source and corrected sun angles; (a) 23:16 GMT, Sept. 17, 1967, A/SPP roll angle +69.48 deg; (b) 01:57 GMT, Sept. 18, 1967, A/SPP roll angle −25.46 deg; (c) 09:06 GMT, Sept. 18, 1967, A/SPP roll angle +97.58 deg; (d) 14:42 GMT, Sept. 18, 1967, A/SPP roll angle −25.46 deg

several hours the leg 1 bolt, oxidizer tank and oxidizer line temperatures also increased in temperature. The retro-engine attach bolt temperature recovered to a value equal to that before the leak. The oxidizer tank recovered to within 30 deg and the oxidizer line to within 20 deg of those temperatures recorded before the leak.

It is shown below that the magnitude of the temperature drop on oxidizer tank 1 indicates that a liquid leak occurred.

It is therefore expected that the tank temperature would increase after the liquid had been depleted. The net drop in the oxidizer tank equilibrium temperature could be indicative of a small, continuing liquid leak or of changing thermal properties, such as a decrease in conductance between the mylar insulation and the walls of the tank. This might result from a tear in the mylar insulation at the base of the oxidizer tank or might result from expanding vapors being trapped between the walls of the tank and the mylar insulation, causing the latter to inflate and thus decrease the contact surface. Both might result from an oxidizer leak at the base of the oxidizer tank 1. Evidence that the latter did occur is given in Figs. 33 and 34. Heat loss from the line to the tank would account for the net decrease in line temperature.

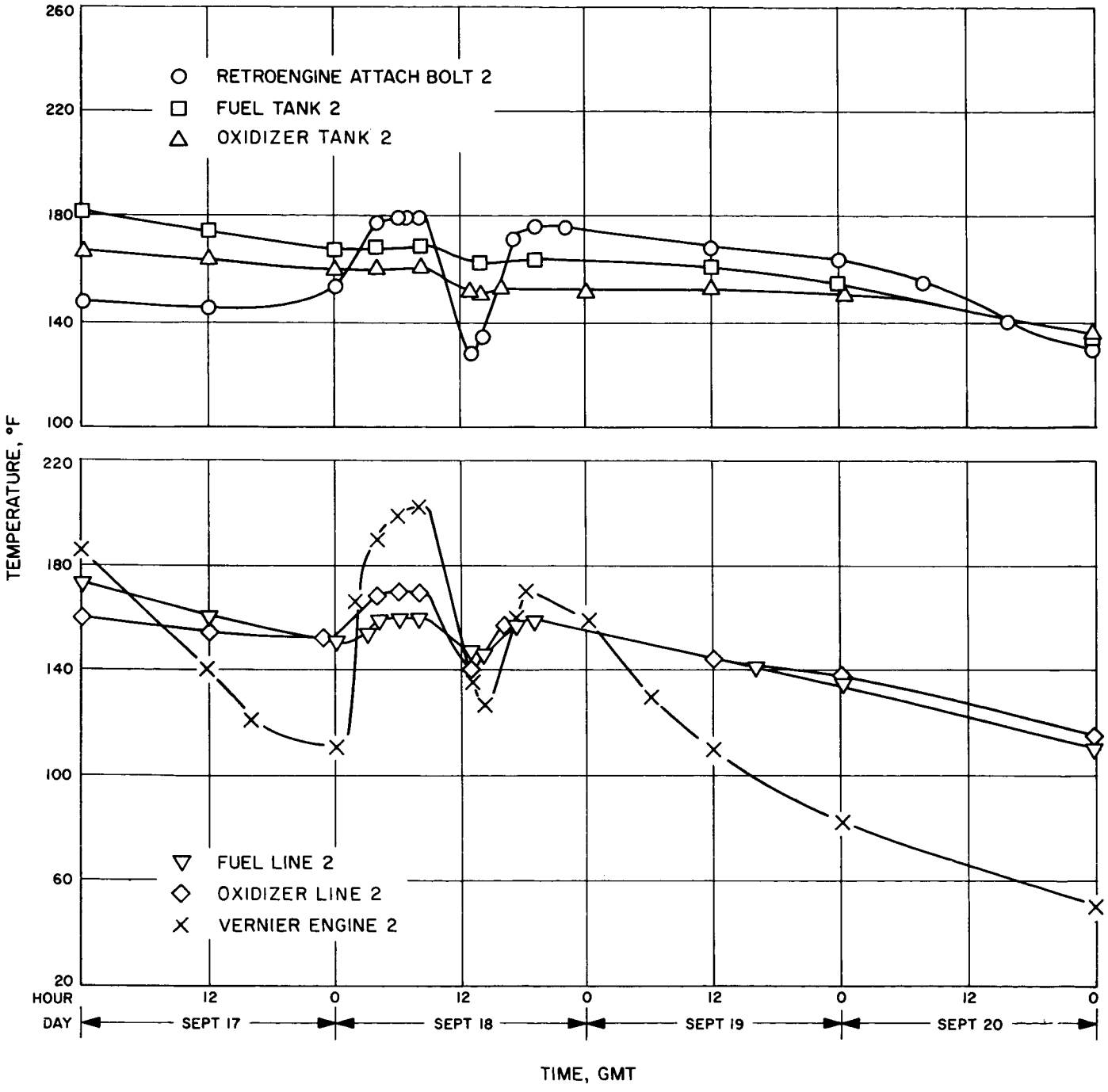

Fig. 31. Leg 2 temperatures during oxidizer leak

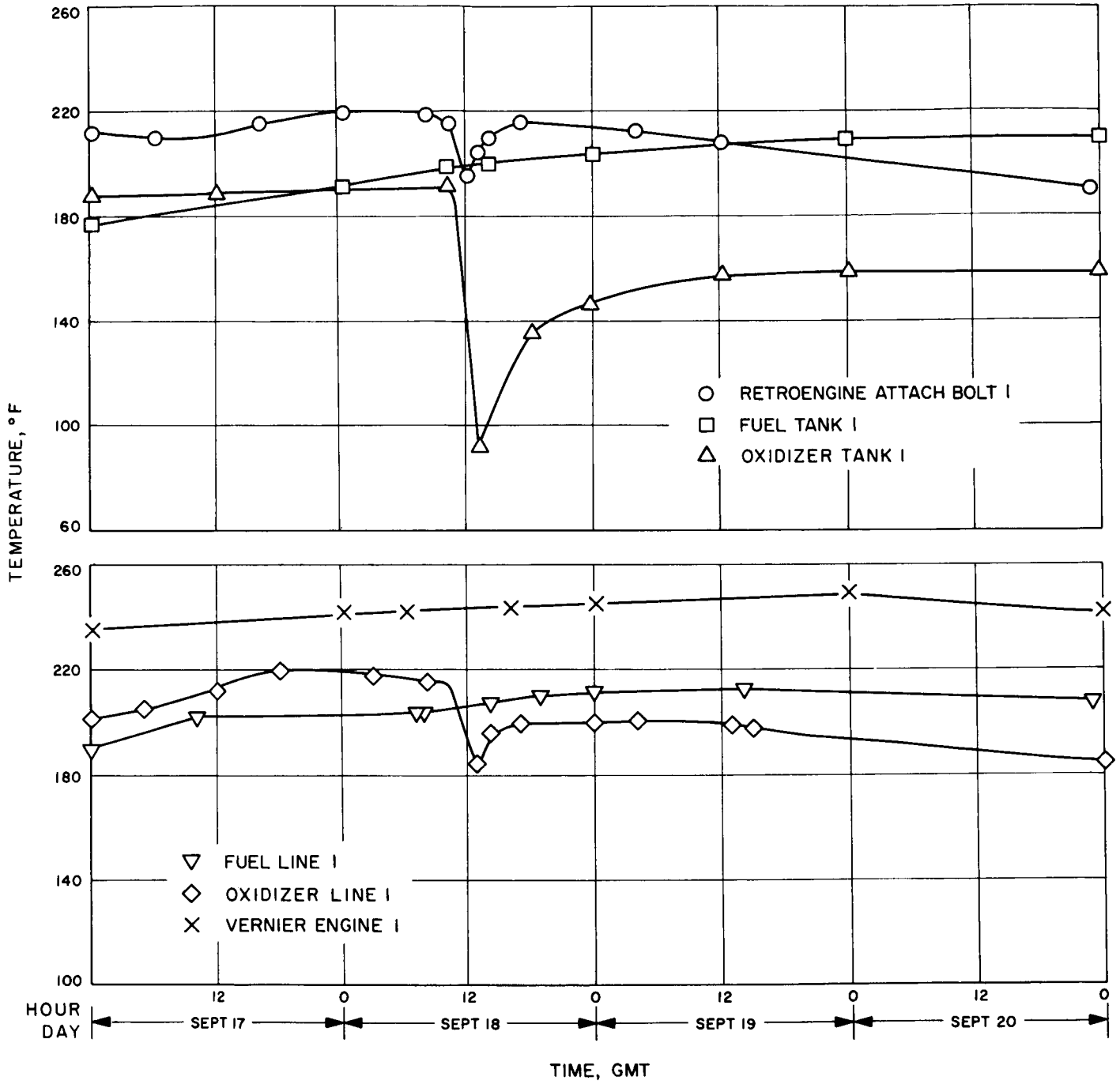

Fig. 32. Leg 1 temperatures during oxidizer leak

Apparently the leak was a liquid leak and not a gas leak. This is indicated by the magnitude of the temperature drop and the fact that the oxidizer pressure had not yet reached the vapor pressure of the liquid when the cooling occurred. Oxidizer pressure is measured by a sensor mounted on oxidizer line 3. The sensor measures the pressure in the line and in oxidizer tank 3. It is also an accurate indicator of the pressure in oxidizer tanks 1 and 2, providing the pressure does not fall below the vapor pressure in either tank, causing the liquid to vaporize and the bladders to expand against the pressurization ports at the top of each tank. If a bladder is forced against a pressurization port, the pressure in oxidizer line 3 is no longer representative.

During the period when oxidizer tank 1 dropped 100°F in temperature, the pressure dropped from 815 to 700 psia, remaining well above the tank 1 vapor pressure of 320 psi. Approximately 8 lb or 151 in.^{3} of liquid oxidizer remained in each oxidizer tank prior to the leak. If the liquid oxidizer were removed from a tank, that tank's thermal capacity would be reduced by 78%. Oxidizer tank 1's temperature dropped 100°F. If most of the liquid oxidizer had already leaked from the tank, the cooling could have resulted from 9 in.^{3} of liquid being trapped in the tank and subsequently vaporized. This is not an unreasonable amount. However, if the leak were a gas leak, the bulk of the liquid would remain in the tank. The oxidizer would vaporize and permeate the bladder to replace the oxidizer vapor being lost due to leakage. Because of the tank's greater mass and thermal capacity, the cooling observed would require that at least 40 in.^{3} of liquid oxidizer be vaporized.

From tank 1 pressure and temperature data, analysis indicates that <4 in.^{3} of liquid oxidizer would vaporize and permeate the bladder during the period when tank 1 temperature dropped 100°F. This is $< 1/10$ of that necessary to explain such a temperature drop. Also, if this were the failure mechanism, similar cooling would be expected on the remaining oxidizer tanks and lines. None was noted on oxidizer tank 3 or line 3. The leak was, therefore, not a gas leak but a liquid leak. At the time of the leak, the engine 1 temperature sensor read 244°F. The temperatures near the head end of the engine and of the adjacent oxidizer line were approximately 280°F. The vapor pressure at this temperature is 1200 psia. Since the oxidizer pressure was only 815 psia, all oxidizer in the engine and adjoining sections of the oxidizer line must have been in the vapor phase. The temperatures of the oxidizer tank and adjoining line were 190° and 215°F, respectively. The vapor pressure at 190°F is 320 psia. The vapor pressure at 215°F is 500 psia. The oxidizer in this region must have been in the liquid phase.

If the leak occurred near the engine, liquid oxidizer would have been forced from the tank and upstream portions of the oxidizer line to the engine. The liquid would boil, and the engine would drop in temperature. Since no change in engine temperature was observed, the leak must have occurred near the base of the oxidizer tank. As such, the expanding vapors in the engine would push the liquid-vapor interface upstream as the pressure dropped. Since no liquid oxidizer would come in contact with the engine and since no significant cooling would result from the expansion of oxidizer vapors, no engine temperature drop would be expected.

There are four fittings near the base of oxidizer tank 1, where a leak could have occurred. One of these would result in a gas leak and the three others would result in liquid leaks. A gas side O-ring seal is positioned between the inside walls of the tank and a Teflon bladder which contains the liquid oxidizer. A liquid side O-ring is positioned between the inside of the bladder and the base of a standpipe, which supports the bladder inside the tank. Both O-rings are made of a Viton A rubber compound. Both seals are located at the base of the tank. If a leak occurred through the gas side O-ring it would be a gas leak. As shown above, the leak was not a gas leak but a liquid leak. If it occurred through the liquid side O-ring it would be a liquid leak. Located just below the O-ring seals are a fill and discharge port to which the oxidizer line is connected, and a fill and vent valve. A liquid leak could have occurred at any of these three fittings. However, based on component reliability histories, the liquid side O-ring is by far the most suspect.

A study of pictures taken by *Surveyor V* of oxidizer tank 1, confirms that the leak did occur at the O-ring seal. Figures 33 and 34 are pictures of the mylar wrap covering oxidizer tank 1. A dimple present before the leak in Fig. 33 is no longer in evidence after the leak in Fig. 34. The pictures indicate that the mylar wrap had been inflated from within, smoothing the dimple and surrounding creases. No other changes in the mylar wrap, except the one which occurred at the time of the leak, have been noted. The mylar is wrapped around the oxidizer tank and tucked at the base of the tank to enclose the O-ring seal. The fill and discharge port and fill and vent valve are separately wrapped. A leak from the O-ring seal would result in inflating the mylar wrapped around the tank. A leak from the latter two fittings would not.

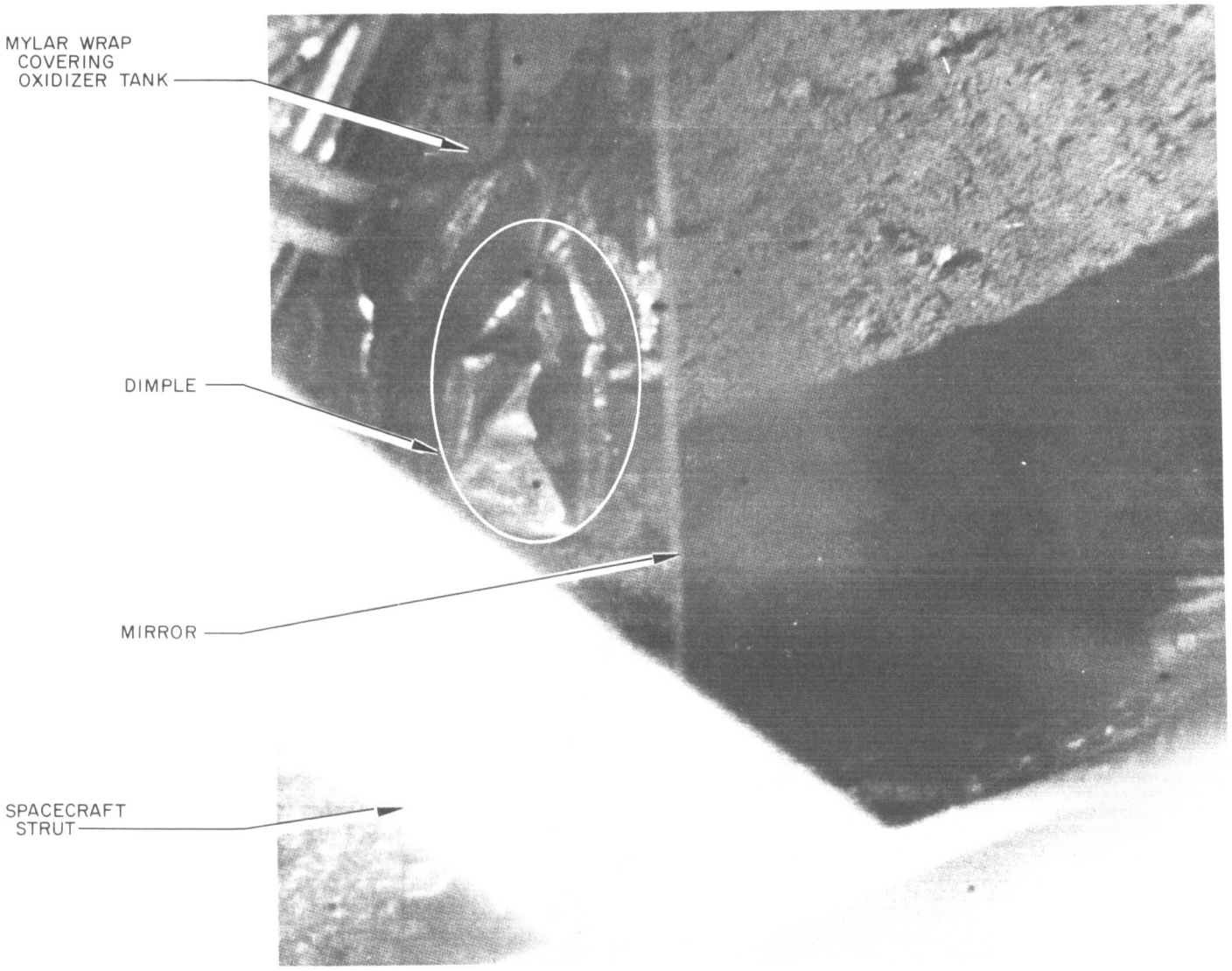

Fig. 33. *Surveyor* photograph of oxidizer tank 1 showing dimple before leak occurred

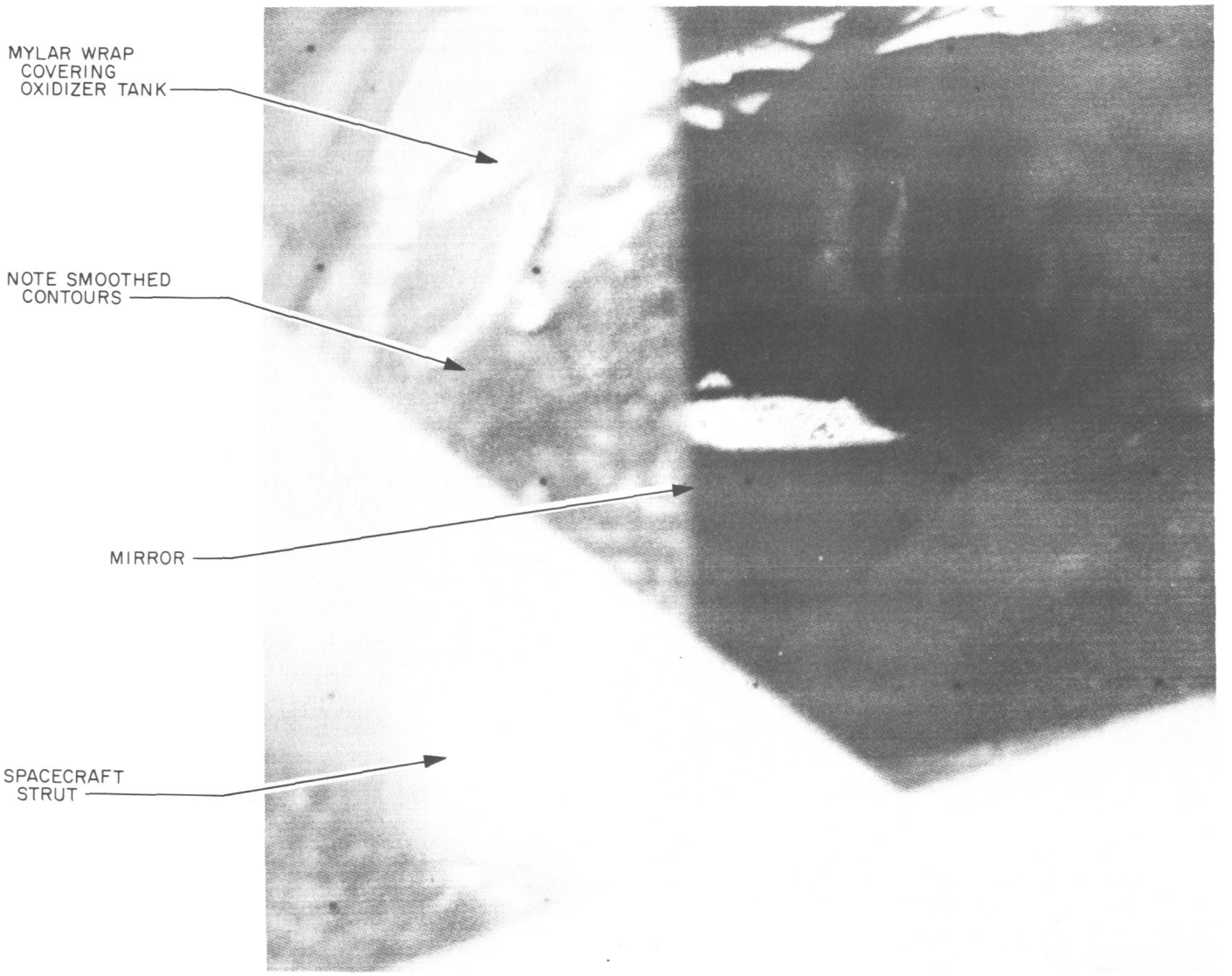

Fig. 34. *Surveyor* photograph of oxidizer tank 1 showing that dimple disappeared following leak

It is concluded that liquid oxidizer leaked through the O-ring seal, that the oxidizer vaporized, inflated the mylar wrap and cooled portions of the tank, line and retro-engine attach bolt. As the liquid in oxidizer tank 1 was depleted, the bladder collapsed around the standpipe, and a pressure gradient developed across the bladder. Liquid trapped in the folds of the bladder, in the inner tube of the standpipe, and in adjacent sections of the oxidizer line boiled once the pressure fell below the vapor pressure of the liquid. This further cooled the oxidizer tank and oxidizer line. The helium and oxidizer vapor remaining in oxidizer tanks 1, 2 and 3 began to permeate the tank 1 bladder and leak through the O-ring at the base of the standpipe. Both helium and oxidizer pressure continued to fall. Based on these findings, tests to determine the O-ring's compatibility in MON-10 were authorized and completed at JPL and HAC. The O-rings are made of a Viton A rubber compound. The tests have demonstrated that the O-rings are severely degraded after 7 days exposure to MON-10 oxidizer at temperatures similar to those seen by the O-ring on oxidizer tank 1 prior to the leak. Also, the rings decompose at temperatures approaching 200°F. Figures 35–37 are enlarged views of three O-ring samples. Table 12 tabulates test data and results.

The sample in Fig. 35 has not been exposed to MON-10. The sample in Fig. 36 was exposed to MON-10 liquid for more than 150 h at ambient temperatures. Some pitting occurred, and there was a 19% reduction in tensile

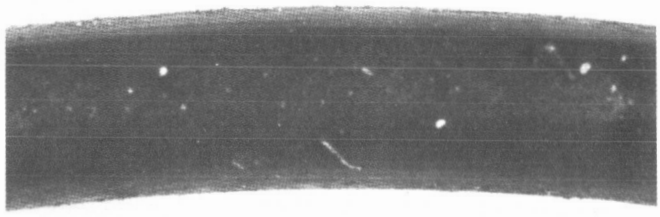

Fig. 35. Enlarged view of unexposed O-ring sample (sample 1)

Fig. 36. Enlarged view of O-ring sample exposed to MON-10 liquid for approximately 7 days at ambient temperature (sample 5)

strength. Figure 37 illustrates a sample which has been exposed to MON-10 liquid for a similar period of time but at higher temperatures than the sample in Fig. 36. Temperatures were increased from 70° to 160°F. The sample has been severely degraded. Tests indicate an approximate 80% reduction in tensile strength. *Surveyor V* oxidizer tank 1 temperature rose from 70° to 190°F over a similar time interval. It is, therefore, concluded that the O-ring failed because of its prolonged exposure to MON-10 at high temperatures.

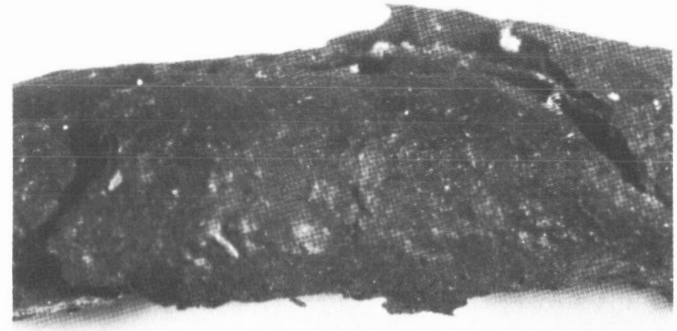

Fig. 37. Enlarged view of O-ring sample exposed to MON-10 liquid for approximately 7 days at temperatures ranging from 70° to 160°F (sample 2)

c. Conclusion. *Surveyor V* began losing oxidizer pressure 7 days after its successful landing on the lunar surface. This was caused by liquid oxidizer leaking through an O-ring seal positioned between the standpipe and bladder at the base of oxidizer tank 1. A temperature drop in the leg 1 oxidizer tank and adjacent components indicates that the leak occurred near the base of oxidizer tank 1. An inflated mylar insulation indicates that the leak probably occurred at either the gas side O-ring located between the base of the tank and the bladder or at the liquid side O-ring located between the bladder and the base of the standpipe. Both are enclosed within the mylar insulation tucked and secured at the base of the tank.

The magnitude of the temperature drop and the fact that the pressure never dropped below the vapor pressure of the liquid indicate that the leak must have been a liquid leak. Therefore, the leak occurred at the liquid side O-ring seal. Tests recently completed indicate that

Table 12. The effect on tensile strength in exposing a Viton-A O-ring to MON-10 at high temperatures

Sample	Time soaked at constant temperature, h					Tensile strengths	
	70°F	100°F	130°F	160°F	Other	Tensile force at rupture, lb	Reduction in tensile strength, %
1	0	0	0	0	0	6.30	—
2	66	48	26	≈10	0	1.16	81.6
3	66	48	26	≈10	0	1.32	79.0
4	66	48	26	≈10	0	1.20	81.0
5	184	0	0	0	0	5.1	19.0

the O-rings are only mildly affected by MON-10 at ambient temperature, but are significantly degraded at temperatures approaching those seen by the O-ring which failed on *Surveyor V*.

It is concluded that the failure resulted from the O-ring's prolonged exposure to MON-10 at high temperatures. Because no such temperatures are experienced until the spacecraft lands on the lunar surface, the anomaly has no significance to spacecraft performance during the transit phase of future flights. However, this analysis does indicate that an O-ring's exposure to high temperatures has become a new constraint in predicting the maximum probable time that the vernier propulsion systems on *Surveyors VI* and *VII* can be exposed to the hot environment of a lunar day and still be expected to function.

D. Deep Space Network Operations

1. Mission E Second Lunar Day and Mission F Operations

a. Pioneer deep space station. During operations for the *Surveyor V* second lunar day, Goldstone transmitted 7141 commands and received 356 television frames. Attempts to revive *Surveyor V* on the third lunar day were unsuccessful.

During mission F, Goldstone provided support for 18 passes, including midcourse maneuver, terminal descent, and lunar day and night operations. The midcourse maneuver portion was executed without any problems, and the spacecraft remained stable and completely controllable. The terminal descent and touchdown sequences were standard. The station was then reconfigured for television and 24 pictures were taken in the 200-line mode. During the remainder of the lunar day, activity at Goldstone included 600-line TV operations, alpha scattering data accumulation, and engineering interrogations. At 10:35:00 GMT on November 17, Goldstone controlled the spacecraft through a successful 8-ft lateral translation.

b. Tidbinbilla deep space station. Canberra initiated mission E second lunar day operations by reviving *Surveyor V* in the first attempt. The signal level was measured at −120 dBmW; subsequent interrogations confirmed that the spacecraft had survived its first lunar night in excellent condition. The solar panel was positioned, and a charge current of 1.3 A obtained. During the mission E second lunar day, Canberra transmitted 2439 commands and accumulated 210 min of alpha scattering data. Attempts to revive *Surveyor V* on the third lunar day were unsuccessful.

During mission F, Canberra provided support for 19 passes, including commanding for the 600-line TV pictures. During the lunar phase of the mission, the station commanded the spacecraft through TV operations, alpha scattering data accumulation, and engineering interrogations.

c. Johannesburg deep space station. The Johannesburg station did not participate in the mission E second lunar day operations; however, the station was committed to revive *Surveyor V* for its third lunar day. This proved unsuccessful.

Johannesburg provided support for the three mission F transit phase passes, including initial acquisition operations.

2. Special Deep Space Instrumentation Facility Station Test, Operations, and Training

a. Mission E second and third lunar days and mission F operations. Madrid participated in the mission E second lunar day operations by commanding and receiving 251 television pictures and performing engineering interrogations. During this period, over 8236 commands were transmitted from this station prior to suspension of operations for the second lunar night. Madrid also participated in the *Surveyor V* revival attempts during its third lunar day. During mission F, this station provided support for 19 passes.

Cape Kennedy support for mission F consisted of a DSIF spacecraft compatibility test, an operational readiness test, a prelaunch countdown phase, and a postlaunch phase lasting through the first 40 min of the flight.

Ascension Island was not committed for mission F.

E. Thermal Engineering

1. Solar Thermal Vacuum Test Support

Thermal performance for STV phases 1A, 2A, 1B, and 4B for SC-7 is summarized in Table 13.

No thermal anomalies occurred during the tests. The larger heater in the SM/SS electronics compartment (7.8 W on SC-7 and 5 W on *Surveyors III* and *IV*) was sufficient to maintain the compartment at the desired level of 0°F.

The first SC-7 STV mission sequence (phase 1A) was performed at high sun beginning at 20:00:00 September 20. The phase was to be a 68-h real-time mission simulation; however, after 32 h and 40 min, it was aborted because of transmitter problems.

The second SC-7 STV mission sequence (phase 2A) was performed at high sun intensity beginning at 03:00:00 September 27. This phase was a simulated 68-h mission sequence followed by TV, alpha scattering, and soil mechanics tests.

Table 13. Thermal performance summary

Flight sensor location by subsystem	Sensor code	Coast phase steady-state temperature, °F			
		SC-7			
		Phase 1A high sun	Phase 2A high sun	Phase 1B low sun	Phase 4B low sun
Vehicle and mechanisms					
Compartment A					
Upper tray	V-15	[a]	54	62[a]	52
Lower tray	V-16	[a]	66	84[a]	66
Transmitter A	D-13	[a]	51	60[a]	51
Transmitter B	D-14	[a]	53	58[a]	48
Main battery	EP-8	[a]	68	91[a]	68
Battery charge regulator	EP-34	[a]	72	89[a]	72
Radiators					
No. 5	V-20	[a]	30	34[a]	26
No. 8	V-25	[a]	25	39[a]	12
No. 2	V-47	[a]	12	21[a]	− 8
No. 3	V-49	[a]	− 34	41[a]	−162
Compartment B					
Upper tray	V-21	[a]	90	68[a]	68
Lower tray	V-22	[a]	93	71[a]	71
Boost regulator	EP-13	[a]	95	73[a]	73
Radiators					
No. 4	V-24	[a]	66	44[a]	44
No. 1	V-45	[a]	74	50[a]	50
No. 5	V-46	[a]	63	39[a]	38
Landing gear assembly					
Crushable block	V-44	− 26	− 28	− 53	− 50
A/SPP mechanism					
Solar panel drive	M-10	75	76	45	62
Elevation axis drive	M-12	− 18	− 17	− 41	− 53
Spaceframe and substructure					
Upper spaceframe					
Near leg 1	V-27	92	94	58	60
Near leg 2	V-35	− 67	− 66	− 85	− 85
Lower spaceframe					
Under compartment B	V-28	62	63	33	35
Under compartment A	V-36	− 15	− 14	− 37	− 30
Retroengine attach points					
Leg 1	V-37	55	52	24	28
Leg 2	V-38	− 35	− 39	− 56	− 53
Leg 3	V-39	64	64	33	36
Propulsion					
Vernier engine thrust chamber assembly					
1	P-7	83	84	48	49
2	P-10	86	86	50	49
3	P-11	80	86	46	45

Table 13 (contd)

Flight sensor location by subsystem	Sensor code	Coast phase steady-state temperature, °F			
		SC-7			
		Phase 1A high sun	Phase 2A high sun	Phase 1B low sun	Phase 4B low sun
Propellant tanks[a]					
Oxidizer 1	P-15	—	68/45[b]	—	74/36[b]
Fuel 1	P-13	—	69/57	—	74/48
Oxidizer 2	P-16	—	67/19	—	73/26
Fuel 2	P-5	—	68/19	—	74/26
Oxidizer 3	P-6	—	68/45	—	75/49
Fuel 3	P-14	—	69/57	—	74/49
Propellant lines					
Leg 1					
Oxidizer line 1	P-8	46	45	25	26
Fuel line 1	P-23	60	60	45	46
Leg 2					
Oxidizer line 2	P-4	21-24	21-24	20-24	20-24
Fuel line 2	P-24	32	20-25	13-17	23
Leg 3					
Oxidizer line 3	P-9	38	33	20-23	20-23
Fuel line 3	P-25	70	79	51	51
Helium tank	P-17	96	98	63	64
Flight control					
Flight control electronics					
Chassis board 1	FC-44	84	86	65	65
Chassis board 6	FC-45	74	76	57	57
Canopus sensor	FC-47	86	90	63	65
Roll gyro	FC-46	177	177	175	176
Pitch gyro	FC-54	175	175	173	176
Yaw gyro	FC-55	175	175	173	178
Roll actuator	FC-71	104	105	69	71
Nitrogen tank	FC-48	75	74	42	44
Radars					
RADVS					
Klystron power supply modulator	R-8	37	39	9	10
Signal data converter	R-9	76	77	44	44
Velocity sensor preamplifier	R-10	22	23	− 7	− 6
Altimeter velocity sensor preamplifier	R-13	29	31	0	2
Altitude marking					
Electronics	R-7	17	17	17	16
Electronic platform	R-6	− 2	− 3	− 4	− 2
Alpha scattering system					
Alpha scattering head	AS-3	49	50	19	19
Alpha scattering electronics	AS-4	− 24	− 24	− 45	− 39
SM/SS					
Auxiliary electronics	SS-12	− 3	− 5	− 8	− 12
Retraction motor	SS-14	−139	−141	−154	−155
Elevation motor	SC-15	−141	−143	−155	−155

Flight sensor location by subsystem	Sensor code	SC-7 phase 1A		SC-7 phase 2A		SC-7 phase 1B		SC-7 phase 4B	
		Steady state	Preoperation warmup	Steady state	Preoperation warmup	Steady state	Preoperation warmup	Steady state	Preoperation warmup
Television									
TV 3 mirror	TV-17	−128	DNA	−137	0	−155	0	−147	−4
TV 3 electrical conversion unit	TV-16	−135	DNA	−131	0	−149	−4	−125	−4

[a]Temperature did not reach steady state.

[b]Denotes temperatures at launch and touchdown.

The third SC-7 STV mission sequence (phase 1B) was performed at low sun intensity beginning at 22:00:00 September 30. This phase was aborted after 50 h and 18 min due to nonthermal malfunctions.

The fourth and last SC-7 STV mission sequence (phase 4B) was performed at low sun intensity beginning at 03:00:00 October 9. This phase consisted of an abbreviated (53 h and 46 min) transit mission sequence. Subsequent to the low-intensity test, a second 15 h and 24 min test was conducted at high intensity, during which time special TV, alpha scattering, and soil mechanics testing took place.

2. Thermal Performance Data for Mission F

The thermal response of *Surveyor VI* throughout the transit phase and lunar day was excellent with the two exceptions indicated below.

a. Vernier line 1 transit thermal behavior. *Surveyor VI* transit thermal data indicate that the quasi-steady state temperature of vernier oxidizer line 1 was approximately 20°F warmer than predicted. Preflight thermal predictions indicated that the vernier line 1 temperature sensor (P-8) would exhibit a quasi-steady state temperature of 30°F; however, the actual quasi-steady state temperature exhibited by the sensor (P-8) was 51°F.

A comparison of the flight data (mission F) and data obtained during *Surveyor VI* STV tests suggests that the peak temperature exhibited by the line during transit was 105°F. The vernier lines upper temperature limit during transit is 110°F; hence, the line upper temperature limit was not violated during the transit mission phase.

Examinations of the vernier line 1 thermal control system have not produced any evidence of a malfunction with the system. Telemetry data indicate that the line heater remained off throughout the transit mission phase. Subsequent to lunar touchdown, the vernier line heater cycled; therefore, the probability of the line heater remaining on during transit is remote. Other possible causes have been investigated and found to be equally remote. The reason for this behavior is not understood at this time.

b. Closed thermal switches on compartments A and B during lunar night. In the first 36 h of the first lunar night of mission F, all nine thermal switches on compartment A and two thermal switches on compartment B failed to open. Three of the stuck switches in compartment A and one additional switch in compartment B are believed by thermal analysis to have opened prior to spacecraft shutdown. Since corrective switch design changes are impractical at this time, analyses have been initiated to predict the effect of stuck switches on SC-7's cooldown and warmup characteristics, with the number of stuck switches as a parameter. These analyses will be used by operations personnel in the event SC-7's switches do stick.

V. Future Projects

ADVANCED STUDIES

A. Introduction

The Advanced Studies Office is responsible for the direction, sponsorship, and, in cooperation with other elements of the Laboratory, the origination of advanced mission and future project studies in the areas of interest and applicability to the Laboratory.

The objective of this effort is to insure that the preliminary technical information and plans for the various potential missions, together with the associated information on spacecraft systems, instrumentation systems, launch vehicle systems, resources, and schedules be available as required. This preliminary mission study information will be used primarily for defining specific flight mission programs and as generalized guidance for Laboratory research and advanced development programs.

Each study conducted by this Advanced Studies Office has been, and will continue to be, documented in a formal final report. This section of the Space Programs Summary is allocated to provide an abstract or summary of the results of each study, including, where appropriate, reference to the final report for additional details.

B. A Program Analysis for Lunar Exploration

At the request of the NASA Office of Space Sciences and Applications and the NASA Office of Manned Space Flight, JPL has been making studies to determine the most effective manner in which the required objectives for lunar exploration can be accomplished, to derive a total exploration program in terms of a mix of specific projects and missions, to identify priority goals, and to help define needed developments. This article presents a resume of the results of this continuing task.

Using the Space Science Board's reasoning and the associated 15 questions (Ref. 1) as a basis, the first step in the scientific part of the study was to devise a rationale that would display logical sequences of investigation. This work resulted in the chart shown in Fig. 1. On this chart there are identified a number of major lines of investigation, each proceeding through characteristic phases ranging downward from initial or gross measurements to later, more refined investigations. The phases are, of course, somewhat related to assumed advances in technology, but they also reflect the intrinsic ordering of any sequential scientific investigation. In the present study we have confined our attention mostly to the early phases, since these are the ones now influencing program decisions, and also since the needs of the later phases are naturally more uncertain at this time.

The next step was to write down sets of measurements that could yield the data required for each phase of each investigation. Of course, some arbitrary choices were

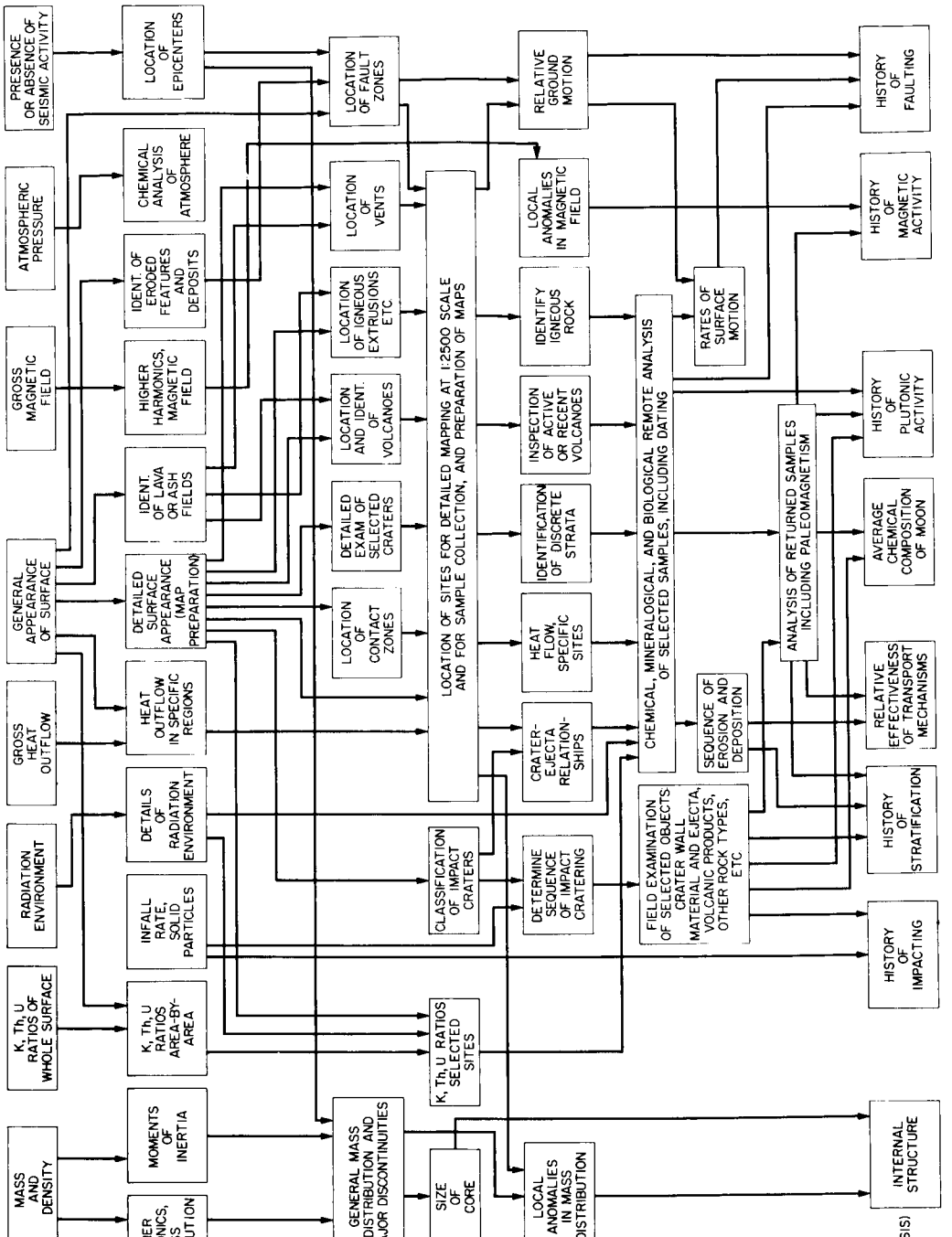

Fig. 1. Major lines of investigation

needed here, since, for example, we could not know in advance how many measurements of a given phenomenon would be needed for a full understanding of it.

The next step in the study was to identify priority requirements. Up to this point we had been considering a program dedicated to answering all recognized lunar questions, without any ordering except that imposed by the investigative logic itself. To be useful for program planning, the study should yield a more selective output. Rather than trying to weigh the relative merits of the several scientific disciplines, we elected to consider the questions and measurements in four categories:

(1) Critical data (priority A).

(2) Cosmogony (priority B).

(3) Exobiology (priority C).

(4) Astrogeology (priority D).

These categories are arranged in priority from the specific goals of lunar science to more general goals. "Critical data" refers to that group of experiments whose results are needed for effective planning of a continuing program. These experiments belong in general to Phase 1 in Fig. 1. For example, an early indication of the presence or absence of seismic activity is essential for planning the lunar seismological program.

"Cosmogony" refers to those lunar questions and measurements which bear on the moon's history and constitution as a planetary body. These measurements are accorded high priority because they may yield information pertinent not only to the moon itself, but also to the origin and evolution of the planetary system. In view of their special importance, these planetological measurements became the subject of a separate study within the JPL effort.[1] The results of this study and their implications are discussed further below.

"Exobiology" refers to the class of experiments that can be done on the moon in support of either techniques or theories in the search for extra-terrestrial life. It is ranked third on our list, not because its intrinsic interest is low, but because the moon is expected to be a less rewarding target than other bodies for at least the early phases of the exbiology investigation.

"Astrogeology" is used here in a restricted sense, to refer to missions in the late, detailed, and extensive phases of a program, similar to the fine-scale mapping and exploitation of unpopulated regions on earth.

By using these categories as a guide, it is possible to place the various investigations in approximate priority order, and then to see whether or not a candidate flight program results in timely achievement of the most urgent measurements.

As mentioned above, special attention has been given to the planetological investigations. This was done, not only because both theory and observation indicate that the moon itself may yield important planetological clues, but also because the results of lunar experiments may be critically important in planning investigations on other planets. Five main questions were identified pertaining to the possible evolutionary paths of the solar system.[1] These questions are as follows:

Q-1. Are the present individual planets and satellites chemically uniform or non-uniform?

Q-2. Did final accretion result in the present array of planets and satellites, or in a collection of bodies that were subsequently modified to yield the present array?

Q-3. Was the (circumsolar) dust cloud homogeneous at the time of final accretion?

Q-4. What was the state of the sun–cloud system when it first appeared as a recognizable entity?

Q-5. Were there large-scale elemental and isotopic non-uniformities in the (initial) contracted nebula?

The lunar investigations which bear most directly on these evolutionary questions are:

(1) Investigation of moon's gross shape and mass distribution, including core, if any.

(2) Investigation of heat flow, magnetism, and interaction with particle-and-field environment.

(3) Investigation of moon's isotopic, chemical, and mineral composition.

The relationships between the major lines of investigation and the five evolutionary questions can be seen in Figs. 2 through 6. Fundamental to all investigations is an adequate mapping program to confirm the validity and show the interrelations of the other measurements.

[1]Adams, J., et al., "A Strategy for Scientific Exploration of the Terrestrial Planets," *Rev. Geophys.* (to be published).

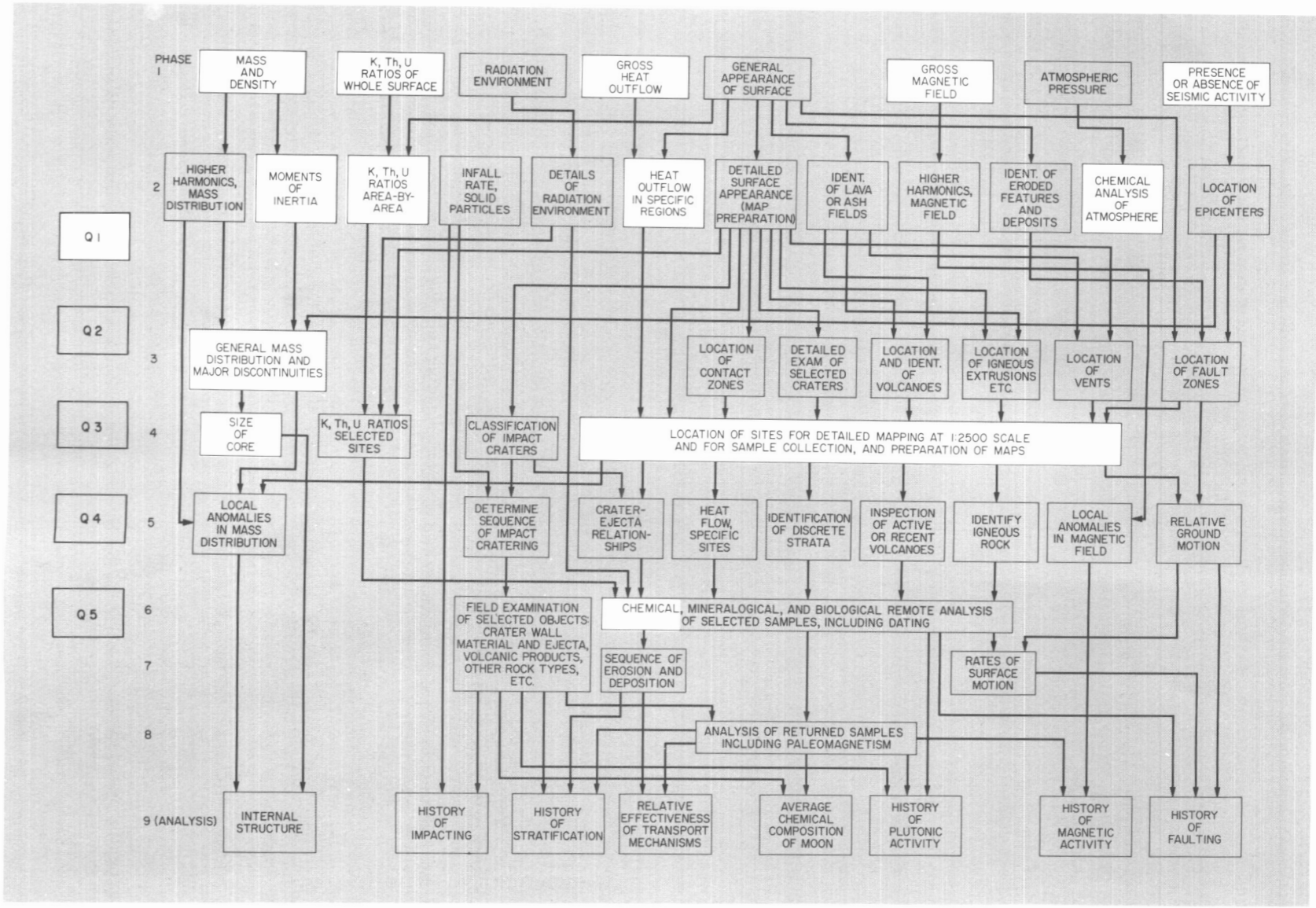

Fig. 2. Measurements pertinent to planetology question 1: "Are the present individual planets and satellites chemically uniform or non-uniform?"

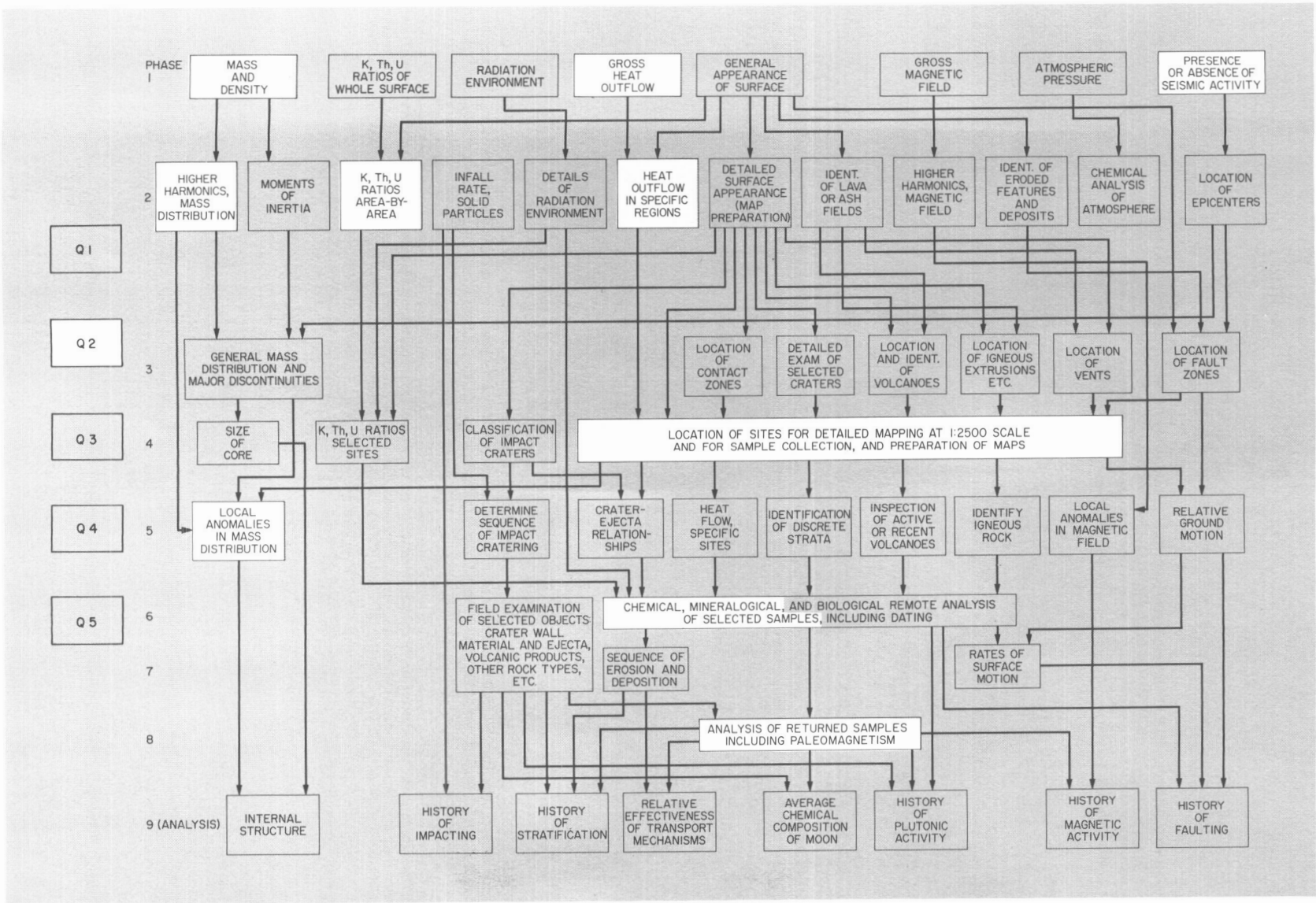

Fig. 3. Measurements pertinent to planetology question 2: "Did final accretion result in the present array of planets and satellites, or in a collection of bodies that were subsequently modified to yield the present array?"

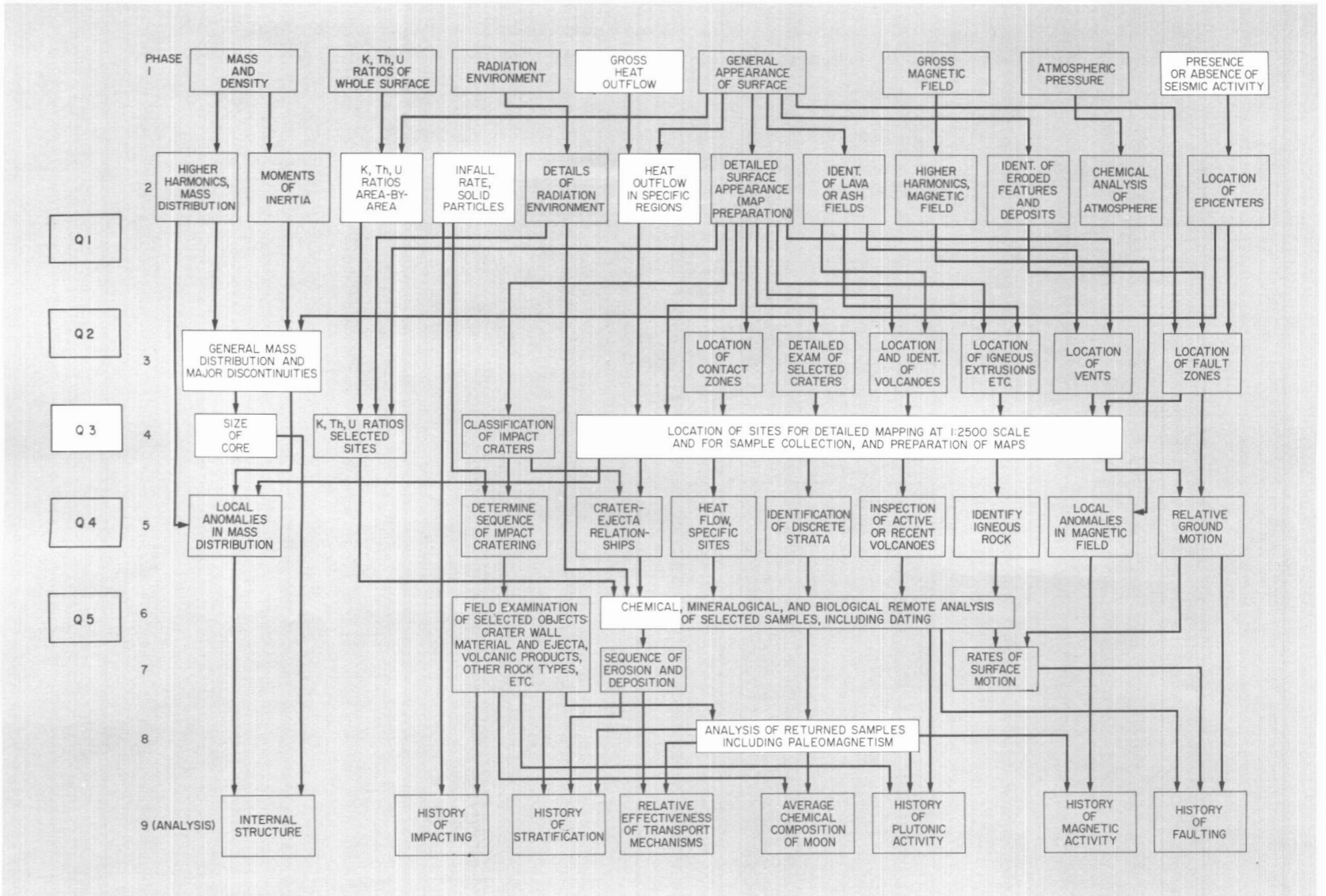

Fig. 4. Measurements pertinent to planetology question 3: "Was the (circumsolar) dust cloud homogeneous at the time of final accretion?"

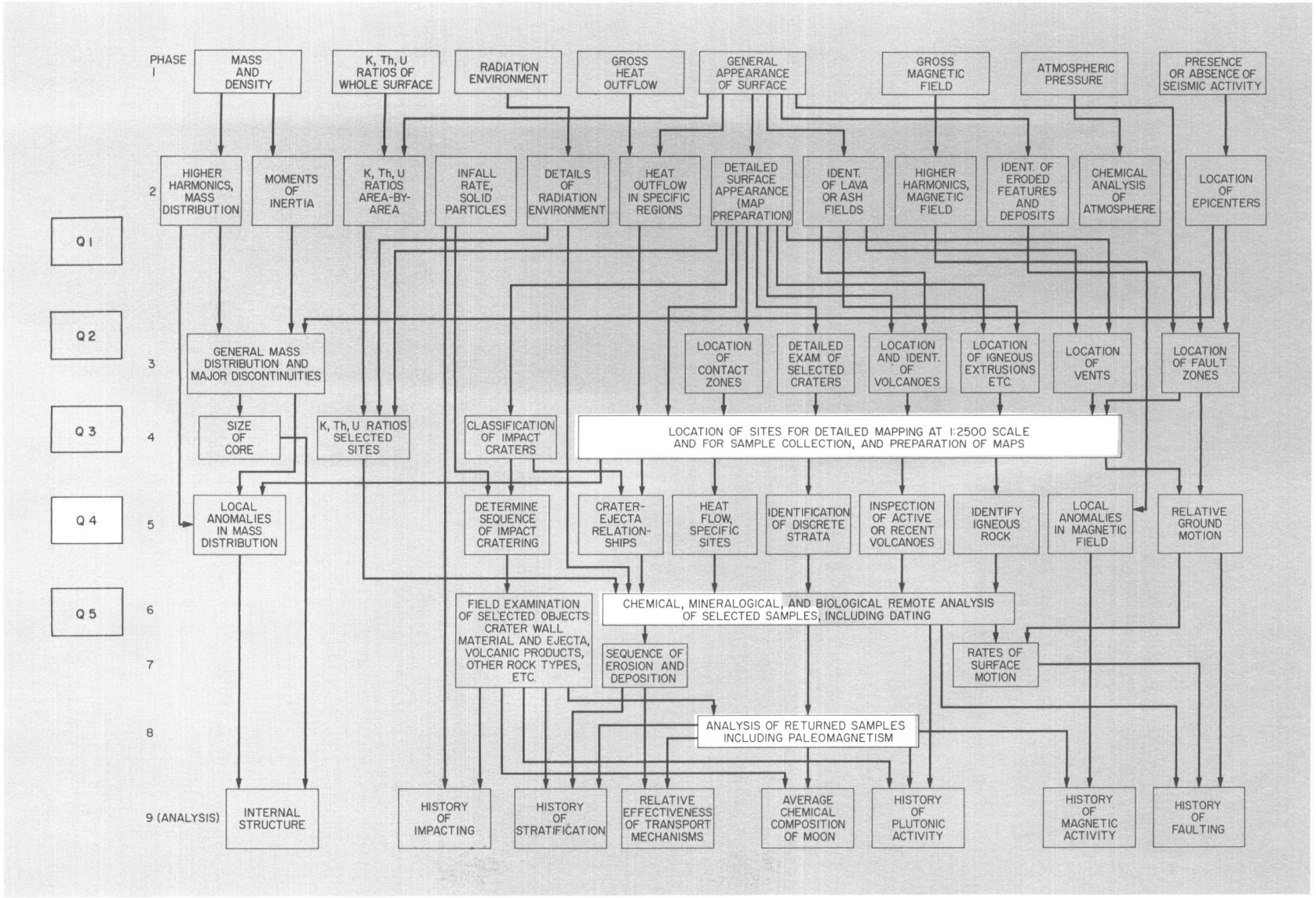

Fig. 5. Measurements pertinent to planetology question 4: "What was the state of the sun–cloud system when it first appeared as a recognizable entity?"

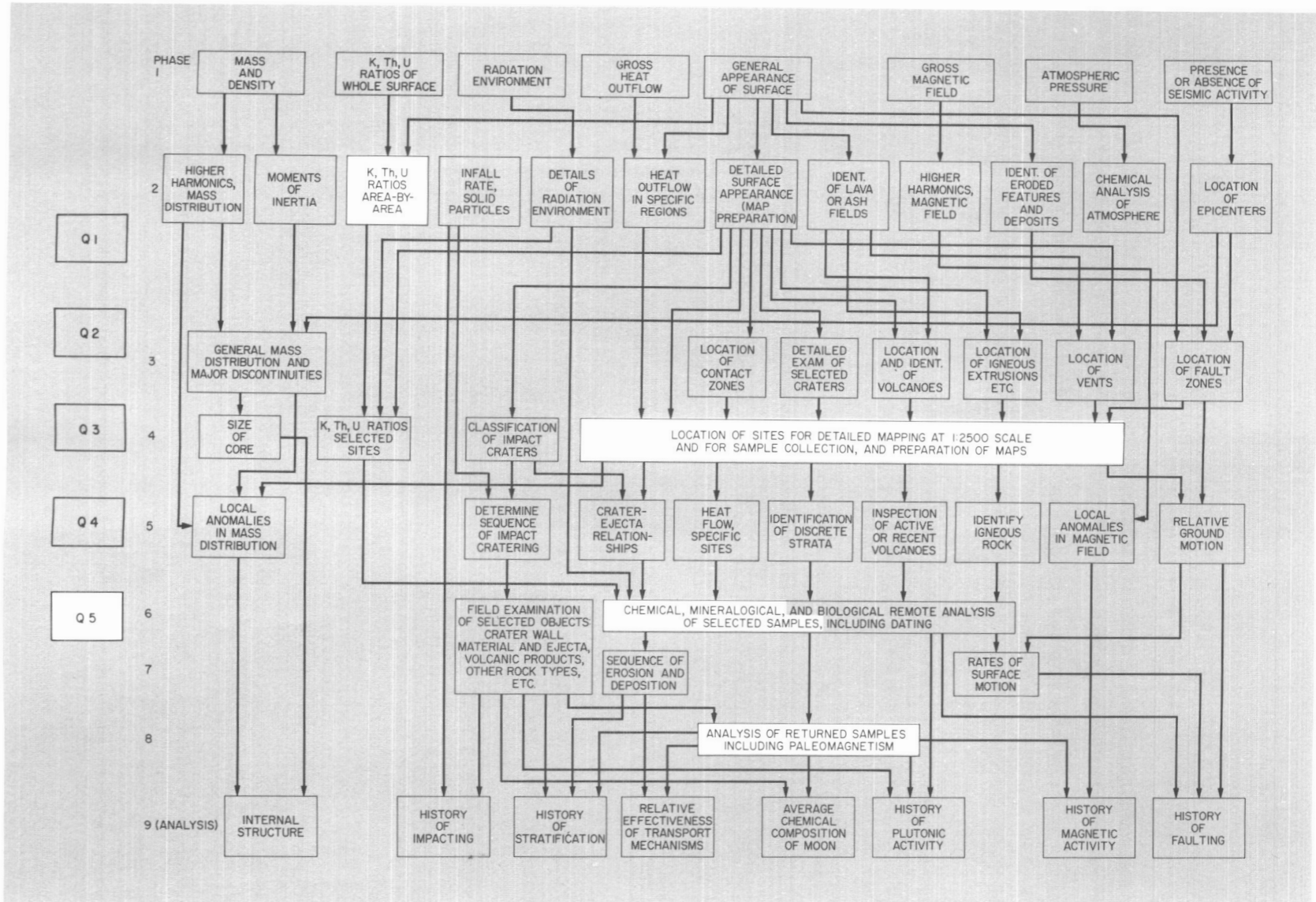

Fig. 6. Measurements pertinent to planetology question 5: "Were there large-scale elemental and isotopic non-uniformities in the (initial) contracted nebula?"

Once the priority measurements in the "critical-data" and "cosmogony" classes were identified, it was possible to begin the evaluation of the flight programs. The main conclusions of the scientific study were such as to require increased emphasis on (1) deep seismic probing, (2) selenodesy, (3) thermal, magnetic, and particle-and-field experiments, and (4) measurements of radioactive-element ratios and extensive sampling and analysis of material collected on the moon. By the same reasoning, relatively less importance was attached to local surface transport mechanisms, isolated tectonic effects, cratering mechanics, or other influences affecting lunar surface details. However, the study has continued to include consideration of these other effects as they influence interpretation of the more fundamental measurements. Also, special attention is being given to the subject of volatile constituents, especially water, because of the large effect that a discovery of available water would have on the later phases of the lunar exploration program.

Given the exploration rationale and the priority goals, the next task in the study was to fit the required measurements into an orderly flight program. As a part of the previous work, instrument lists (SPS 37-44, Vol. II, pp. 40–43; SPS 37-45, Vol. II, pp. 58–64) had been prepared, giving descriptions of the experimental equipment complements that could be carried by orbiting or landing spacecraft. Experiments and instruments for manned exploration are given in Ref. 2. With the aid of these lists and the measurement sets for each phase, as listed in Fig. 1, it was possible to prepare a mission planning chart (Table 1). In Table 1 the first column lists the measurements from Fig. 1. The following columns list the objectives, instruments, and spacecraft believed applicable for each measurement, plus explanatory remarks.

The major conclusion that can be drawn from Table 1 is that there are some high-priority lunar measurements which will not be made very soon if present flight-program plans are followed. If near-future lunar flights are limited to *Apollo* and modest extensions of *Apollo*, there will be no early opportunity to perform the following types of measurements:

(1) Simultaneous particle-and-field measurements on the surface and in orbit, including accurate mapping of the lunar magnetic environment.

(2) Operation of a long-baseline seismic net.

(3) Surface sampling, with on-site analysis and/or sample return to earth, in moon's polar regions and remote, rough areas.

(4) Subsurface probing in regions (e.g., polar areas) where theory or observation suggests possibility of finding recoverable water.

(5) Topographic mapping of selected areas in support of the above and other investigations.

The first class of measurements could be made by small orbiters (IMP or *Pioneer*-type spacecraft) operating in combination with ALSEP or *Surveyor* payloads on the lunar surface. The IMP or *Pioneer* spacecraft are preferable to larger spacecraft because of (1) their spin stabilization, which permits rapid measurement of field vector components, (2) their nonmagnetic design and construction, (3) their small mass and consequent small induced-radiation background, and (4) their relative independence of other mission constraints such as illumination, rendezvous maneuver criteria, etc. Because of these advantages it has been recommended that IMP or *Pioneer*-type spacecraft be carried aboard *Apollo* or AAP vehicles and ejected after reaching lunar orbit. Also, a study of the experimental criteria for such missions has been made; the results are given in an internal document.[2] The *Explorer 35* mission is providing valuable initial data for planning such investigations.

The second class of measurements requires (1) landings at three or more widely-separated points on the lunar surface, and (2) simultaneous operation of the landed seismometers over a time period reasonably long compared with the (now unknown) frequency of natural seismic events. These requirements suggest use of *Surveyors* in combination with ALSEP. Use of ALSEP alone would require manned flights scheduled closely so that the last seismometer would be delivered while the first one still had several months of life remaining.

The third class of measurements, surface sampling, presents special problems. *Apollo* and AAP flights are expected to yield adequate sampling data within their areas of access. For *Apollo* these areas will be equatorial, flat mare sites selected primarily for safety, with sample collection limited to a region within about 1 km of the landing point. For AAP the constraints are less definite at present. There is a possibility of reaching the middle latitudes of the moon, and also a possibility of landing close enough to steep, rough, or unique features (e.g., Copernicus) so that, with the aid of transport vehicles, astronauts can reach the sites of interest.

[2] *Scientific Objectives and Requirements of a Lunar Orbiter to Investigate the Field and Particle Environment of the Moon*, July 1967 (JPL internal document).

Table 1. Mission planning chart

Measurement	Science objective (priority)	Science instruments	Spacecraft[a]														Remarks
			Unmanned					*Apollo*			AAP						
			Orbiter I	*Orbiter II*	*Surveyor*	Landers	Rovers	ALSEP	Geology	Sample return	CSM	IMP/*Pioneer*	ALSEP	LSSM	LFU	Base	
Phase I																	
(1) Three moments of inertia—range and doppler tracking of orbiter with transponder. Orbit should be inclined to equator.	B,D,A	Tracking of orbiter	S	P													Measurement is being carried out. Radio or laser ranging from landers or ALSEP could provide additional data.
		Tracking of IMP/*Pioneer*										P					
(2) K,Th,U ratios of whole surface.	B,D,A	Gamma ray spectrometer	P	P							P	P					May be carried out on *Orbiter 6, but if not, will not be done until* early '70s with CSM or orbiter Block II.
(3) Gross radiation environment—high- and low-energy particle detectors such as electrostatic analyzers and gamma ray detectors *in lunar orbit. Desire* long lifetime and elliptical orbit.	A,D	Radiation detectors		P								P					These experiments are not being done. Expect to get data from a combination of landers and extrapolation of earth data.
(4) Gross heat outflow—best done in survey mission by polar orbiter.	B,D,A	Infrared radiometer		P													Will not be done before early '70s on such vehicles as orbiter Block II and CSM.
		Microwave radiometer		P													
		Thermal mapping									P						
		Microwave imager									P						
(5) General surface appearance—orbiter and lander photographs with orbiter resolution of 100 m or better.	A,D	Photo imaging	S														Measurement is being carried out.
		Survey camera			S												
(6) Gross magnetic fields—three-axis magnetometer on orbiter.	A,D	Vector magnetometer										P					Can be done on unmanned photographic orbiter but IMP/*Pioneer* would do it best.
		Helium magnetometer		P													
(7) Atmospheric pressure—red head in low altitude lunar orbit. Desire long lifetime.	A	Red head or trigger gauge		P													Unless flown on orbiter Block II, this measurement will not be accomplished; however, surface measurements during *Apollo* and AAP are scheduled.

(8) Presence or absence of seismic activity—operation of instrument over period of at least 6 mo and at several locations.	A,B,D	Single-axis seismometer			P													Will probably be done first as part of *Apollo* (ALSEP).
		Passive seismic				P		P					P					
Phase II																		
(9) Higher harmonics of mass distribution.	B,D	Tracking of orbiter		P														This measurement will probably be satisfied in the normal course of the lunar program.
		Radio and laser ranging			P	P												
		Gravity gradiometer										P						
		Laser-radio ranging												P				
(10) Radial mass distribution—three-axis long-period seismometer net if moon has elastic wave source.	B,D	Passive seismic				P		S						P				Really need a net for this measurement which allows simultaneous data from widely separated geographic points.
		Passive seismic																
		Passive seismic												P				
(11) K,Th,U ratios area by area—detail study of gamma ray distribution. Desire low-altitude polar orbit. Measurement (2) may have satisfied this.	D,B	Gamma ray spectrometer		P								P						It should be noted that if *Orbiter 6* does not fly, this measurement may not be accomplished.
		Gamma ray spectrometer																
(12) Infall rates of solid particles—long-life micrometeorite detectors either in orbit or on surface.	D,A,B	Meteor dust detector	S	P								P						Some information is being obtained by orbiter Block I; however, this measurement requires data obtained from both orbiters and landers.
		Micrometeorite ejecta			P	P								P				
		Dust detector												P				
(13) Details of radiation environment—high- and low-energy particle detectors on orbiters and ground stations. Ground stations would act as base for orbiter observations.	D,A,B	Radiation experiments		P	P			S					P	P				These experiments are not being done. Will make some ground measurements as part of *Apollo* ALSEP.
(14) Heat outflow in specific regions—this is a followup on measurement (4), includes both orbiter and ground measurements.	D,B	Thermal mapping		P														If not accomplished in Phase I, this observation has high priority here.
		Microwave surface imager		P														
		Thermal mapping										P						
		Multifrequency microwave spectrometer										P						
		Heat flow						S										
		Heat flow in 3-m holes												P				
		Subsurface probe															P	

Table 1 (contd)

Measurement	Science objective (priority)	Science instruments	Spacecraft[a]															Remarks
			Unmanned					*Apollo*			AAP							
			Orbiter I	*Orbiter II*	Surveyor	Landers	Rovers	ALSEP	Geology	Sample return	CSM	IMP/*Pioneer*	ALSEP	LSSM	LFU	Base		
(15) Detail surface appearance < 10 m resolution and stereo of whole moon.	D,A	Photo imaging		P														Can be done by unmanned mapper as orbiter Block II, and can be done by CSM. Data to be achieved and retrieved only when needed.
		CSM cameras									P							
(16) Identification of lava and ash fields—surface composition measurements from lunar orbiter to be correlated with measurement (15) and ground truth data.	D	Radar		P														The ground truth for this measurement can come from mineralogy-petrology measurements by landers, rovers, *Apollo* and AAP geology and sample return. It should be realized that these features may be recognized best by visual imaging.
		Gamma ray spectrometer		P														
		Thermal neutron detector		P														
		Thermal mapping		P														
		X-ray fluorescence		P														
		Microwave surface imager		P														
		Imaging radar									P							
		Gamma and x-ray spectrometer									P							
		Thermal mapping									P							
		Multifrequency microwave spectrometer									P							
		CSM imaging system									P							
		Photo imaging experiment	S	P														
(17) Higher harmonics of magnetic field—a three-axis magnetometer in polar orbit.	D	Magnetometer (vector)						S			P	P	P					This measurement most probably will require an IMP/*Pioneer* spacecraft in combination with surface observations for base control. Best done by combination IMP/*Pioneer* plus ALSEP or combination IMP/*Pioneer* plus lander.
(18) Identification of eroded surfaces and deposited layers—measurements from lunar orbiter to be correlated with measurement (15) and surface studies.	D	Radar		P														Most of the data for this will probably come from visual imaging. Much information is being obtained by the orbiter Block I series of spacecraft. Will need ground-truth for correlating orbiter data.
		Gamma ray spectrometer		P														
		Thermal neutron detector		P														
		Thermal mapping		P														
		X-ray fluorescence		P														

		Microwave surface imager		P												
		Photo imaging experiment	S	P												
		Photo imaging experiment									P					
		Imaging radar									P					
		Gamma and x-ray spectrometer									P					
		Thermal mapping									P					
		Multifrequency microwave spectrometer									P					
(19) Chemical analysis of the atmosphere—instruments for this should be carried on low-altitude polar orbiter plus emplaced at possibly two ground sites.	D,B	Quadrupole mass spectrometer		P												The ground data for this measurement appears to be coming along; however, measurements will be difficult from the manned missions because of outgassing. This measurement is best done on a combination of orbiter Block II and ALSEP. Also, measurement should be done early in lunar program.
		Gas chromatograph				P										
		Lunar atmosphere experiment				P										
		Ion detector						S								
		Pressure gauge						S								
		Sample return								S						
		Ion mass spectrometer											P			
		Lunar atmosphere experiments											P			
(20) Location of epicenters—three long-period, three-axis seismometers separated by hundreds of kilometers and operating simultaneously.	B,D	Passive seismic arrays				P		P					P			The three scheduled *Apollo* ALSEP missions will give a start on this; however, a reasonable solution to this measurement will require many years of seismic-net operation. Will probably also require a tripartite net on backside.
Phase III																
(21) Physical libration.	D,B	Ranging (radio and laser)				P										
		Laser-radio ranging network											P			
(22) Radial discontinuities in mass—if moon is seismically active, seismic measurements in Phase II may show the core-mantle discontinuity. If moon is not seismically active, this measurement will require large-scale active seismic experiment and must be delayed to a later phase.	B,D	Passive seismic arrays				P		S					P			If moon is seismically active and considering the long lifetime for both the *Apollo* and AAP ALSEP, we should have good information on this measurement by the middle '70s.

Table 1 (contd)

Measurement	Science objective (priority)	Science instruments	Spacecraft[a]														Remarks
			Unmanned					*Apollo*			AAP						
			Orbiter I	*Orbiter II*	*Surveyor*	Landers	Rovers	ALSEP	Geology	Sample return	CSM	IMP/*Pioneer*	ALSEP	LSSM	LFU	Base	
(23) Location of contact zones—visual examination from the surface of specific regions selected on the basis of Phase II maps. Roving vehicle traverses probably required—field geology.	D	Roving vehicle science					P										The data for selecting these sites is probably available from ground-based telescopic observations and *Orbiter I* data; however, orbiter Block II or CSM images will certainly enhance site selection. The *Apollo* geologist may observe this type of feature; however, a specific mission to observe contact zones will probably not be accomplished until AAP.
		Apollo-geology sample return						S	S								
		LSSM science												P			
		LFU science													P		
		Lunar base studies														P	
(24) Detailed examination of selected craters—ground study of classic crater types. For the larger craters and any detail study, this observation will require considerable mobility and long stay times—field geology.	D	Roving vehicle science					P										This measurement is only marginally within the capabilities of the AAP stay times and the range of the LSSM and LFU. The *Apollo* astronaut will accomplish some preliminary observations on small craters in the landing area.
		Apollo-geology sample return							S								
		LSSM science												P			
		LFU science													P		
		Lunar base studies														P	
(25) Location and identification of volcanoes—includes ground studies of selected sites chosen from Phase II maps—field geology.	D	Roving vehicle science					P										Orbiter mapping data for study of these sites can be provided from the orbiter Block II or CSM spacecraft but specific sites may not be visited before LSSMs and LFUs are available. Will likely involve traverse over rough ground.
		LSSM science												P			
		LFU science													P		
		Lunar base studies														P	
(26) Location of igneous extrusions—includes ground studies of selected sites chosen from Phase II maps—field geology.	D	Roving vehicle science					P										Same as above.
		LSSM science												P			
		LFU science													P		
		Lunar base studies														P	

(27) Location of gas vents—includes ground study of some sites—field geology.	D	Roving vehicle science					P										Location of some sites from orbiter visual data and remote sensors. In addition to the geology of classic areas would also like to study any gas emissions. This latter task will probably require the use of LSSM or more probably LFU to emplace instruments.
		LSSM science												P			
		LFU science													P		
		Lunar base studies														P	
		Ion mass spectrometer											P				
		Lunar atmosphere experiment											P				
(28) Location of fault zones—includes ground studies of selected features, field geology.	D	Roving vehicle science					P										Location of some of these features will be accomplished from Phase II mapping, but others will require detail ground mapping by a geologist to locate them. Ground studies will probably require considerable mobility and long stay times; also, active seismic or other geophysical techniques will be useful.
		LSSM science												P			
		LFU science													P		
		Lunar base studies														P	

[a]S = Scheduled, P = Planning.

It now appears likely that *Apollo* and early AAP sampling data may not be definitive for the whole moon, because of the limited regions and durations of access. Therefore, the concepts of longer-range surface exploration vehicles have been examined. These vehicles fall into two classes: (1) manned, traveling laboratories and (2) unmanned, instrumented, sample-collecting mobile machines. Vehicles in the first class would require so much advancement of technique that many years would pass before they could be in use upon the moon. Vehicles in the second class would also require significant new engineering development but could be available sooner and at much smaller cost.

The fourth class of investigations listed above (subsurface probing and search for aquifers) may require a major engineering development in deep drilling on the moon. Alternatively, it may require that a *Surveyor* or *Apollo*-class spacecraft, carrying one or another of the drills already being tested, be landed in a high-latitude mare-border region. If conditions are favorable, ice may be trapped within a few centimeters of the surface near the poles. However, a slight reduction in trapping efficiency (or a major shift in the orientation of the moon's poles during geologic time) would be enough to place the ice boundary deep below the surface. Therefore, preliminary experiments, such as neutron spectrum measurements from orbit,[3] polar exploration by remotely controlled roving vehicles, or the previously mentioned polar landings of instrumented *Surveyors*, should be considered.

The fifth class of activities (metric mapping), is recognized as a necessary adjunct to surface exploration. It may be partly achieved by instrumentation aboard orbiting manned spacecraft. However, additional photographic orbiter flights, with some engineering and calibration improvements, also appear necessary for the economical achievement of the required mapping coverage.

The JPL study to date has not identified any items in the approved NASA flight program plan that are unnecessary or scientifically undesirable for the lunar exploration rationale represented by Fig. 1. It has—as described previously—identified some additional lunar missions, not included in the present approved program, which would be highly desirable on scientific grounds. Some of these missions (e.g., *Surveyor* seismic and IMP/*Pioneer* particle-and-field experiments) would be only minor extensions to the present program. Others (e.g., orbital metric mapping and *Surveyor* polar landings) would involve substantial spacecraft procurements but could and should be done as straightforward applications of existing technique. Still others (e.g., remote-area roving sampling, and deep drilling, if required) would require new engineering developments. In order to gain an understanding of the problems presented by the remotely controlled roving mission, the JPL group has started an engineering study of surface vehicles. In order to put reasonable bounds on the rover configurations to be studied, the following logic has been applied:

(1) The most urgent remote-area sampling investigations can probably be done by an instrument payload (SPS 37-45, Vol. II, pp. 58–64) similar to the payloads originally intended for *Surveyor*; namely, a coordinated group of collection and sensing devices with an aggregate weight of 100 to 200 lb. Some of this weight would be devoted to imaging and on-site chemical, mineral, and isotopic sensing, but some of it would also be used for storing collected samples which the rover would eventually bring to a rendezvous site for retrieval and return to earth. In the present study the return is assumed to be carried out by a manned vehicle; unmanned sample-return systems, as previously studied for *Surveyor*, could also be considered if necessary.

(2) Previous studies indicated that a separable rover, delivered as payload by *Surveyor* and hence limited to a *total* mass of 100 to 200 lb, could be useful in local surveys, and prototype vehicles were built. However, it was recognized that such small vehicles, with a *payload* mass of only 10–30 lb, would have marginal performance for the long-range sampling mission.

(3) A reasonable upper limit on size for an automated rover would be one compatible with delivery to the lunar surface by an unmanned LM spacecraft, as has been envisioned in studies of the LSSM, a vehicle with a mass of about 1000 lb.

(4) Between these lower and upper size limits, there is probably a feasible vehicle design which can perform the most urgent sampling measurements, while still being small and light enough to be delivered (1) as an integral package ("*Surveyor*-on-wheels") launched by *Centaur*, (2) as payload aboard a

[3] *Scientific Objectives and Requirements of a Lunar Orbiter to Investigate the Field and Particle Environment of the Moon*, July 1967 (JPL internal document).

single-launch, manned AAP mission, or (3) as a separable payload item aboard an unmanned soft-lander launched by a vehicle intermediate in size between *Centaur* and *Saturn V*. (A fourth delivery mode—launch from an orbiting AAP-class manned spacecraft—might be of interest but has not yet been considered in detail.) Each of these three delivery modes is compatible with a roving vehicle in the 600–800 lb mass range, with the requisite instrument payload of 100 lb or more; i.e., with an investigative capability similar to that originally planned for *Surveyor*, but augmented by (1) the ability to deliver material samples for return to earth, and (2) the ability to take the samples from particular selected spots along a traverse, rather than just from a single, random point.

Though all of the three delivery modes mentioned above would give about the same gross mass (600–800 lb) for the roving vehicle itself, there would be significant differences in performance, cost, and development time. The first mode (integral vehicle design, *Centaur* launch) is the least costly and represents the smallest departure from existing technique. But the performance of the rover is constrained by (1) *Centaur* injection mass capability and (2) incorporation of the guidance, control, and propulsion subsystems required for transit to and landing on the lunar surface. The parts of these systems which can not be used after landing for navigation or locomotion become surplus and have either to be jettisoned or carried as excess burden during the roving mission.

The second delivery mode (rover as payload on manned LM) eliminates the need for transit and descent subsystems on the rover, enhancing the payload potential for any given gross rover mass. But it does couple the rover to the manned flight schedule, it requires the solution of new interface problems on the LM, and it competes with other LM payload items such as a drill or other instruments, or expendables for lengthening the astronauts' stay on the moon. The cost of this mode is likely to be higher than that of the first mode, unless the LM-associated costs are excluded.

The third delivery mode (rover as payload on an unmanned lander about three times the size of a *Surveyor*) offers the greatest flexibility in design of the roving mission, but it requires not only the new engineering development of the rover itself, but also the development of a new lunar-soft-landing spacecraft and the adoption of an intermediate-size launch vehicle (such as a *Saturn I* or *Titan III* with upper stage) not previously used in the lunar program, and so is likely to be the highest-cost option.

In addition to the cost differences, there is another effect that must be considered in comparing modes. In each lunar project to date, as development difficulties were encountered, scientific objectives were compromised. This experience suggests that any future projects having primarily scientific goals should incorporate only a minimum of new engineering development. For the sampling mission, there is no escaping the need for locomotion and navigation on the moon. These are new engineering requirements, and the development program should be laid out so that they have a chance of being met with a minimum compromise of mission goals, and so that after the technical problems are mastered, enough resources remain to complete the scientific program. Of the modes considered, the *Centaur*-launch mode appears least demanding of new development and hence has been selected for the baseline rover design to be analyzed in the JPL study. The automated LSSM might also be a candidate, but it does require the development of the unmanned LM and the dual-launch AAP mission profile. If a satisfactory sampling mission can be executed by the smaller rover with only one *Saturn V* launch (to return the collected samples to earth) it is clearly the least costly and the least demanding of new developments, of all the options examined.

In the NASA 1967 summer conference on lunar science and exploration (Ref. 3) the scientific requirements for surface mobility were reaffirmed and various mobile systems were considered. Studies of these concepts are continuing; the purpose of the JPL part of this effort will be to provide valid technical information on small, long-range vehicles capable of carrying those instruments needed for the early exploratory investigations in areas remote from manned-landing sites on the moon.

References

1. *Space Research, Directions for the Future.* Space Science Board, National Academy of Sciences, National Research Council, Washington, D. C., 1965.

2. *Conference on Lunar Exploration and Science,* NASA SP-88. National Aeronautics and Space Administration, Washington, D. C., 1965.

3. *1967 Summer Study of Lunar Science and Exploration,* conference held at University of Santa Cruz, Calif., from July 31 to August 13, 1967, NASA SP-157. National Aeronautics and Space Administration, Washington, D. C., 1967.

C. Study of a 1973 Venus Capsule/ Lander Mission

1. Introduction

The Advanced Studies Office has recently completed a study of a mission to the planet Venus in the 1973 opportunity. The mission considered consists of a flyby spacecraft and a capsule/lander which descends through the atmosphere and, for a short time, survives and operates on the surface. Such a mission would allow complementary scientific measurements, not only from near-Venus space, but also while traversing the atmosphere and from the surface of the planet.

The objectives of this study were two-fold:

(1) To determine the differences between a 1973 Venus flyby capsule mission and a previously studied 1973 Venus-Mercury mission, assuming that the two had identical Venus science objectives.

(2) To determine the requirements for postlanding survival on the surface of the planet Venus.

Considered individually, the implications of these two objectives are quite different. The first requires that an optimum mission be designed to satisfy the Venus science objectives so that a comparison can be made between the two missions. The second objective necessitates an in-depth study of the technological problems of landing on Venus, together with the problems of short-term capsule survival.

2. Study Guidelines and Constraints

The launch vehicle considered is the *Atlas SLV-3C/ Centaur* with the *Surveyor* shroud. Capability of this vehicle at the energies required ($C3 = 18$ km^2/s^2) is adequate to launch a planetary vehicle weighing up to 1500 lb. This implies that, from a weight standpoint, the Venus-Mercury planetary vehicle and the one for this mission are quite similar. Furthermore, the spacecraft functions for the two missions are much alike, i.e., to deliver a capsule for entry into the Venus atmosphere and to make flyby measurements. Indeed, the primary difference is that the Venus-Mercury spacecraft must investigate Mercury as well as Venus. It was, therefore, decided that the bulk of the attention during the study should be spent on the mission and capsule/lander designs and that the spacecraft should be heavily based on the Venus-Mercury design.

For the capsule/lander, the related objective specifies a definition of technology requirements. Since this was the case, a constraint was adopted that the simplest possible lander design would be sought. The model environments on Venus are so severe that there is a major difficulty just in surviving on the surface for a short time, hence it is felt that this study shows the minimum price to be paid for Venus surface operations. Pursuant to these observations, the following guidelines and constraints were adopted:

(1) Science objectives of Ref. 1.

(2) 1973 Venus launch opportunity.

(3) *Atlas/Centaur* launch vehicle.

(4) Flyby spacecraft plus atmospheric probe plus surface surviving payload.

(5) Emphasis on comparison to the Venus-Mercury mission and the requirements for post-landing survival.

(6) Spacecraft design based on the Venus-Mercury mission.

(7) Minimum complexity lander design:
   (a) The same subsystems will be used for both descent and post-landing.
   (b) Braking will be only by aerodynamic means.
   (c) No post-landing erection or orientation mechanism will be provided.
   (d) Surface lifetime will be sufficient to return one frame of science data.
   (e) No surface-exclusive science instruments are included in the baseline; i.e., only descent instruments are to be used on the surface.

(8) Wide range of atmosphere models.

(9) Limiting surface conditions for survival.

It should be emphasized that the post-landing science mode chosen (guideline 7e) is not necessarily representative of the way in which an actual lander would be designed. Rather, this mode was chosen because it was adequate to satisfy the study objective and avoided the problem of selecting a scientifically optimum complement of post-landing instruments.

3. Study Approach

The greatest question pertaining to the capsule/lander design is that of the environment on Venus. Because so

little is known about the planet, it is necessary to design for a wide range of atmospheric temperatures and pressures. Surface composition and structure are even more uncertain and are not even amenable to the wide ranging model solution. Hence, the approach used was to design for reasonably severe impact/post-landing conditions, then to find limiting conditions on the nature of the surface which preclude certain operations.

The technical approach taken was first to formulate a mission that was scientifically attractive, i.e., best met the Venus portion of the science objectives given in Ref. 1. Potential mechanizations for flying this mission were then developed, and baseline designs for both the spacecraft and the capsule/lander were formulated.

4. Mission Design

Launch for this mission would be by an *Atlas/Centaur* in late November 1973 with arrival in mid-March 1974. At 12 days before encounter, the capsule would be separated from the spacecraft and deflected onto an impact trajectory. During the first several minutes of capsule cruise, one-way communications are established with the earth via an S-band link. Following separation of the deflection rocket and an antenna, all systems, except a timer, are shut down to conserve power.

Approximately halfway through the cruise phase of the capsule mission, the communications system is turned on for several minutes to transmit engineering data on the condition of the capsule. Shortly before entry, capsule power is again turned on so that communications can be established and the capsule's status ascertained before it enters the atmosphere. The capsule is also despun at this time to ½ rad/s to improve atmospheric dynamics. Atmospheric entry speed is approximately 36,000 ft/s. (The low approach and entry speeds were purposely selected for this mission design to alleviate heat shield requirements.) Entry angles for the landing sites selected are about −60 deg, and the angle of attack at entry is less than 35 deg. Although lower angles of attack reduce heat shield requirements, they also increase dispersion and preclude impact at the most scientifically attractive point. The point chosen for descent and landing is 10 deg on the sunlit side of the terminator. Hence the capsule enters 26 deg from the subearth point and 80 deg from the subsolar point.

Entry and blackout are nearly simultaneous, with blackout duration lasting 12 to 14 s. During blackout, details of the deceleration profile and light level data are stored for later transmission. At the end of blackout, the capsule has decelerated to near Mach 1 with the velocity vector almost vertical, and the heat shield and backup structure are jettisoned. Real-time communications are not immediately established, since lock-up may take several minutes, but predetection recording is used throughout. During descent, the scientific measurements are made, and real-time data are interleaved with that stored during blackout. The resulting data stream is transmitted directly to earth at 30 bit/s.

Descent times and impact speeds are based on the model atmospheres of Ref. 2 extended to surface pressures of 4 to 50 atm. Descent times are between 15 and 70 min and impact speeds range from 10 to 30 m/s. No parachute is deployed during descent; retardation is only from the aerodynamic drag on the capsule. Landing shock is absorbed by polyimide fiberglass resin impact limiter. The impact point is intentionally chosen to be quite far from any of the radar-identified surface features (Ref. 3) since these seem to be locally rough terrain.

The final resting attitude of the capsule is random, hence six antennas for post-impact communications are provided. An on-board sensor notes the direction of gravity and selects the three antennas that are up and transmits sequentially over them. The post-impact lifetime is sufficient to allow transmission of science data collected at landing. The final demise of the lander is due either to heat leaking into the subsystems or to battery exhaustion.

5. Capsule/Lander Design

The capsule/lander design is characterized by simplicity so that vital technology requirements can be easily identified. The design has the following features:

(1) The same subsystems are used in both the descent and post-landed phases. For instance, the transmitter used for descent is also used after landing.

(2) Atmospheric braking is by ballistic means only; there are no parachutes or retrorockets.

(3) After landing, the capsule operates without benefit of a righting or orientation system.

(4) Lifetime on the surface is sufficient to return at least one frame of scientific data.

The overall configuration of the capsule/lander is shown in Fig. 7 just after separation from the spacecraft. The diameter of the heat shield is 40 in. Weight at spacecraft separation is 268 lb. The heat shield and

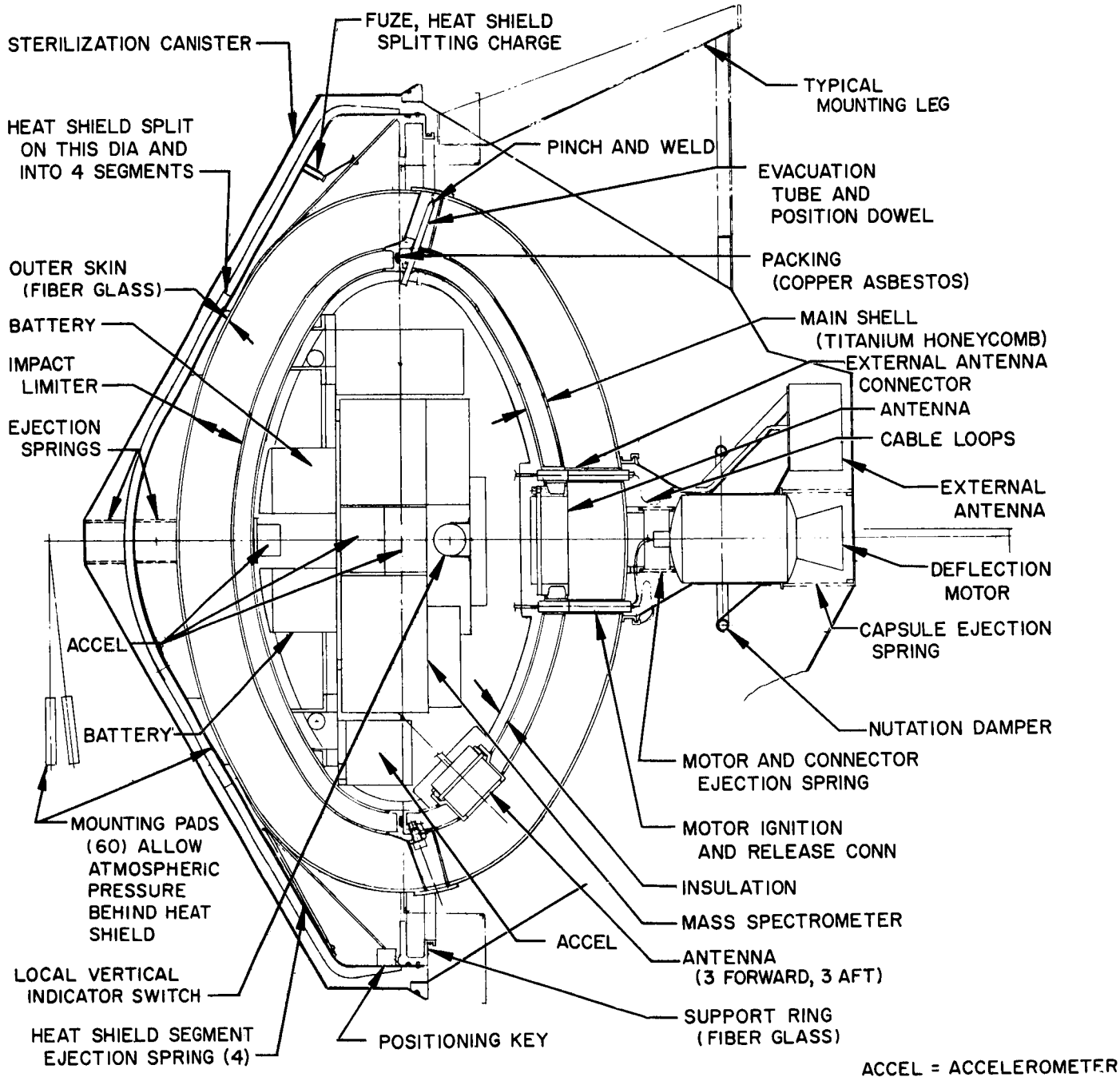

Fig. 7. Capsule/lander configuration

backup structure are removed, thus reducing descent weight to 212 lb.

6. Conclusions

The flyby/capsule portion of this mission differs from the Venus-Mercury mission in the following respects:

(1) Sunlit landing sites are available with a direct-to-earth communications link.

(2) Considerably lower entry speeds accrue from the free Venus trajectory selection. Entry speeds are 36,000 ft/s rather than 43,000 ft/s.

(3) Earth occultation trajectories pass behind the planet as seen from the earth, which enhances the occultation results.

(4) Lower periapsis altitudes are available; 2500 km was chosen.

(5) The near-planet trajectory can be selected to overfly some of the radar identified surface features.

(6) There is no TV on the spacecraft.

The requirements for short-term post-landing survival on the Venus surface are the following:

(1) Direct-to-earth communications are necessary.

(2) The penalty to an atmospheric descent probe is not severe; the weight of the capsule/lander is approximately 75 lb more than an equivalent capsule which operates to impact only.

(3) If the atmosphere is within the design range, the probability of successful post-landing operations is quite high (greater than 90%).

(4) Operations on the surface, in particular access from the capsule, are severely limited by the hostile Venus environment. Hence, extension beyond the modest capabilities of the first-generation vehicle is still an open question.

References

1. Brereton, R. G., et al., *Venus/Mercury Swingby with Venus Capsule: Preliminary Science Objectives and Experiments for Use in Advanced Mission Studies,* Technical Memorandum 33-332. Jet Propulsion Laboratory, Pasadena, Calif., May 1, 1967.

2. Evans, D. E., Pitts, D. E., and Kraus, G. L., *Venus and Mars Nominal Natural Environment for Advanced Manned Planetary Mission Program,* NASA SP-3016, Second Edition. NASA Manned Spacecraft Center, Houston, Tex., 1967.

3. Carpenter, R. L., *Study of Venus by cw Radar—1964 Results,* Technical Report 32-963. Jet Propulsion Laboratory, Pasadena, Calif., Mar. 1966. (Also appears in *Astron. J.*, Vol. 71, No. 2, Mar. 1966.)

Abbreviations

AAP	*Apollo* applications program
AC	attitude control
A/DC	analog-to-digital converter
ADSS	automatic data switching system
AFETR	Air Force Eastern Test Range
AG	approach guidance
ALSEP	*Apollo* lunar surface experiments package
A/SPP	antenna/solar panel positioner
BCE	bench checkout equipment
CC & S	central computer and sequencer
CDC	command data console
CIT	California Institute of Technology
CSM	command and service module
DAS	data automation system
DSIF	Deep Space Instrumentation Facility
DSN	Deep Space Network
DSN/ NASCOM	Deep Space Network/NASA Communications Network (world-wide)
DTM	development test model
DTRB	development test request bulletins
FAT	flight acceptance test
FCN	formal change notice
FMC	Fansteel Metallurgical Corp.
FPAC	flight path analysis and command
HAC	Hughes Aircraft Company
IDS	interim data sheets
IMP	Interplanetary Monitoring Probe
IPL	image processing laboratory
IRR	infrared radiometer
IRS	infrared spectrometer
JPL	Jet Propulsion Laboratory
LFU	lunar flying unit
LM	lunar module
LSSM	local scientific survey module
MDR	master data record
MOS	Mission Operations System
MMTS	multiple mission telemetry system
ODR	original data record
OSE	operational support equipment
PN	part number; pseudo noise
PVT	performance verification test
RADVS	radar altimeter and doppler velocity sensor
RFP	request for program
RTV	reentry test vehicle
SAF	Spacecraft Assembly Facility
SFOF	Space Flight Operations Facility
SI	Sargent Industries
SIPM	star identification program
SM/SS	soil mechanics/surface sampler
SN	Serial Number
SNR	signal-to-noise ratio
SPAA	spacecraft performance analysis area (in SFOF)
SPAC	spacecraft performance analysis and command
SPE	static phase error
SSAC	space science analysis and command
SSD	space sciences division
STCDS	system test complex data system
STV	solar thermal vacuum
TAT	type approval test
TC	temperature control
TCP	telemetry and command processor
TFR	trouble and failure reports

Abbreviations (contd)

TMCA	Titanium Metals Corporation of America	UCB	University of California, Berkeley
TTY	teletype	UVS	ultraviolet spectrometer
TV	television	VCO	voltage-controlled oscillator
TWX	teletypewriter exchange	VPS	vernier propulsion system